MEMBRANE FOULING MITIGATION IN WATER FILTRATION USING PIEZOELECTRICS

by

Obinna Aronu

A Thesis

Submitted to the Faculty of Purdue University

In Partial Fulfillment of the Requirements for the degree of

Master of Science in Mechanical Engineering

Department of Mechanical and Civil Engineering

Hammond, Indiana

December 2020

THE PURDUE UNIVERSITY GRADUATE SCHOOL
STATEMENT OF COMMITTEE APPROVAL

Dr. Harvey Abramowitz, Chair
Department of Mechanical and Civil Engineering

Dr. A.G. Nnanna, Co-Chair
Department of Mechanical and Civil Engineering

Dr. Xiuling Wang
Department of Mechanical and Civil Engineering

Dr. Chandramouli Viswanathan Chandramouli
Department of Mechanical and Civil Engineering

Approved by:
Dr. Chenn Zhou

This thesis is dedicated to my mum, Mrs. G.N Aronu for her love towards us her children and her endless prayers for me during this research

ACKNOWLEDGMENTS

This thesis presented a unique learning ground and challenge to me and will not be complete without recognizing the untiring efforts of some persons who took it upon themselves to ensure that this work comes to completion. Professor. George Nnanna for giving me the opportunity to work under Purdue Water Institute and his supervisions during this research. I really appreciate what you did for me. Professor Harvey Abramowitz for being such a gentle supervisor. His advice and numerous significant contributions to this research. It was a privilege having you as my supervisor. Professor Gokarna Aryal, for making out time to supervise my work even though he was not officially appointed as my supervisor. His timely response to my mails and meetings when called upon. He is one of a kind. Professor Chandramouli Viswanathan Chandramouli and Professor Xiuling Wang for serving as my committee members, lending their invaluable time, knowledge and expertise to this work.

Dr. G.N Aronu and his wife Dr. Otito-Anaka Aronu for their love and support during this research. My mum Mrs. G.N Aronu for all her prayers and words of encouragements during this master's program. My former colleagues at the Water Institute, Michael Ozeh for always being there when called upon for advice and important contributions and David Okposio for his special way of relieving the tense atmosphere in the lab, Uzumma Ozeh and Ashreet Mishra. Williams Oged for his technical assistance during this research. Janice Novosel for her guidance in the formatting of this thesis.

My boss at the Grounds department, John Bachmann for his patience and for being such a good boss. My colleagues at the Grounds department, Isaac Facen for always sparing some pocket change for my lunch, Sam Naranjo for always making out time to teach me no matter how little the job seems, Rob Sager and Eric Popa. The Purdue Water Institute for providing the grant for this research. Most of all to God almighty for seeing me thus far.

TABLE OF CONTENTS

LIST OF TABLES

LIST OF FIGURES

LIST OF ABBREVIATIONS

PVDF	Polyvinylidene Fluoride
TMP	Transmembrane Pressure
NF	Nanofiltration
RO	Reverse Osmosis
MF	Microfiltration
UF	Ultrafiltration
PVC	Polyvinyl chloride
MBR	Membrane bioreactors
CA	Cellulose Acetate
PSF	Polysulphone
PES	Polyethersulphone
PE	Polyethylene
PP	Polypropylene
MW	Molecular Weight
MWCO	Molecular Weight Cut-Off
EPS	Extracellular Polymeric Substances
SOC	Synthetic Organic Compound
NOM	Natural Organic Matter
SMP	Soluble Microbial Products
PZT	Zirconate Titanate
$C_aSO_4.XH_2O$	Hydrated Calcium Sulphate
C_aCO_3	Calcium Carbonate
SiO_2	Silicon Dioxide
$M_g\ (OH)_2$	Magnesium Hydroxide
$Ca\ (PO_4)_2$	Calcium Phosphate
SEM	Scanning Electron Microscope
EDS	Energy-Dispersive Spectroscopy
DI	Deionized
TDS	Total dissolved Solids

NaOH	Sodium Hydroxide
DOE	Design of Experiment
OPRD	Organic Process Research and Development
OFAT	One-Factor-At-A-Time
OVAT	One-Variable-At-A-Time
TTT	Top-Top-Top
TBT	Top-Bottom-Top
TSD	Top-Side-Down
Q_P	Flowrate (g/s)
$\overline{Q_P}$	Average flowrate (g/s)
ρ_w	Density of water (kg/m^3)
J_n	Normalized flux
J_{inst}	Instantaneous flux (Lm^{-2}h^{-}1)
J_{Max}	Maximum flux (Lm^{-2}h^{-}1)
C	Carbon
O	Oxygen
F	Fluorine
Na	Sodium
S	Sulphur
Ca	Calcium
K	Potassium
Si	Silicon
Al	Aluminum
Fe	Iron
Mg	Magnesium

ABSTRACT

The clogging of filtration membrane by particles otherwise known as fouling is a major concern in membrane filtration technology due reduction of flux, membrane lifespan and system performance, with an associated increase in process and operating costs in industries that utilize membrane in their production process. Cleaning or replacement of a fouled membrane requires production to be interrupted or the entire system to be shut down. This is because the cleaning or replacement of the fouled membrane requires production to be interrupted for the cleaning process or the entire system to be shut down for the replacement process to take place, leading to great losses to the industries involved. Many approaches have been devised over the years to tackle this problem, of which not only undermine the performance of the filtration membrane but also contribute to great losses to industries that apply them. Cheaper and more efficient means of fouling control remains the key to solving this problem.

A water filtration system is proposed that uses piezoelectric crystals attached on a tubular polyvinylidene fluoride (PVDF) membrane to increase flux and delay the clogging of the pores of the filtration membrane (by particles). Filtration tests with mud solution showed that the membrane vibrated with piezoelectrics reduced the clogging of the pores and increased permeate flux of the filtration process as compared to the non-vibrated membrane. To optimize the permeate flux production of the system and fouling reduction, the effects of voltage, concentration and location of piezoelectric crystals were investigated. An equation to best fit the experimental data was developed which can help in the optimization of the variables.

1. INTRODUCTION

1.1 Overview

The major limiting factor in membrane separation process is the fouling of the membrane and the consequent reduction in flux **[1,2]**. Membrane fouling occurs when the unwanted, suspended and dissolved solutes are deposited on the membrane surface and into the pores leading to a decline in permeate flux and an increase in transmembrane pressure **[3,4]** resulting in loss of performance, reduction of membrane lifespan, which in turn increases the process and the operating costs **[5]** in industries. The cleaning of the fouled membrane requires production to be interrupted for the process to take place while the entire system must be shut down for the replacement process to take place, hence the losses. At present, there is no available solution to completely prevent membrane fouling in industries **[6]**.

Vibrating the membrane with such turbulence promoters as electric motor, gases etc. and backwash have proven to be some of the ways of achieving high permeate flux, but still with their numerous disadvantages **[7]** which pose a lot of threats to industries that employ membrane in their production processes. Some of the chemicals used in chemical cleaning can oxidize the membrane surface leading to the partial severing of the membrane polymers thereby shortening the lifespan by changing the functional groups, mechanical properties and physical structure of the membrane **[8]**. Also, the high chemical cost, production flow interruption, the threat to the environment due to disposal difficulty make this approach a little less effective. Backwash often resorted to by industries involves flow reversal from the permeate side to the feed side, creating mechanical stress that erodes the extremely thin top layer of the membrane making it unsuitable for some membrane configurations. It not only requires a working flux twice higher than that of the filtration **[9]** resulting in more energy consumption, but also requires a stop in normal production flow leading to a loss of useful production time. The associated production losses incurred by these industries runs into millions of dollars when quantified **[10]**.

Because of their light weight, piezoelectrics have been applied in many processes and structures including radar structures **[11]** and energy harvesting **[12]**. It recently gained popularity as one of

the turbulence promoters suitable for all types of membranes and provides cheaper and more portable means of mitigating fouling. Various research on piezoelectrics have proved that the physical vibration of membranes using piezoelectrics is very effective in fouling reduction. For instance, Coster et al **[13],** applied AC-voltage in the frequency range of 0.5-3kHz to a piezoelectric polyvinylidene fluoride membrane during which polyethylene glycol water solution was filtered leading to a 10-100nm range of membrane displacement which was able to increase the flux more than that of the non-vibrating membrane. Kuscer et al **[14],** developed a piezoelectrically-driven vibrating system used in filtration of humic acid solution. Vibrating the membrane at the frequency of 100kHz with a voltage of $100V_{pp}$ led to a reduction in flux decline by 59% when compared with the flux decline in a non-vibrating ceramic membrane. Darestani et al **[15]** imparted piezoelectric properties to polyvinylidene fluoride (PVDF) microfiltration membranes through electrical poling and used it to study the effects of operational factors on membrane fouling. This was able to drastically reduce the fouling of the membrane. This work is a continuation of **[16]** in which vibrating the membrane with piezoelectric crystals produced a permeate flux 86% more than that of the headline and **[17]** in which piezoelectric crystals were found to reduce concentration polarization after the first 1 hour of the filtration time and optimization of the system was recommended. The anti-fouling effects of vibrating piezoelectric crystals on ultrafiltration membranes as well as three variables namely voltage, piezoelectric crystal location and feed water concentration were investigated in this work. The results revealed that the interstitial cracks introduced between the cake layers by the vibratory action of the piezoelectric crystals was the major source of fouling reduction for the vibrated membrane. Also, results from the investigated variables revealed that vibrating the membrane with low voltage, keeping the feed water concentration at low or medium level and placing the crystals at Top-Bottom-Top (TBT) locations would yield the highest permeate flux.

1.2 Research Objectives and Research Questions

This work aims at presenting an effective method of reducing membrane fouling in water filtration, using piezoelectrics to optimize permeate flux and eliminate backwash. To achieve the said objective, the variables that needed to be investigated were first identified. Once identified, the number of experiments to be run were determined using a Design of Experiment (DOE). The following research questions were generated to help achieve the afore-mentioned objectives:

RQ 1. What are the most important variables for reducing membrane fouling in UF system incorporating piezoelectrics for vibration?
RQ 2. What range of the variables should be tested?
RQ 3. What combination of the level of the variables will optimize the permeate flux?

2. LITERATURE REVIEW

2.1 Membrane Technology

Early studies on membranes can be traced back to the eighteenth-century philosopher scientists **[18]**. Up to the nineteenth and early twentieth century, they were basically used in the laboratory to develop physical/chemical theories without any commercial purpose. Today, membranes (Fig. 2.1) which are physical barriers that allow certain compounds to pass through depending on their physical and /or chemical properties **[19]** have become very popular in the last two decades **[20]** and have gained high acceptance in the domestic sector, drinking water purification units and many industrial sectors like food, medicine, pharmacy, biotechnology, chemical, industrial effluents and waste water treatments **[21]**, employ membranes due to many advantages they have over separation methods like evaporation, adsorption and absorption, gas-separation, chemical separation, pervaporation etc.

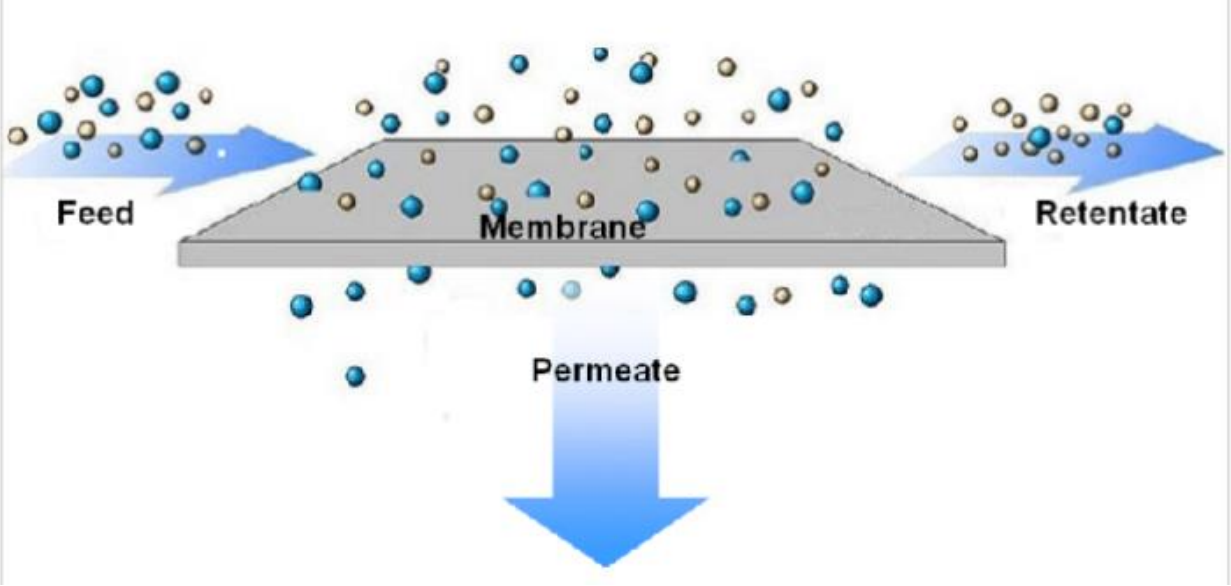

Figure 2.1. Membrane based separation process **[22]**
Image credit: researchgate.net

Advantages of using membranes include their potential to remove microorganisms, inorganic salts, organic pollutants, flexibility of operation and cost effectiveness, less energy requirement for operation, high availability of membrane materials. The high purification potential of membrane separation processes makes it possible to meet the requirements applicable to advanced wastewater treatment for protection of water and ground water resources. In wastewater treatment plant (Fig 2.2), membranes play important roles where they are used to make water safer for human consumption and have been used to replace the conventional filtration methods due to their lower cost of treatment, minimum to no use of chemicals, low maintenance cost over the conventional methods and high clean water quality production **[23].**

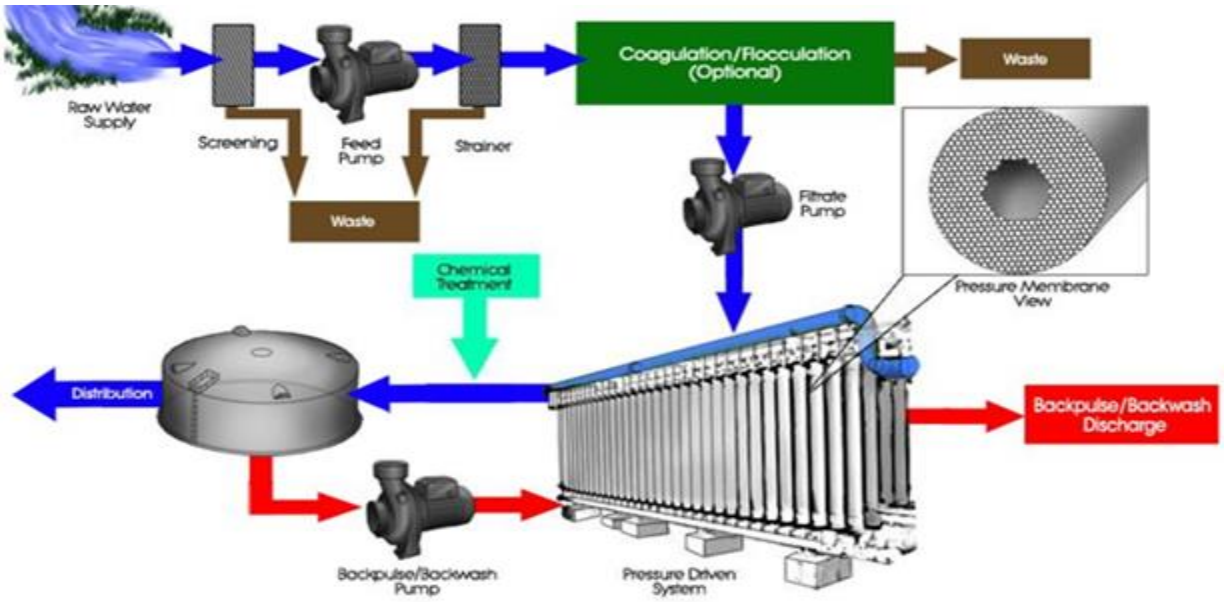

Figure 2.2. Membrane separation process used in the water treatment industry.
Image credit: http://tiny.cc/26aniz

There are basically 3 possible streams (Fig 2.3. left) in the membrane process: the feed stream, the retentate stream and the permeate.

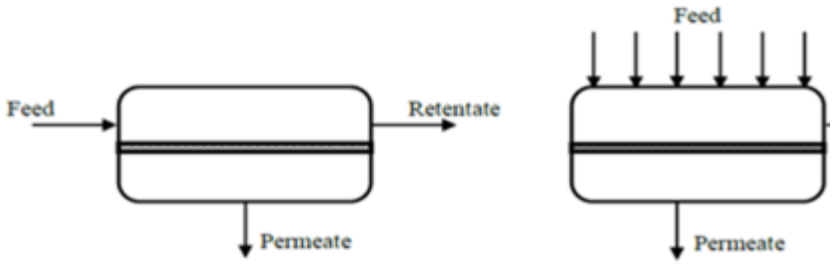

Figure. 2.3. Membrane filtration streams with crossflow mode (left) and dead-end mode (right) **[19]**

The feed stream consists of the water which contains the compound to be separated, the retentate consists of the compounds that cannot pass through the membrane while the permeate consists of those compounds that are able to pass through the membrane **[20]**. The operation of a membrane can either be done on dead-end mode (Fig 2.3. right) or crossflow mode (Fig 2.3. left). In dead-end mode (order wise) known as full-flow stream, there is no retentate stream. This mode is suitable for operations with low-solids in water.e.g. ultrafiltration of apyrogenic pure water production while in cross-flow filtration mode, some of the feed water is collected as a concentrate (or retentate) stream and is suitable for waters having significant loading and /or membrane of limited permeability **[20].** Crossflow filtration mode has been found to be better than dead-end mode because of its higher mass transfer, higher energy savings and retention efficiency **[21].** It prevents solute build-up on the feed side of the membrane. Dead end type on the other hand enhances gel formation and concentration polarization and is usually used to study the worst-case scenario of fouling [**18].**

2.2 Membrane Classification

The advances in membrane technology has led to the development of different types of membranes. This gives rise to different classifications which include nature of driving force, membrane configuration, membrane material and the nominal size of separation achieved.

2.2.1 Classification Based on the Nature of Driving Force

This groups the membrane processes into two: the constant flux process and the constant pressure process. In the constant flux process, the membrane is driven to keep a constant flux while reduction in flux continues due to membrane fouling. In order to meet the production demands and balance the effect of reduced flux, the transmembrane pressure (TMP) which is the pressure difference along the membrane is usually increased, leading to an increased force of the feed water on the membrane thereby allowing the flux to remain relatively constant. In constant pressure operation, the flux decreases when the membrane begins to foul while the pressure is kept constant.

2.2.2 Classification Based on Membrane Configuration

This puts the type of membrane inside the membrane module into consideration. Module is used to describe a complete unit comprising the membrane, the pressure support for the feed, the permeate and concentrate structure as well as the overall support structure **[24].** Classification based on configuration includes flat sheet membranes, spiral wound membranes, hollow fiber membranes, tubular membranes and emulsion membranes.

2.2.2.1 Spiral Wound- Membrane

The spiral wound-membrane (Fig. 2.4) is mainly used in Nanofiltration (NF) and Reverse Osmosis (RO) water treatment. It is not commonly used in Microfiltration (MF) and Ultrafiltration (UF) because it does not allow for backwash which is often required for MF and UF in order not to get clogged up or fouled **[23].** It comprises several large sized membrane sheets and a porous cloth at the permeate side attached to the perforated pipe lying in the center and rolled around the perforated pipe into a circular shape thereby making the fluid flow within the module to be in a spiral formation.

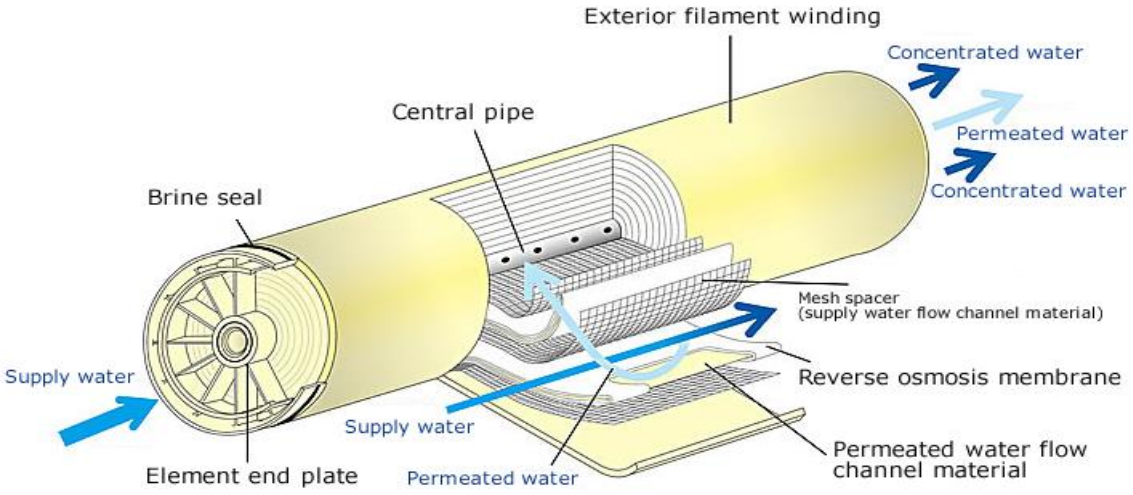

Figure 2.4. Spiral wound membrane **[25]**
Image credit: muro-chem.co

2.2.2.2 Hollow Fiber Membrane

The hollow fiber membrane utilizes thousands of long, porous filaments ranging from 1-3.5mm wide which are potted in a polyvinyl chloride PVC shell for water filtration. The hollow fiber membrane is used for all types of filtration from MF to RO but is mostly used for MF and UF configuration in water treatment because of its backwash ability which is very essential for MF and UF applications and does not require extensive pretreatment prior to utilization.

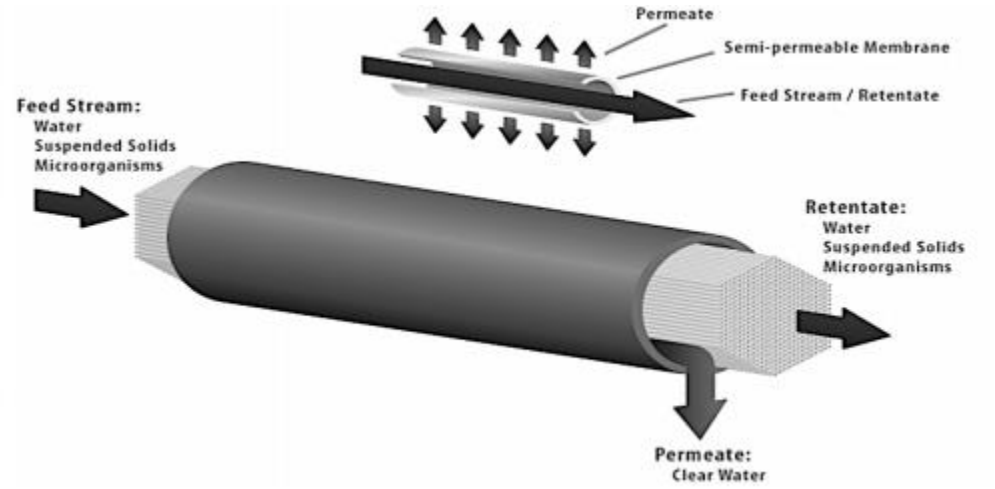

Figure 2.5. Hollow fiber module with in-side out flow system **[26]**
Image credit: Synderfiltration.com

With a packing density as high as 40,000 m^2/m^3 (compared to spiral wound and tubular modules which are usually from 30 to 1000m^2/m^3 and 130 to 300 m^2/m^3 respectively), higher membrane surface area within smaller module size, they find application in membrane bioreactors (MBR), RO pretreatment, industrial/wastewater, juice processing biotech applications etc. This membrane treats the feed in two different ways. When the feed water enters into the center of the membrane and the permeate is collected along the outer surface of the membrane, the in-side out flow (Fig. 2.5) is achieved, on the other hand, if the feed water is fed along the outer surface of the membrane and the permeate is collected from the inside of the hollow fibers, an outside-inflow system is achieved **[19].**

2.2.2.3 Tubular Membrane

The tubular membrane (Fig. 2.6) is an extension of the hollow fiber membrane. In this, one or a bundle of tubular membranes are used as the filtration mechanism. A tubular membrane has a porous wall tube with the membrane inside and is used when the feedwater has a high concentration of suspended solids or the feedwater has a potential to plug the membrane pores. When the feedwater is pumped into the membrane tube, the permeate filters through the membrane and gets collected at the permeate side while the rejected concentrate continues to flow through the center of the feed tube.

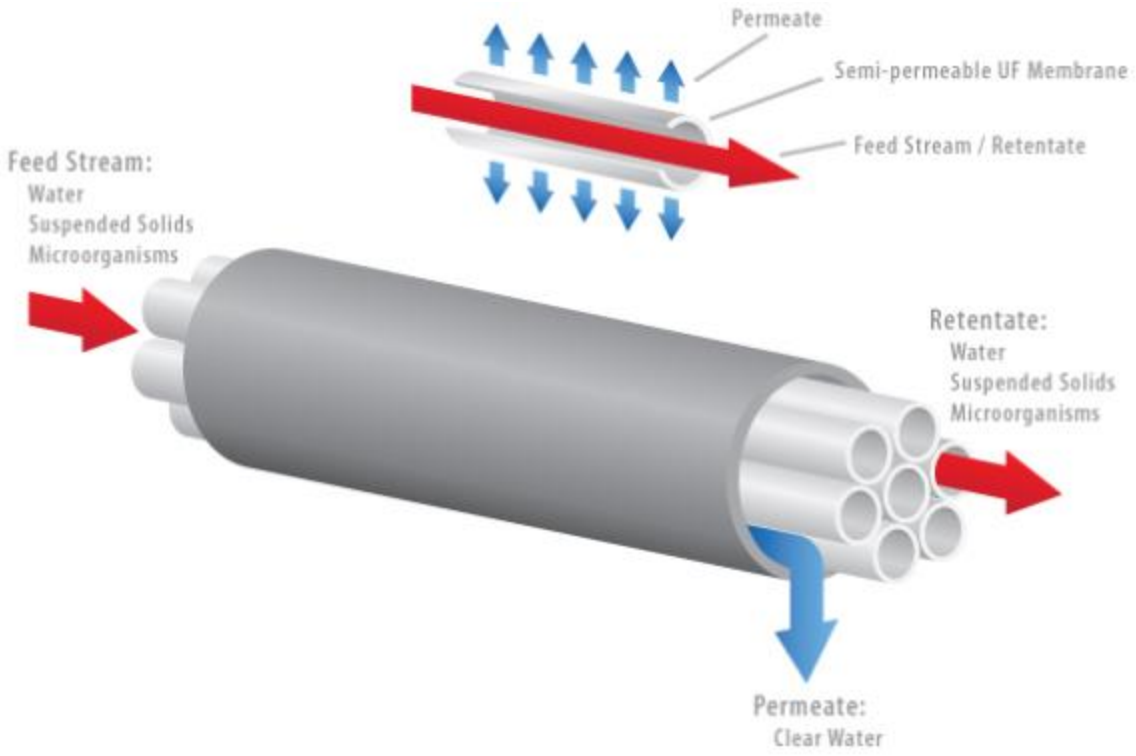

Figure 2.6. Tubular membrane with in-side out flow system **[27]**
Image credit: Synderfiltration.com

2.2.3 Classification Based on Membrane Material

Cellulose, cellulose acetate (CA) and ethyl cellulose being the first commercial membranes **[18]**, **[28]** and having low chemical resistance, could not withstand extreme conditions that are required in some industrial applications. These were overtaken by the synthetic membranes which have been more researched and commercialized for both domestic and industrial uses. These synthetic membranes may be composed of organic substances (polymers) or inorganic substances (ceramics) with polymeric materials being widely studied for the reason of its mechanical strength, flexibility and chemical stability. Due to its excellent chemical composition and thermal stability, Polysulphone (PSF) has gained wide usage as membrane material **[29]** while other polymers like polyethersulfone (PES), polyvinylidene fluoride (PVDF), polyvinyl chloride (PVC), polyethylene (PE), polypropylene (PP), polyamide, chitosan are other membrane materials that are been

constantly researched and used in recent years. Today, a larger portion of the membrane of the membrane market has been overtaken by the PVDF membrane **[24].**

2.2.3.1 PVDF Membrane

The PVDF is a semi crystalline polymer unit of $-(CH_2\,CF_2)_n-$ **[30].** Due to its high mechanical strength, good chemical resistance and thermal stability with excellent aging resistance which are important for membrane separation processes, it has found application in all membrane types except for RO **[24]**. Among many other good qualities of PVDF is its processability which makes it a good candidate for the preparation of flat sheet, hollow fiber and tubular membrane **[30].** These numerous qualities of the PVDF has made it one of the promising UF and MF membrane materials for industrial applications as compared to other polymeric materials **[31]** and is currently being explored for applications in membrane contactor and membrane distillation **[6], [30]**. However, the application of PVDF has been found to be limited because of fouling in water treatment and wetting (hydrophobicity) in membrane contactors, thereby reducing the efficiency of the membrane and degrading its performance. A lot of advances have been made to correct these limitations by way of material screening, surface engineering and pore tuning **[32], [33], [34]**.

2.2.4 Classification Based on the Nominal Size of Separation Achieved

Depending on their particle size exclusion capabilities and the pressure required to drive the membrane, membranes are categorized into micro-filtration (MF), ultra-filtration (UF), nano-filtration (NF) and reverse osmosis (RO) (Fig. 2.7).

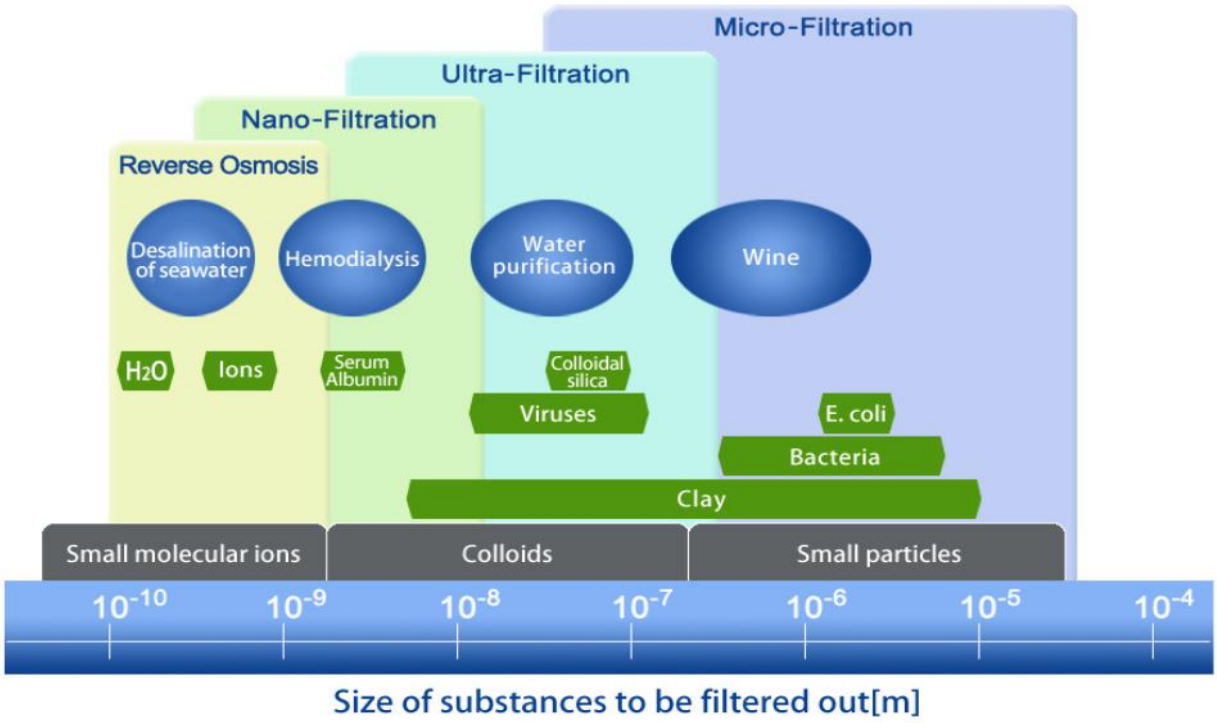

Figure. 2.7. Classification of membrane filtration based on size exclusion **[28]**
Image credit: bing.com

These membranes have different pore-sizes which depend on the size of the particle they are configured to allow to pass through them when they are used for filtration purposes. While the MF and UF membranes are regarded as low-pressure membranes because they require less driving power, the reverse is the case for NF and RO membranes since they require higher driving pressure for operation. Membranes can reject particles that are bigger than their nominal pore sizes.

2.2.4.1 Reverse Osmosis

RO membranes are considered non-porous because of their small pore sizes that are less than 2nm with the dense layer within their polymer matrix. They do not sieve particles rather they rely solely on diffusion of water across their dense layer and macromolecular exclusion from the produced permeate. They generally reject particles smaller than $1x10^{-4}$µm to $1x10^{-3}$µm. RO requires treatment to prevent fouling.

2.2.4.2 Nanofiltration

NF filtration utilizes straining to remove particles and allows ionic species like sodium and chloride to be removed from feed water through diffusion across the macromolecule pores of the membrane. NF membranes reject particles between $1x10^{-3}$µm to $1x10^{-2}$µm and are achieved through its pores which are generally less than 2nm. NF requires pretreatment to prevent fouling.

2.2.4.3 Ultrafiltration

This selectively separates macromolecules of 1,000-200,000Dalton molecular weight from solvent and dissolved solutes **[35].** Based solely on molecular size for separation, UF separates extremely small particles and dissolved molecules from fluids. It retains materials ranging from 1k to 1000k molecular weight (MW) while allowing salts and water to pass through. It retains materials larger than the rated pore-size and is used typically to separate proteins from buffer components for buffer exchange and desalting. UF membranes are applied to supplement some other treatment processes like coagulation, sedimentation, flocculation and for pre-treatment purposes in reverse osmosis plants **[36].** UF membrane technology is vastly applied in various industrial processes like food, pharmaceuticals, biotechnologicals, pure-water production, seawater production and desalination. **[37],[38]**. Among the many benefits of ultrafiltration that gives it wide application are its ability to simultaneously concentrate and desalt solutes, does not require phase change that often denatures labile species (that are likely to change) , can perform either at room temperature or in a cold room and is gentle to solutes unlike some processes like precipitation **[14].**

2.2.4.4 Microfiltration

These are membrane separation processes that utilize filters with pore size of approximately 0.03 to 10 microns (1 micron = 10^{-6} m), a molecular weight cut-off (MWCO) of greater than 1000,000 daltons and relatively low feed water operating pressure of approximately 100 to 400kPa (15 – 60psi). When used, microfiltration membranes prevent the passage of sand, silt clay, giardia lamblia and cryptosporidium cysts, algae and some bacterial species into the filtered fluid but does not totally prevent viruses from passing through. When used with disinfectants, MF controls the passage of these microorganisms into the filtered fluid.

2.3 Fouling of Membrane

Fouling in membrane technology is used to describe the process of deposition or adsorption of colloids, particles, macromolecules (like proteins, polysaccharides), salts etc. on the membrane surface and/or inside the pores or pore walls **[18], [6]** leading to great decline in flux, change in selectivity and separability during filtration operation thereby shortening the lifespan of the membrane. Fouling is of economic importance in membrane technology because it limits the productivity of the membrane **[18]** and increases its operating cost **[6], [39], [40]**. Although one of the ways of mitigating fouling and improving membrane separation is by cleaning the membrane, this often results in an increased operation cost since it requires the stoppage or interruption of normal operation leading to a waste of useful operation time. Many efforts are being made to reduce fouling while the operation time is not tampered with until it becomes very necessary. Some methods devised for fouling reduction range from operation parameter optimization (like the operation pressure, temperature, crossflow velocity, flocculation pretreatment), optimizing the design of the membrane module structure (like its shape, length-diameter ratio, casting form, the packing density of the membrane) **[6],** the current method of fouling control by shear stress generation **[41]** (like cross-flow, piezoelectrics, gas-sparging and ultrasonic-inducements) **[39], [4], [42]** brought about by the relative motion between the surrounding fluid and the membrane, to the actual washing of the membrane otherwise known as backwashing.

2.3.1 Fouling Classification

A deeper look at membrane fouling reveals that there are various ways of categorizing the fouling of membranes.

2.3.1.1 Classification Based on Foulant Type

Classified based on the foulant type are:

2.3.1.1.1 Biofouling

Biofouling occurs when biofilms of extracellular polymeric substances (EPS) and microbial cells matrix are formed on the membrane **[43], [44], [45], [40].** This refers to the deposition/retention, growth and metabolism of bacteria cells or flocs on the membrane. It constitutes one of the most

common and serious issues in membrane technology, especially in applications like waste-water treatment, membrane bioreactor, bio separation, reverse osmosis and desalination **[46].**

2.3.1.1.2 Colloidal Fouling

Colloidal fouling occurs when organic / inorganic particles or colloids block the pores of membranes leading to cake formation or concentration polarization. This also refers to the fouling of the membrane with colloidal particles in the size range of a few nanometers to a few micrometers **[47].** Such foulants include clays, silts, silica salts, humic acid and hydroxides of heavy metals.

2.3.1.1.3 Inorganic Fouling or Scaling

This occurs as a result of the precipitation of salt crystals (usually calcium and magnesium salts) unto the membrane due to supersaturation during filtration. Such salts as $CaSO_4.XH_2O$, $CaCO_3$, SiO_2, $Mg(OH)_2$ and $Ca_3(PO_4)_2$ are the major causes of inorganic fouling. Inorganic substances are believed to contribute less than 15% of membrane foulants in nanofiltration plants for the treatment of surface water **[56]**. The mechanism of inorganic fouling involves the crystallization of salt ions that were precipitated from the bulk solution and particulate fouling.

2.3.1.1.4 Organic fouling

In this, dissolved organic matter (DOM) occurs in the form of synthetic organic compound (SOC), natural organic matter (NOM), soluble microbial products (SMP) [**18].** The interactions of chemical properties with the membrane material and strong effects of organic types make it difficult to identify the fouling mechanism of organic fouling. For NOM, humic substances have been identified to be the major foulants which cause severe irreversible fouling in pressure-driven membrane process through adsorption and blocking resulting in flux decline **[56]**

2.3.1.2 Classification Based on their Relative Resistance to Cleaning

When classified based on their relative resistance to cleaning we have reversible and irreversible fouling **[41].** Operating below the critical flux has been identified by researchers as the best approach of fouling control especially for reversible and irreversible fouling **[56].**

2.3.1.2.1 Reversible Fouling

Reversible fouling is the type that is easily removed by certain cleaning methods. This is usually caused by loosely attached foulants which if not controlled build up on top of one another forming a cake layer. Usually occurs due to external deposition of material (cake filtration) on the membrane. The mechanisms of reversible fouling involve concentration polarization and cake layer formation **[49].**

2.3.1.2.2 Irreversible Fouling

This is the type that remains after the cleaning. Irreversible fouling is further divided into hydraulically irreversible which cannot be cleaned by hydraulic means and chemically irreversible which is the irreversible fouling left after chemical cleaning **[10].** This can be caused by pore blocking, strongly attached foulants, gel layer formation or biofilm formation. Many researchers point out that irreversible cannot be removed by any method including chemical method **[50][51],** however some other researchers established that irreversible fouling can be removed by chemical reagent but repeated chemical cleaning results in poor membrane performance and degradation **[52][53].**

2.3.2 Fouling Mechanism

No matter the category of fouling, there are basically three stages in fouling, they include: adsorption, pore-blocking and cake formation **[10].** In adsorption, the deposited particles/solutes on the membrane interact with the membrane, pore-blocking occurs when the pores of the membrane are fully or partially closed by colloids and particles. Pore-blocking occurs at the initial stages of filtration when the membrane surface is bare of deposits thereby exposing the pores to direct interaction with the incoming particles. Adsorption and pore-blocking in internal pore surfaces occur if the foulants (colloids) are smaller than the membrane pores (i.e. solutes). Cake formation occurs when layers of particles build up on each other on the surface of the membrane leading to additional resistance to the permeate flow. Four fouling mechanisms (Fig. 2.8) are easily identifiable, this includes: complete blocking, standard blocking, intermediate blocking and cake filtration.

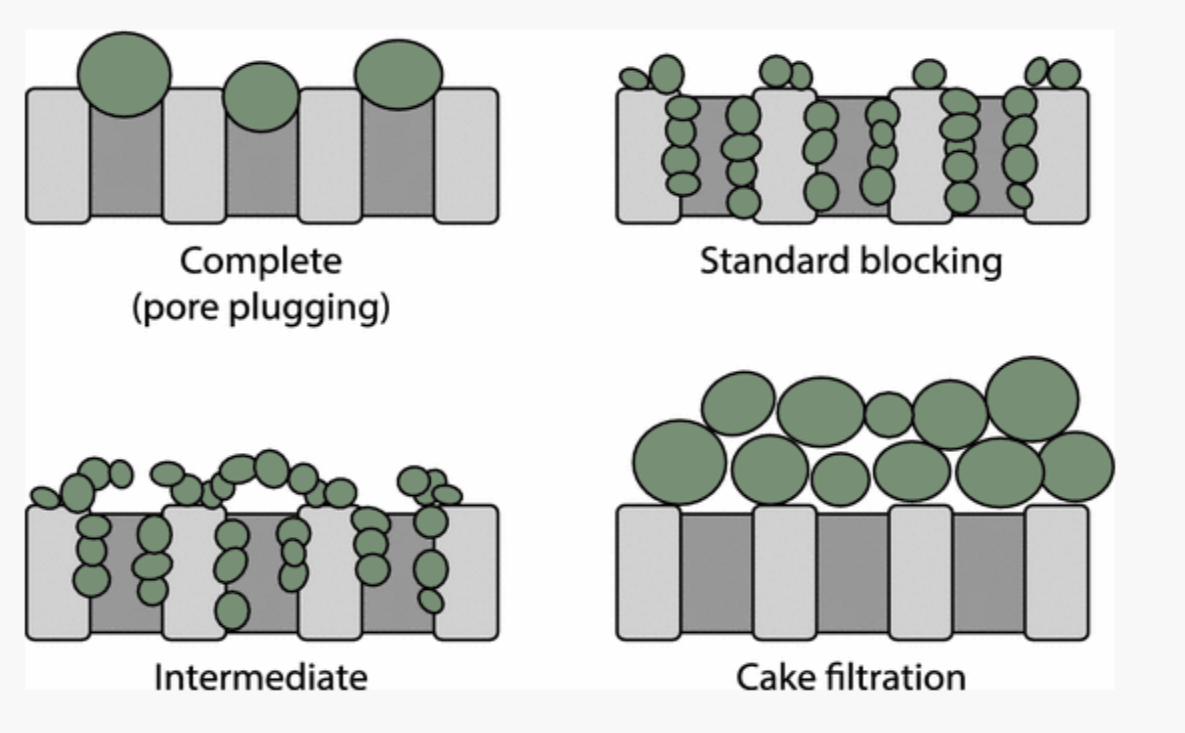

Figure 2.8. Illustrations of several membrane fouling mechanisms **[47]**

In complete pore blocking, large particles block the pores of the membrane, thereby preventing water from passing through. This is basically caused by occlusion of pores with particles. In this, superimposition is not possible. For standard blocking, particles whose sizes are smaller than the pore-size enter the pore and deposit on the internal pore surfaces with their whole length causing the narrowing of the pore size and consequent reduction in flux. Intermediate blocking is quite like complete blocking but in this case, the particles have the capability to deposit on the top of other deposited particles. Superimposition is possible in this case. In cake filtration, an impermeable layer of particles is formed on the entire surface because of the deposition and accumulation of particles whose diameters are larger than that of the membrane pore size. It is believed that cake filtration is generally reversible by water flushing or backwashing **[47].** There have been many contradictory reports regarding the main factors that cause fouling. While some claim that the solutes are the main factors, others claim that it's the suspended solids or colloidal material **[24]**. Whatever the cause may be, there is an urgent need for fouling control. Three operating conditions have been pointed out as the driving factors that mitigate fouling: TMP, feed water characteristics and membrane characteristics **[54]**.

2.4 Piezoelectric crystals

The Curie brothers in 1880 **[55]** observed the phenomenon of piezoelectricity (Fig. 2.9). The term piezoelectricity is derived from two Greek words: *'Piezo'* meaning to squeeze or press and '*Electron'* which refers to amber, a source of electricity. Piezoelectricity (also referred to as direct piezoelectric effect) is a reversible physical process that occurs in some materials whereby an electric dipole moment is generated when stress is applied to the material. The indirect piezoelectric effect (electrostriction) refers to the generation of strain with the application of electricity to the material **[56].** This molecular phenomenon that is observed at the macroscopic level **[57],** originates from the non-centrosymmetric nature of the materials i.e. crystals not having a center of symmetry in their structure giving rise to electric dipoles within the material.

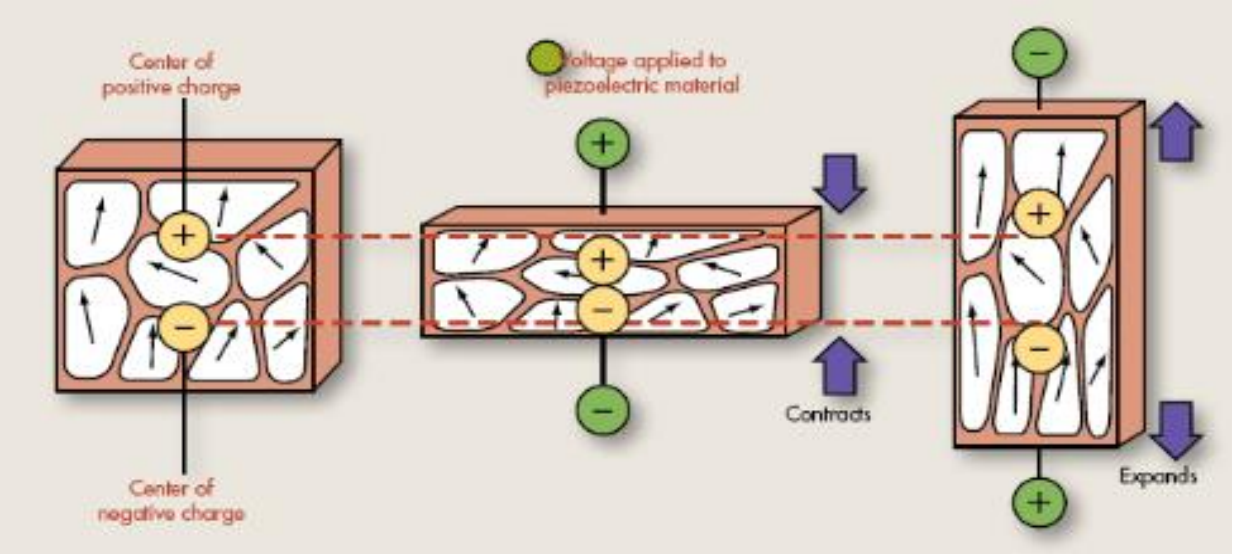

Figure 2.9. The Piezoelectric effect **[58]**

The unit cells in most crystals are symmetrical in nature but that of piezoelectric crystals are asymmetric in nature but they are still electrically neutral due to the cancelling out of a positive charge by the neighboring negative charge. Today, piezoelectric materials are applied in numerous devices like actuators, sensors, motors, high voltage and power applications, energy harvesting devices, medical applications and water filtration. forming the basis for a multi - billion-dollar

worldwide market **[59]**. In water treatment, piezoelectric materials such as lead zirconate titanate (PZT) are integrated in the water treatment system design to reduce fouling **[4]** while in some other cases, membranes like the PVDF membranes are made piezoelectric by the process of poling in which the membrane is subjected to a strong electric field and high temperature where the domain orientation becomes aligned thereby making the membrane piezoelectric **[11]** . Fouling reduction by piezoelectric effect is basically due to the local turbulence generated on the membrane by the piezoelectric crystals **[60]**.

3. MATERIALS AND METHODS

3.1 The Membrane

Ultrafiltration with tubular membrane was adopted for the membrane fouling experiment because of its use in pure-water production **[37]**, its ability to simultaneously concentrate and desalt solutes, does not require phase change and ability to perform either at room temperature or in a cold room **[14]**. PVDF membrane material was the material adopted for the experiment due to its processability which made it a good candidate for preparing tubular membrane **[30]**, the high mechanical strength and thermal stability with excellent aging resistance **[24]**.

Figure 3.1. Tubular PVDF ultrafiltration membrane

This polyvinylidene fluoride (PVDF) ultrafiltration membrane (FP100) (Fig. 3.1) with a nominal retention character of 100,000MW as used in this present study was supplied by Membrane Specialists LLC, Hamilton, USA. The effective membrane length is 32cm. Table 3.1 presents the characteristics of the membrane (FP100) used for the fouling experiments.

Table 3.1. The characteristics of the membrane

Membrane characteristics	Properties
Membrane name	FP100
Membrane material	PVDF
Pore size (nm)	8
Molecular weight cutoff	100kD
PH range	1.5-12
Operating pressure (bar)	10
Temperature (°C)	80
Generic specification	UF
Hydrophilicity	1
Membrane shape	Tubular
Inner diameter	12.10
Effective diameter length (mm)	320
Effective membrane area (mm^2)	12.10

3.1.1 SEM Characterization

The neutral (clean) membrane as well as the fouled membrane were respectively analyzed before and after the fouling experiment using the Phenom XL G2 desktop Scanning Electron Microscope (SEM) (Fig.3.2). This provided the respective complex structures and highly magnified images of both the neutral and the fouled membranes' surface topography which were later used for better comparison.

Figure 3.2. SEM for membrane characterization

With this microscope, the image of the inner surface of the membrane (Fig.3.3) was taken. The white dots as observed on the membrane are production defects and not the pores of the membrane. The membrane pores are so small that they could not be captured by the SEM microscope. This makes it impossible for extremely small particles and dissolved molecules to pass through it. It retains materials larger than the rated pore size (8nm) and allows only water to pass through it.

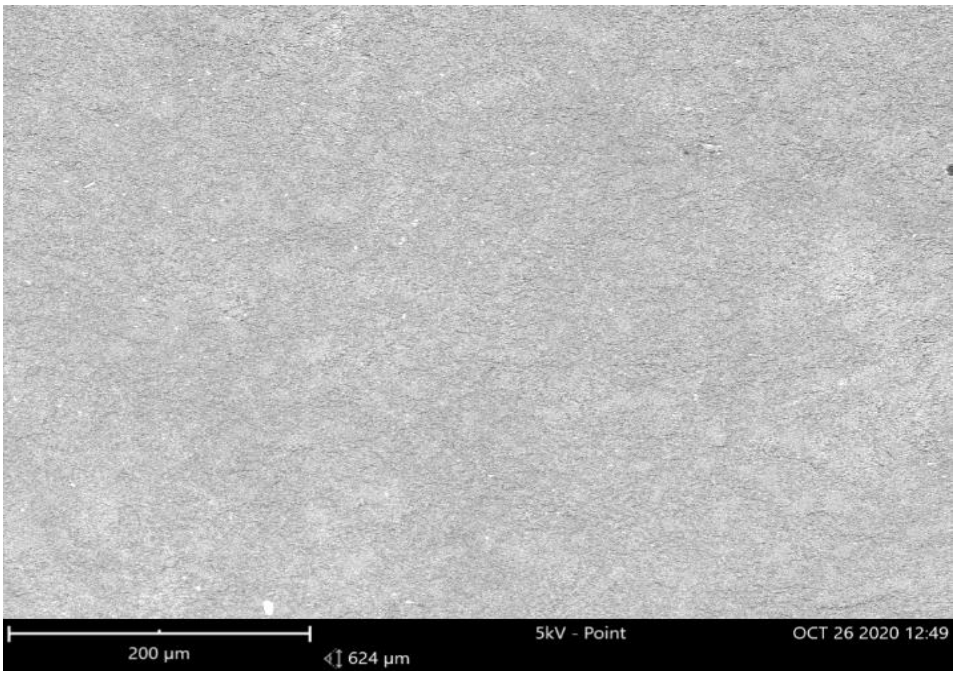

Figure 3.3. SEM image of the inner surface of the neutral membrane.

The Energy-Dispersive Spectroscopy (EDS) analysis (Fig. 3.4) which revealed the elemental constituents of the neutral membrane was also carried out using the microscope.

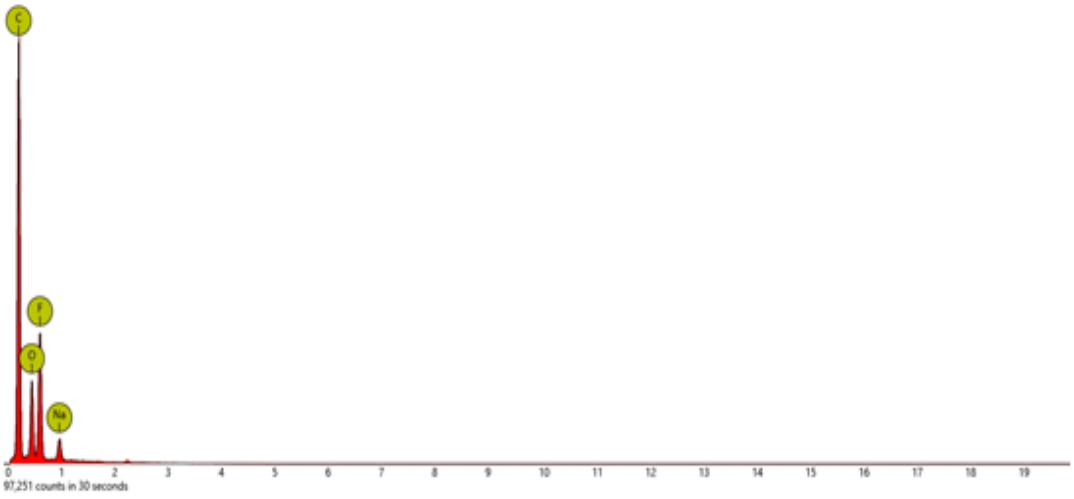

Figure 3.4. EDS analysis of the neutral membrane

With this the elemental constituents of the neural membrane at any point on the membrane were observed to be carbon, oxygen, fluorine and sodium. Table 3.2 presents the proportion by mass of these elements in the neutral membrane, this in turn was used as a reference to compare the EDS analysis of the fouled membrane. With this the elements that cause the fouling of membrane were identified.

Table 3.2. The constituents of the neutral membrane observed during the EDS analysis.

Element Number	Element Symbol	Element Name	Atomic Conc.	Weight Conc.
6	C	Carbon	71.05	62.05
9	F	Fluorine	14.34	19.81
8	O	Oxygen	12.36	14.38
11	Na	Sodium	2.25	3.76

3.2. The Membrane Module

The membrane module fabricated to suit the inside-out flow pattern of the filtration setup consists of 11" clear PVC tube whose both ends were fit into Fernco PI056-215 flexible couple 1-1/2 x 2inch and covered by schedule 40 PVC bushing 1-1/2 x 1/2inch (Fig. 3.5.).

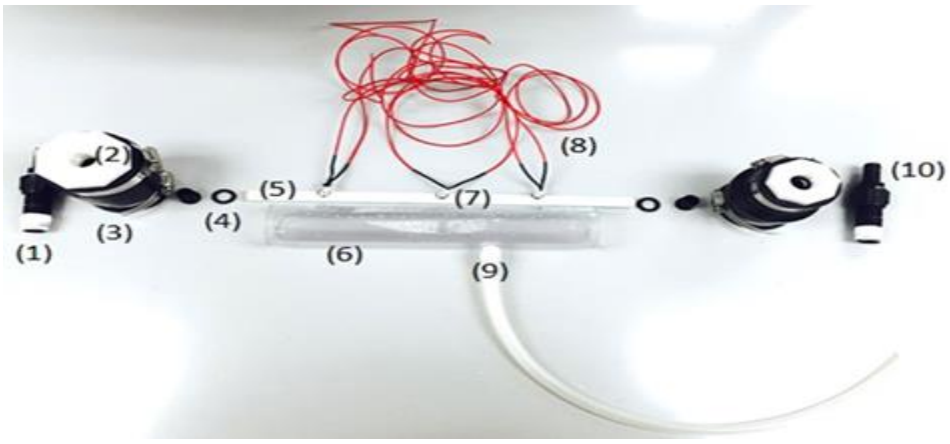

Figure 3.5. The membrane module assembly
Notations: 1- Rain bird swing coupling, 2- Schedule 40 PVC bushing, 3- Flexible coupling 1-½ X2, 4- Rubber gasket, 5- UF membrane, 6- Clear PVC tube, 7- Piezoelectric crystals, 8- Insulated PVC coated 30 AWG wire, 9- Exit hose for filtered water, 10- Cut-off riser.

To ensure that the UF membrane is tightly held in place while avoiding leaks, the 1/2”x 3/4"x 6” cut off riser was attached to the Rain bird swing pipe coupling on both sides. These serve as both the inlet and outlet points for the feed water used for the filtration experiment. The assembled parts of the membrane module are presented in (fig 3.6). The parts for the membrane module were supplied by ACE hardware Indiana USA.

Figure 3.6. Assembled parts of the membrane module

3.3. The Piezoelectric Crystals

The crystals (flat coin vibration motor) (Fig. 3.7) used for the experiment were supplied by Sparkfun Electronics, Incorporated, 6333 Dry Creek Parkway, Niwot, USA. These were used to vibrate the membrane in order to destabilize the particles from settling on the membrane and subsequent blockage of the pores. These vibration motors are a popular choice in many applications due to their small size and the enclosed vibration mechanism. The two cables are connected to the positive and negative sources of voltage which energizes them and make them vibrate on the membrane surface where they are attached.

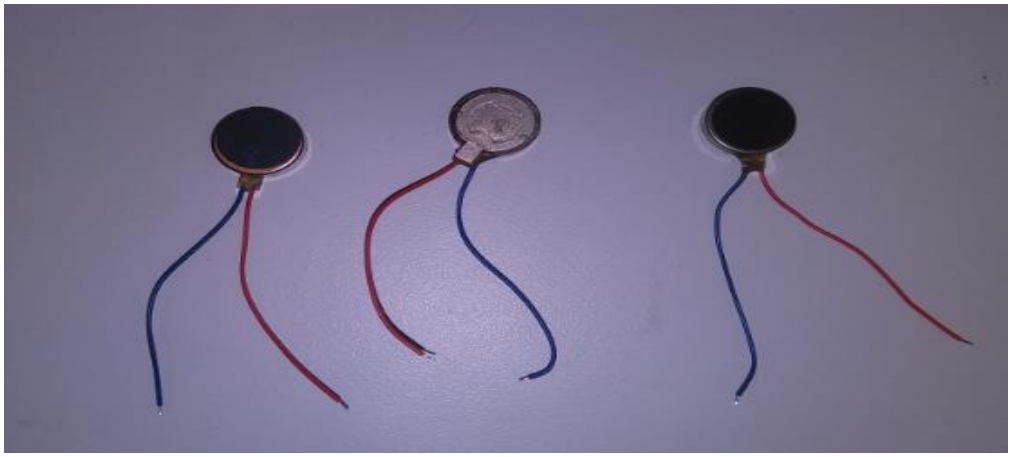

Figure 3.7. The crystals (10mm x 3mm mini vibration motor)

3.3.1 The Reliability Test

Because the crystals would be in contact with liquid (in this case water) for a long time there arose the need to test its suitability for the environment. This was achieved by connecting the crystals to voltage source while immersed in 500g of water (Fig. 3.8). The crystals could vibrate in the water for 6 hours with a close monitor. The crystals maintained their vibration for 6 hours and were brought out and observed carefully. They were not in any way affected by the medium in which they were immersed. It was concluded that the crystals would be able to operate effectively in water and would be able to perform as expected for the fouling experiment since each of the experiments lasted for 4.5-5 hours.

Figure 3.8. Reliability test of the crystals in water

This reliability test conducted for the crystals was important as it helped to ascertain not only the survival of the crystal in the medium but also the maximum length of time it would be able to operate effectively in water without breaking down.

3.4 The Feed Water

The feed water is basically made from surface soil of different concentrations, which place them into the low, medium and high category. These concentrations are mixed with the right proportion of D.I water and tested for the different characteristics before the fouling experiment is conducted.

3.4.1 Preparation of the Feed Water

The feed water which is categorized into low, medium and high concentration (Fig. 3.9 a-c) were prepared by mixing 2grams, 3grams and 4grams (of garden soil) respectively with 500grams of Deionized (DI) water. A uniform mixture of the DI water and the garden soil is obtained by stirring the mixture with the magnetic stirrer for 5 minutes (Fig. 3.10). The magnetic stirrer employs a rotating magnetic field to cause a stir bar immersed in the feedwater to spin very quickly thereby stirring the mixture and making it uniform. After stirring the mixture, it is left alone for 20 seconds. This is to allow for sedimentation which makes the heavier and larger sand particles to settle at the bottom leaving the muddy water on top. This muddy top portion of the feed water is carefully collected for the fouling experiment while the sedimented bottom part of the feed water is discarded.

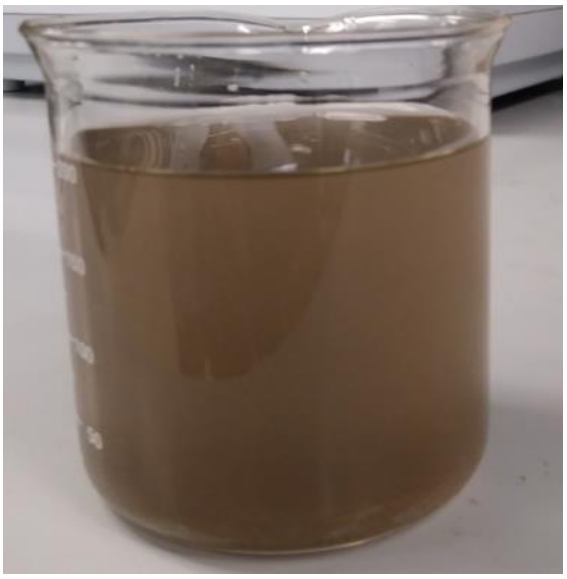

(a)

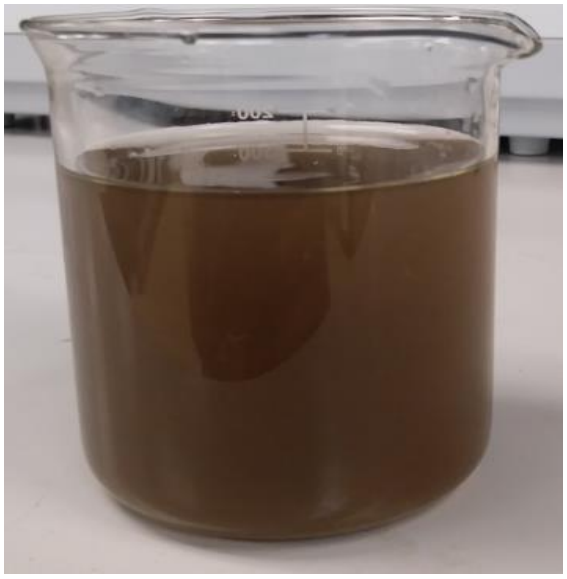

(b)

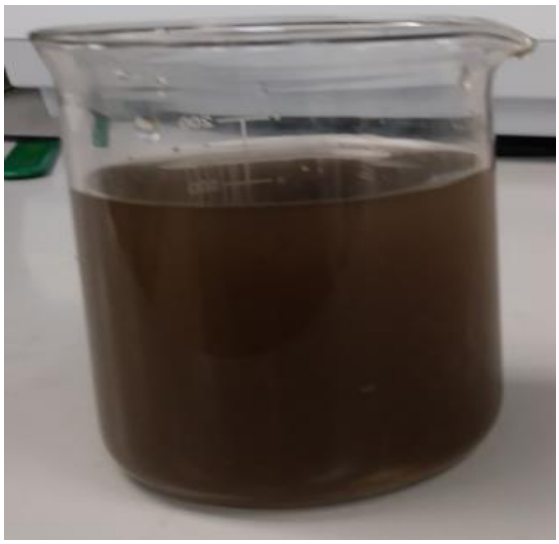

(c)

Figure 3.9 (a) Low concentration feed water (b) Medium concentration feed water (c) High concentration feed water

Figure 3.10. Uniform mixing of the feed water using the magnetic stirrer

After collecting the top portion of the feed water, it is tested for the different characteristics as follows:

3.4.1.1 Turbidity Level

This is a measure of the cloudiness or haziness of a fluid which is caused by many particles that are generally visible to the naked eye. The measurement of the turbidity level of a water sample involves the use of light beams (also known as incident light) with defined characteristics to determine the semi-quantitative presence of particulate matter in the water sample.

Figure 3.11. The HACH 2100N Turbidimeter

The material present in the water sample scatters the incident beam which is detected and quantified relative to a traceable calibration standard. The HACH 2100N turbidimeter (Fig. 3.11) was used to measure the relative clarity of the feed water by measuring the amount of light scattered by particles suspended in the feed water sample.

3.4.1.2 TDS, Conductivity, Salinity

The total dissolved solids (TDS) is a measure of all organic and inorganic substances (minerals) that are contained in the feed water and in the filtered permeate after filtration. The conductivity is a measure of the feedwater and permeates' ability to carry an electrical current while the Salinity of the feedwater and that of the permeate is a measure of the saltiness or the amount of salt that dissolves in them. These properties were respectively measured using the APERA instruments EC60 (Fig. 3.12).

Figure 3.12. APERA instruments EC60

3.4.1.3 The PH

PH is the measure of hydrogen ion concentration. The PH of the feedwater as well as the permeate were measured using OAKTON PH/mV/ºC meter (PH 510 series) (Fig. 3.13).

Figure 3.13. OAKTON PH meter

3.4.1.4 The Dissolved Oxygen Level

This is the level of dissolved oxygen in both the feed water and permeate. For the experiment, this property was determined using the dissolved oxygen kits (fig. 3.14) supplied by CHEMetrics, Inc. 4295 Catlett road, Midland, VA 22728 USA.

Figure 3.14. The dissolved oxygen kits

With the help of these precision instruments, the characteristics of both the feedwater, the DI water and the permeate were taken and recorded as presented in Table 3.3.

Table 3.3. Characteristics of the water samples used for the fouling experiments

Property	Feed Water			DI Water
	Low	Medium	High	
Turbidity ±5%	157	252	382	0.057
pH ±0.1	6.08	6.02	5.87	5.89
Conductivity ±3% (µS)	22.2	21.5	27.7	0.9
Dissolved oxygen ±0.2ppm (mg/L)	5.0	5.0	5.0	8.0
Salinity ±0.02ppt	0.01	0.01	0.01	0.0

3.5. Membrane Cleaning

The membrane was cleaned before every experiment as recommended by Membrane Specialists (the suppliers). The cleaning kit (Fig. 3.15) is basically made of NaOH and DI water. The cleaning involves flushing the membrane with NaOH solution. The NaOH solution was made by mixing 2grams of NaOH to 1000ml of DI water. This is circulated through the system for 5 minutes while the pressure control valves are fully open. The opening of the pressure control valve is to allow the NaOH solution to flow freely through the membrane without penetrating through the membrane and being collected as permeate. The Full opening of the pressure valves allows for free circulation of the NaOH solution (throughout the system) from the feed section to the retentate section without anyone being collected as permeate. During this, the PH of the circulated water rises to 10-12.

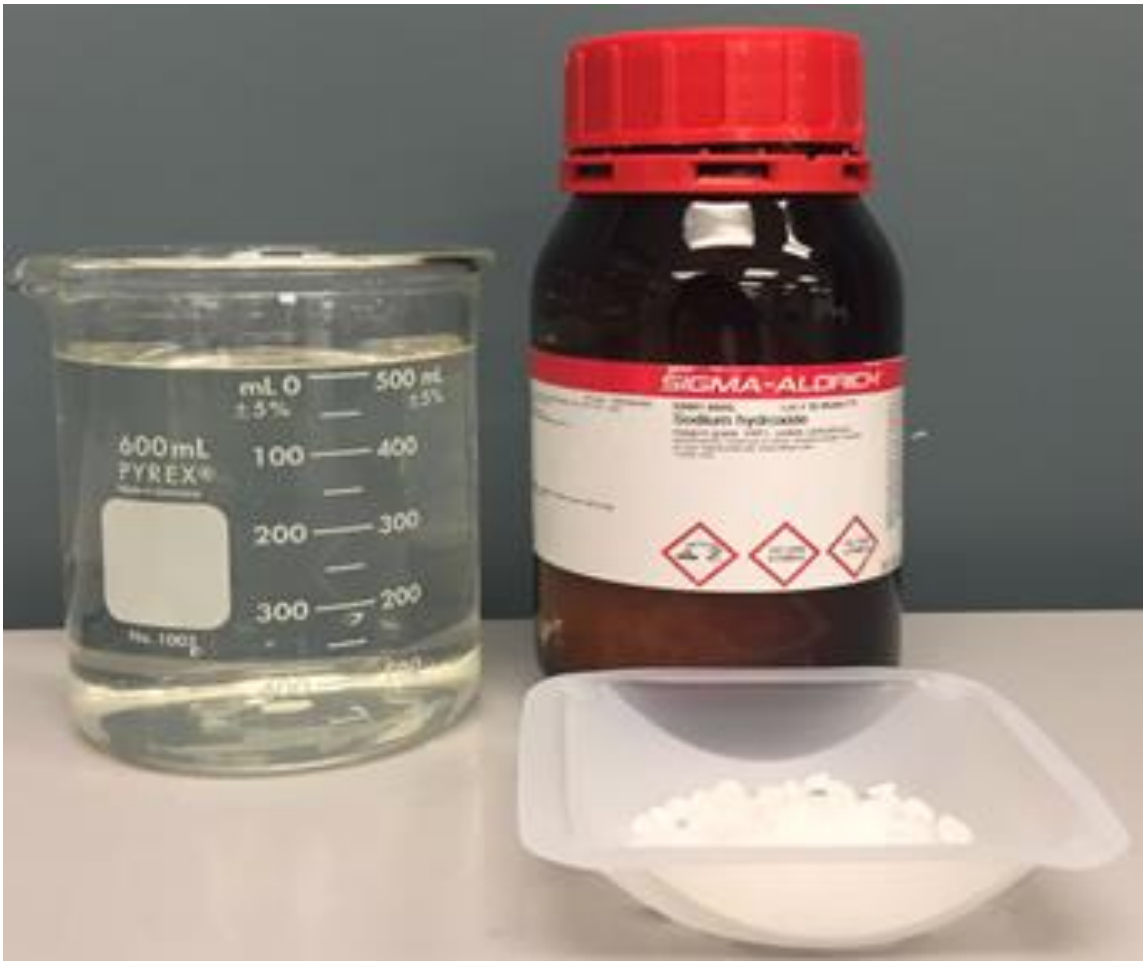

Figure 3.15. Membrane cleaning kit

After this, the system is equilibrated i.e. to bring it back to a pH of 7. This is achieved by rinsing the system with DI until the pH returns to 7. At this point, the membrane is ready for the filtration experiment to commence. In theory, the lack of ions means that the deionized water should have a pH of 7, however when DI water comes in contact with atmospheric carbon dioxide, it absorbs the carbon dioxide and produces carbonic acid which reduces the pH of the deionized water to as little as 5.5 depending on the amount of carbon dioxide it was able to absorb. This explains the low pH value of 5.89 for D.I water as recorded in Table 3.3. Therefore, during the equilibration of the system, the target pH value of the DI water was usually 5.89. The cleaning is also done after each experiment thereby making the system clean for better performance.

3.6. Experimental Procedure for the Membrane Fouling Experiment

To determine the fouling reduction capability of the piezoelectrics on the membrane, the flux performance was studied in a specially designed inside-out crossflow filtration setup (Fig. 3.16). All the filtration experiments were performed at a transmembrane pressure of 5 psi, a temperature of 22^{o}C ± 2 and the pressure control valves were set to inlet pressure of 15psi and outlet pressure of 10psi. During the experiment, the feed water was passed through the membrane module (Fig. 3.17) where it was filtered. The filtered water (the permeate) was collected in the permeate tank where the mass was measured at a specific time interval of 60s, while the unfiltered water (the retentate) was circulated back to the feed tank where it was recirculated round the system throughout the filtration period.

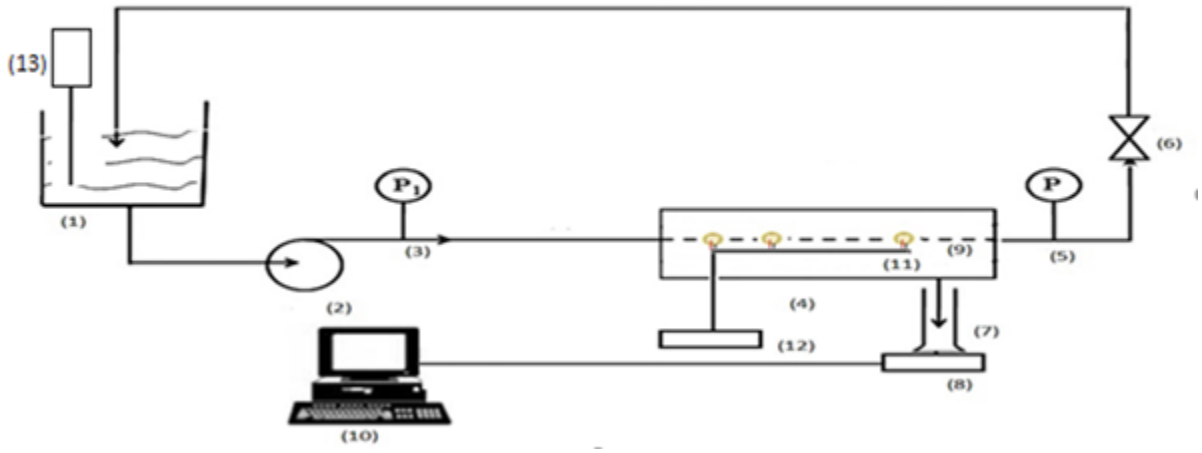

Figure 3.16. Schematic of inside-out crossflow filtration setup for the fouling experiment **[49]**
Notations : 1- feed tank, 2- peristaltic pump, 3- inlet pressure gauge, 4- UF membrane cartridge, 5- outlet pressure gauge, 6 – flow control valve, 7- filtered water tank, 8- weighing scale, 9- UF membrane, 10- desktop computer for data acquisition, 11- piezoelectric (flat coin vibration motor) attached to the UF membrane, 12- power supply, 13- magnetic stirrer.

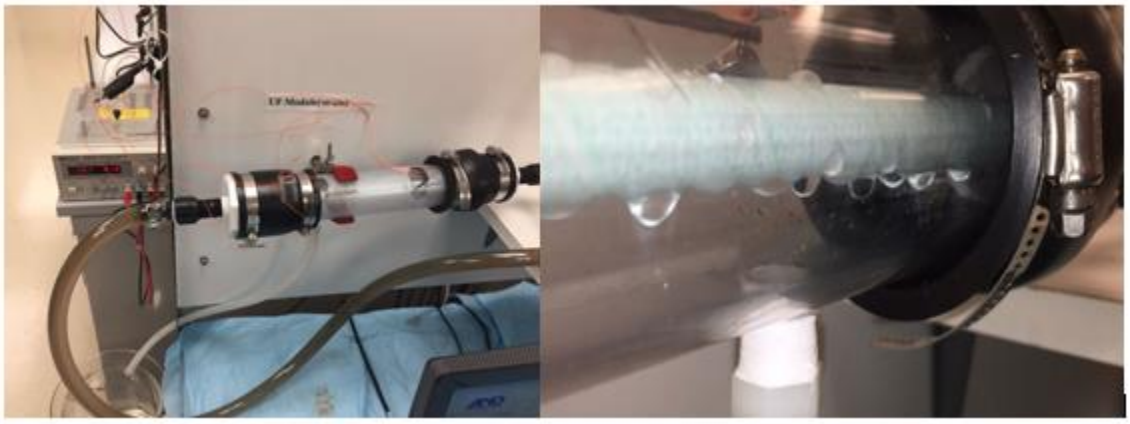

Figure 3.17. The membrane module during the filtration process

The change in the cumulative mass of the permeate as a function of time was recorded as the flow rate (Q_p) in (g/s), the average flow rate $(\bar{Q}_p)$ obtained over a certain period was recorded while the flux (J) in ($Lm^{-2}h^{-1}$) was calculated as follows:

$$Q_p = \frac{\Delta m}{\Delta t}\ (g/s) \qquad (1)$$

$$\bar{Q}_p = \frac{1}{N}\sum_{P=1}^{N} Q_p\ \ (g/s) \qquad (2)$$

$Where\ N = \ Total\ number\ of\ \ flow\ rates\ recorded\ during\ the\ experiment.$

$$J\ = \frac{Q_p}{\rho_{wA}}\ (Lm^{-2}h^{-1}) \qquad (3)$$

Δm is the mass of the permeate collected during a period Δt, $\rho_w$is the density of water and A is the membrane effective area. The normalized flux (J_n) calculated as the ratio of the flux at any instance (J_{inst}) to the maximum flux (J_{max}) was obtained during the experiment as follows:

$$J_n = \frac{J_{inst}}{J_{max}} \qquad (4)$$

The filtration performance was studied using mud solution made by mixing garden soil of different masses (whose grain size is less than 1mm) to 500g of DI water. The different characteristics of

the suspension were recorded as presented in Table 3.3; the piezoelectric actuators strategically placed on the membrane were driven at different voltages for different concentrations of the mud suspension. For comparison, experiments without any vibration order wise known as the base case were also performed. To ensure the accuracy of the result obtained, the used membrane was replaced and analyzed after each experiment.

3.7. Statistical Design of the Experiment (DOE)

Statistical design of experiment is a structured, organized method for determining the relationships between factors affecting a process and the output of that process **[61]**. This concept dates to the twentieth century (1920 to be precise) **[62].** It came into existence through the contribution of the famous statistician Sir Ronald Fisher to statistics. Having been characterized as "a genius who almost single-handedly created the foundations for modern statistical science, he published books **[63]**,**[64]**,**[65]** which are the pillars of statistical thinking in science and industrial applications. He further highlighted the need to consider statistical analysis during the planning stages of research rather than at the final phases of experimentation **[61]**.

It has been identified as a powerful approach to optimizing processes in industries **[66]**. The pharmaceutical industry **[67]** has seen a great increase **[68]** in the application of DOE in the development of its pharmaceutical process between 2003 - 2013 as can be seen from the increased volume of DOE-related publications in Organic Process Research and Development (OPRD). The traditional optimization approach of varying- one- factor or variable- at- a- time known as OFAT or OVAT suffers many drawbacks like; not being able to provide quantitative information needed to rank the importance of process variable **[69]**, not being able to uncover the optimal conditions since the outcomes are highly dependent on the starting point, not being able to separate the "noise" (which is the inherent run-to-run variation of a system) of a reaction from the actual improvement unless a significant number of reactions are repeated using the same conditions **[66]** etc.

The DOE approach is preferred over the traditional optimization approach due to its ability to eliminate researcher bias often leading to reaction conditions that have not been previously considered. The most important advantage being its ability to quickly detect how interactions between factors can affect product yield and quality **[66]**. The simultaneous variation of parameters employed by DOE makes it more efficient than the traditional approach of varying one

factor/variable at a time. Although running the DOE approach seems daunting and time consuming at the beginning, due to the numerous experiments to be carried out (usually defined at the beginning unlike the traditional approach), the quality and thoroughness of the information obtained outweigh the effort. DOE employs factorial experiments which consist of a systematic variation of two or more variables at once **[69]**. For three level experiment, each variable is set to either a high, medium or low value according to standard pattern. Experimental runs are conducted for each possible combination of variable settings. To adopt a full DOE approach, the following steps (Fig. 3.18) were taken during this research;

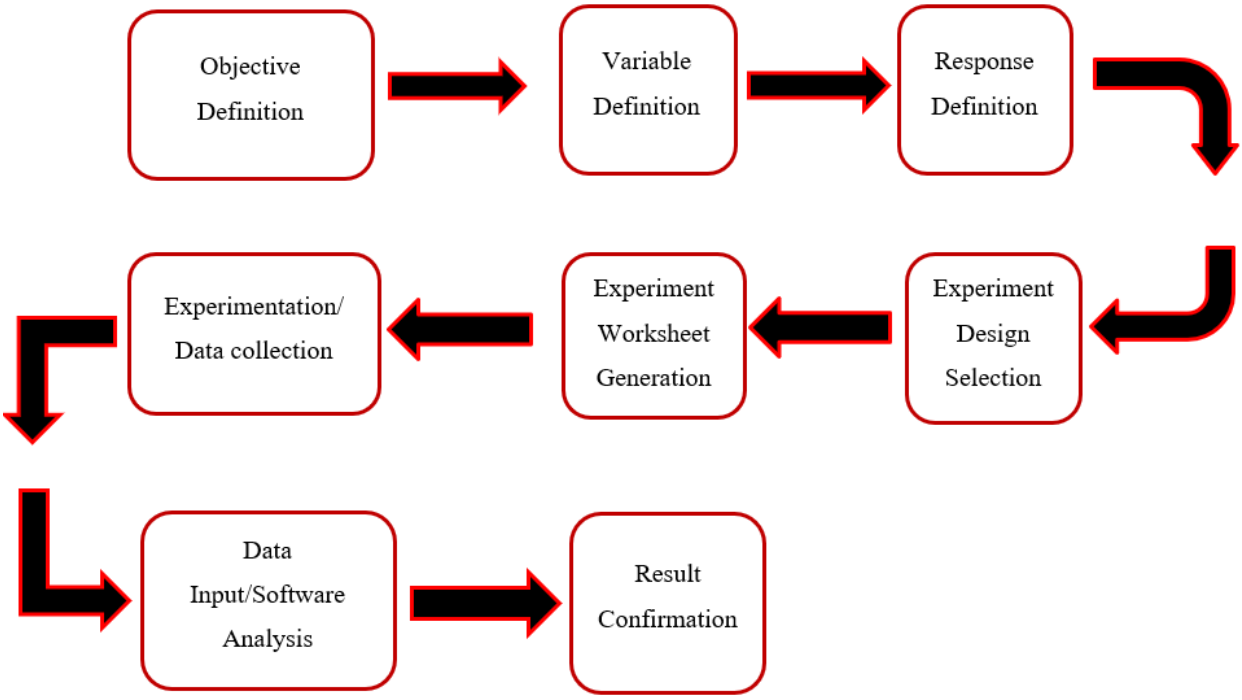

Figure 3.18. Flow diagram for steps adopted for a full DOE

1. Define the objective: Here, the process issues to be resolved are identified. The objective in most cases (this research inclusive), is to optimize the process (production of permeate flux). However, some process conditions are "locked" which shifts the goal to merely understanding the robustness around existing conditions. For this case, the robustness is simply examining the impact of small changes (if any) in the continuous factors (those variables to which numerical values can be assigned) on the outcome.
2. Define the factors/variables and their ranges: The determination of variables/factors to include depends solely on the available resources. When many variables are involved, more

experiments are conducted which leads to more time and materials spent during the optimization. It is therefore imperative that the variables are prioritized (using available process knowledge) into groups and assigned high, medium and low settings for the selected variables as in the case of three-level factorial design.

Three important variables namely; soil concentration (A), voltage (B) and location of Piezoelectric crystals (C) (Fig. 3.19 a-c) were identified as the most important variables to be considered for the research as presented in Table 3.4. The number of crystals was kept constant at 3.

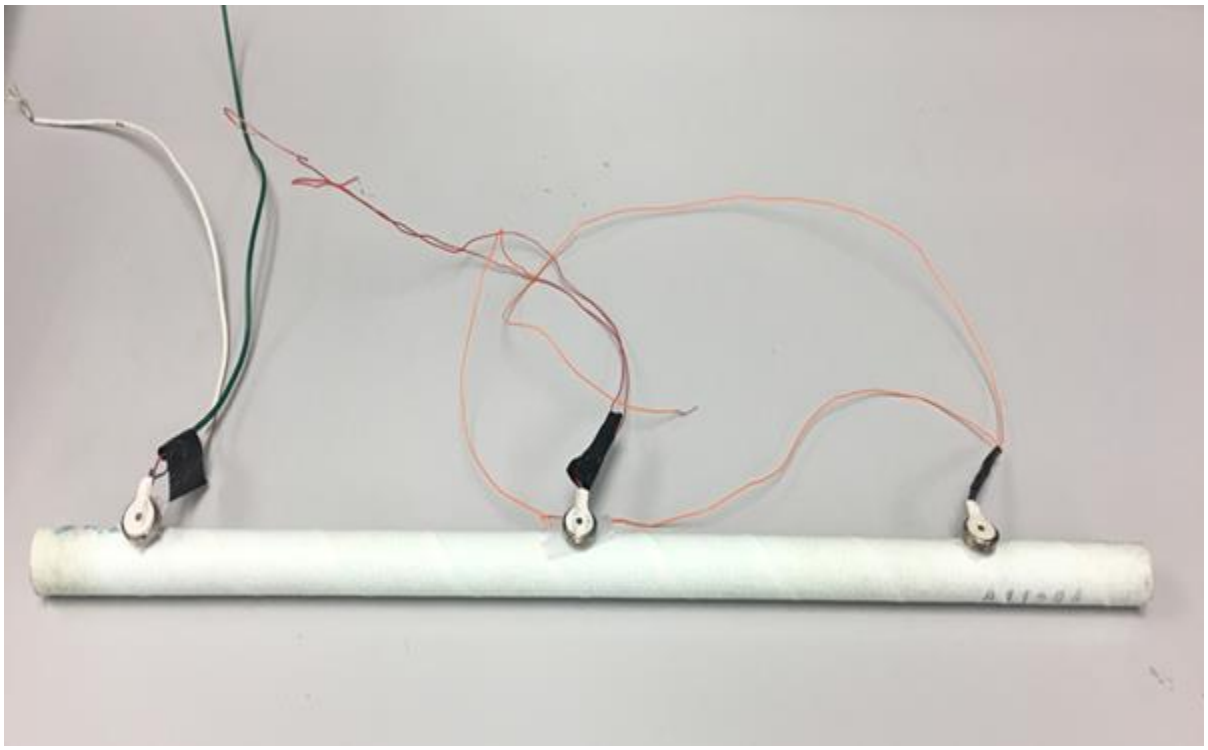

(a)

Figure 3.19 (a) The Top-Top-Top (TTT) crystal location configuration (b) The Top-Bottom-Top (TBT) crystal location configuration (c) The Top-Side-Down crystal location configuration

Figure 3.19. cont’d

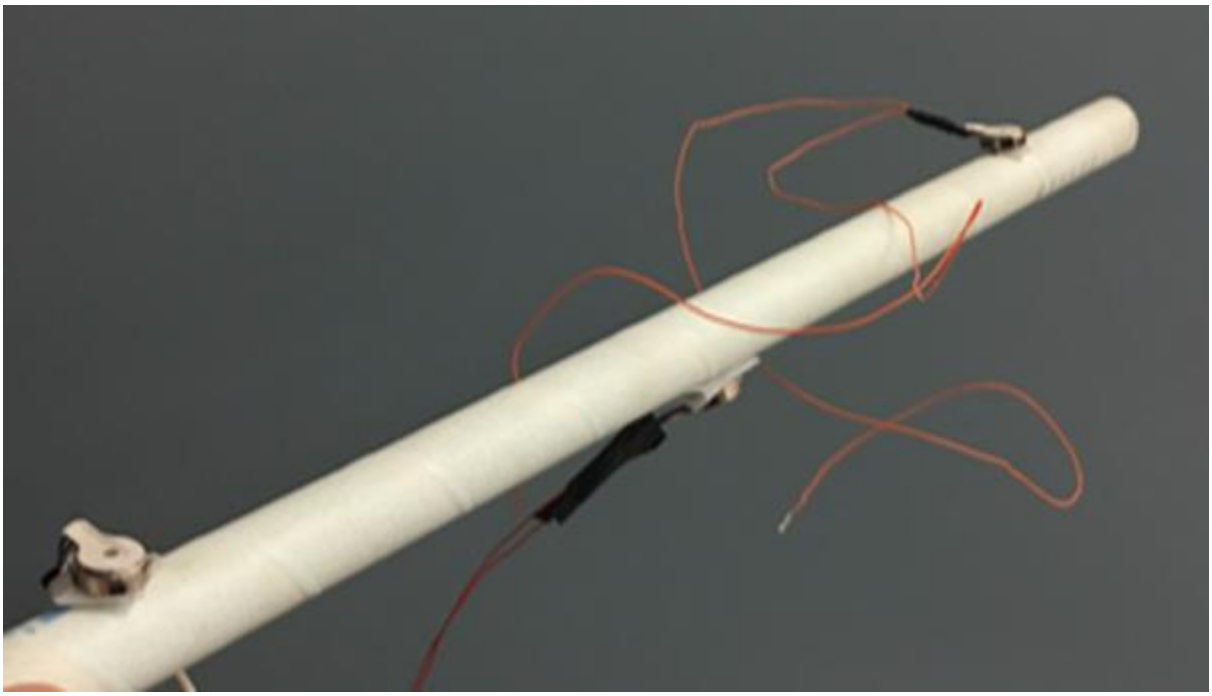

(b)

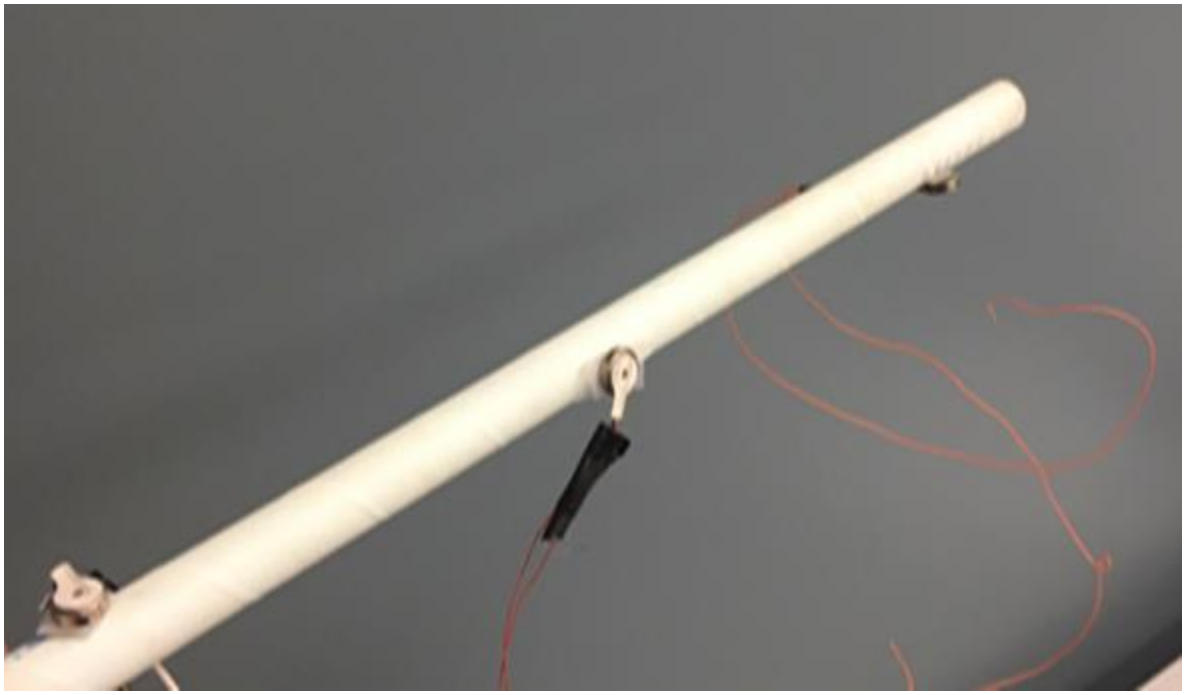

(c)

Table 3.4. The variables and their levels

Variables	Low (Level 0)	Medium (Level 1)	High (Level 2)
Soil concentration (A)	2 grams of soil to 500 grams of water	3 grams of soil to 500 grams of water	4 grams of soil to 500 grams of water
Voltage (B)	2V	3V	4V
Location of crystals (C)	Equal spacing: All on top (TTT)	Equal spacing: One on top, one on the side and one on the bottom (TSD)	Equal spacing: Two on top, the middle one on the bottom (TBT)
Number of crystals	3	3	3

3. Response definition: In illustrating the application of the three-level factorial design of the membrane fouling experiment, the experimental responses which are the measurable outcomes of the process are respectively the flowrate and the permeate flux. The decline in these parameters were measured over a time period (t) is due to the continual clogging up of the membrane by foulants during water filtration while being vibrated with crystals. Experimentally determined values of the permeate flux and the flowrate are calculated using equations 1 - 3.

4. Selection of the experimental design: Three variables were selected for investigation; namely, voltage, soil concentration and crystal location. Three-level factorial design was developed which led to the categorization of the variables into low, medium and high levels/settings as presented in table 3.4. Low category (Level 0): Voltage is 2V and soil concentration is 2 grams of soil to 500 grams of water and crystal location is top-top-top (TTT). Medium category (Level 1): Voltage is 3V and soil concentration is 3 grams of soil to 500 grams of water and crystal location is top-side-down (TSD). High category (Level 2): Voltage is 4V and soil concentration is 4 grams of soil to 500 grams of water and crystal location is top-bottom-top (TBT). The designation for this design is 3^3, signifying three factors studied at three levels. This gives rise to a total of twenty-seven experimental runs (Table 3.5) needed for the DOE approach. These experiments were conducted in two runs which are namely; run 1 and run 2, making it a total of fifty-four experiments conducted and fully analyzed in this research.

5. Generation of experiment worksheet: All the above information was used to generate the list of experiments to be performed (Table 3.5). These experiments were conducted in two runs namely; run 1 and run 2 with each run comprising a total of twenty-seven experiments. In general, fifty-four experiments were conducted during this research.

Table 3.5. The twenty-seven experimental runs conducted

Test	A	B	C
1	Ratio of 2g of soil per 500g of water	2V	Equally spaced: all crystals on top (TTT)
2	Ratio of 2g of soil per 500g of water	2V	Equally spaced: crystal on top, crystal on side, crystal at the bottom (TSD)
3	Ratio of 2g of soil per 500g of water	2V	Equally spaced: middle crystal on bottom while the other two are on top (TBT)
4	Ratio of 2g of soil per 500g of water	3V	Equally spaced: all crystals on top (TTT)
5	Ratio of 2g of soil per 500g of water	3V	Equally spaced: crystal on top, crystal on side, crystal at the bottom (TSD)
6	Ratio of 2g of soil per 500g of water	3V	Equally spaced: middle crystal on bottom while the other two are on top (TBT)
7	Ratio of 2g of soil per 500g of water	4V	Equally spaced: all crystals on top (TTT)
8	Ratio of 2g of soil per 500g of water	4V	Equally spaced: crystal on top, crystal on side, crystal at the bottom (TSD)
9	Ratio of 2g of soil per 500g of water	4V	Equally spaced: middle crystal on bottom while the other two are on top (TBT)
10	Ratio of 3g of soil per 500g of water	2V	Equally spaced: all crystals on top (TTT)
11	Ratio of 3g of soil per 500g of water	2V	Equally spaced: crystal on top, crystal on side, crystal at the bottom (TSD)
12	Ratio of 3g of soil per 500g of water	2V	Equally spaced: middle crystal on bottom while the other two are on top (TBT)
13	Ratio of 3g of soil per 500g of water	3V	Equally spaced: all crystals on top (TTT)
14	Ratio of 3g of soil per 500g of water	3V	Equally spaced: crystal on top, crystal on side, crystal at the bottom (TSD)

Table 3.5. cont'd

15	Ratio of 3g of soil per 500g of water	3V	Equally spaced: middle crystal on bottom while the other two are on top (TBT)
16	Ratio of 3g of soil per 500g of water	4V	Equally spaced: all crystals on top (TTT)
17	Ratio of 3g of soil per 500g of water	4V	Equally spaced: crystal on top, crystal on side, crystal at the bottom (TSD)
18	Ratio of 3g of soil per 500g of water	4V	Equally spaced: middle crystal on bottom while the other two are on top (TBT)
19	Ratio of 4g of soil per 500g of water	2V	Equally spaced: all crystals on top (TTT)
20	Ratio of 4g of soil per 500g of water	2V	Equally spaced: crystal on top, crystal on side, crystal at the bottom (TSD)
21	Ratio of 4g of soil per 500g of water	2V	Equally spaced: middle crystal on bottom while the other two are on top (TBT)
22	Ratio of 4g of soil per 500g of water	3V	Equally spaced: all crystals on top (TTT)
23	Ratio of 4g of soil per 500g of water	3V	Equally spaced, crystal on top, crystal on side, crystal at the bottom (TSD)
24	Ratio of 4g of soil per 500g of water	3V	Equally spaced, middle crystal on bottom while the other two are on top (TBT)
25	Ratio of 4g of soil per 500g of water	4V	Equally spaced all crystals on top (TTT)
26	Ratio of 4g of soil per 500g of water	4V	Equally spaced, crystal on top, crystal on side, crystal at the bottom (TSD)
27	Ratio of 4g of soil per 500g of water	4V	Equally spaced, middle crystal on bottom while the other two are on top (TBT)

6. Experimentation / data collection: The conducted experiments as described in section 3.7, was performed under the same conditions for run 1 and run 2 respectively. However, the pump used in run 1 was different from that used in run 2. This was because, after conducting the twenty-seven experiments of run 1, the pump broke down, which led to the purchase of another pump of similar specification as that of run 1. This new pump was used to conduct the twenty-seven experiments of run 2. The permeate flux of the membrane fouling experiment was taken every sixty seconds and recorded over a period of four and half hours. The flux reading needed as input data for the software was taken before the steady state of the fouling experiment. Steady state of the experiment is the time when there

is little or no change in the permeate flux or flow rate of the experiment. At this time, the membrane has been completely clogged up by particles and is at its cake formation stage. It was observed that on the average, the steady state of the experiment was arrived at, after two hours of the experiment. So, 25%, 50%, 75% and 100% experimental flux readings were taken and recorded within 2 hours of the experiment which is before the steady state i.e. at 0.5-hour, 1 hour, 1.5 hour and 2-hour intervals respectively as recorded in Tables 3.6 and 3.7 for run 1 and run 2 respectively.

Table 3.6. Run 1 experimental results

Run	Test	Concentration (A)	Voltage (B)	Crystal Location (C)	25% Experimental Flux ($Lm^{-2}h^{-1}$)	50% Experimental Flux ($Lm^{-2}h^{-1}$)	75% Experimental Flux ($Lm^{-2}h^{-1}$)	100% Experimental Flux ($Lm^{-2}h^{-1}$)
1	1	0	0	0	43.50	32.35	33.75	37.00
1	2	0	0	1	42.50	41.25	33.75	33.75
1	3	0	0	2	40.50	40.00	32.00	30.00
1	4	0	1	0	31.25	25.50	23.50	24.50
1	5	0	1	1	27.50	24.00	21.25	19.75
1	6	0	1	2	31.50	33.75	30.75	23.50
1	7	0	2	0	33.75	33.00	15.75	48.75
1	8	0	2	1	27.25	21.50	19.25	19.00
1	9	0	2	2	50.25	42.25	40.75	29.50
1	10	1	0	0	28.00	22.50	21.00	20.00
1	11	1	0	1	34.00	27.75	22.50	18.25
1	12	1	0	2	23.50	25.50	22.75	23.00
1	13	1	1	0	45.75	33.50	29.25	24.25
1	14	1	1	1	38.00	38.00	32.25	29.00
1	15	1	1	2	41.50	32.00	26.25	22.75
1	16	1	2	0	46.25	41.00	32.75	27.25
1	17	1	2	1	22.25	19.00	16.00	15.75
1	18	1	2	2	44.50	39.50	34.25	29.25
1	19	2	0	0	35.00	31.50	29.50	22.75
1	20	2	0	1	31.75	26.75	25.50	23.50
1	21	2	0	2	54.75	44.50	34.00	37.00
1	22	2	1	0	23.75	20.00	17.50	16.85
1	23	2	1	1	23.50	19.50	18.25	18.00
1	24	2	1	2	19.75	17.75	16.00	13.75
1	25	2	2	0	26.75	26.00	26.84	22.00
1	26	2	2	1	50.5	47.25	41.75	34.00
1	27	2	2	2	50.50	40.75	38.50	35.50

Table 3.7. Run 2 experimental results

Run	Test	Concentration (A)	Voltage (B)	Crystal Location (C)	25% Experimental Flux ($Lm^{-2}h^{-1}$)	50% Experimental Flux ($Lm^{-2}h^{-1}$)	75% Experimental Flux ($Lm^{-2}h^{-1}$)	100% Experimental Flux ($Lm^{-2}h^{-1}$)
2	1	0	0	0	40.50	33.75	30.50	29.25
2	2	0	0	1	38.52	27.00	29.50	23.50
2	3	0	0	2	37.50	36.00	25.00	28.00
2	4	0	1	0	37.50	34.50	30.75	31.00
2	5	0	1	1	33.25	31.00	29.00	29.50
2	6	0	1	2	32.00	29.50	27.75	26.00
2	7	0	2	0	36.50	26.75	24.95	24.60
2	8	0	2	1	35.00	27.75	23.50	26.25
2	9	0	2	2	36.25	31.00	28.75	26.00
2	10	1	0	0	20.75	23.75	21.25	21.00
2	11	1	0	1	30.75	31.75	29.75	31.00
2	12	1	0	2	42.25	41.25	39.62	38.50
2	13	1	1	0	36.50	31.25	30.50	28.25
2	14	1	1	1	40.00	34.00	35.00	32.75
2	15	1	1	2	43.25	31.50	28.25	28.25
2	16	1	2	0	33.00	28.75	26.50	23.75
2	17	1	2	1	34.75	34.25	29.50	23.25
2	18	1	2	2	35.25	28.50	26.50	21.50
2	19	2	0	0	28.25	29.25	26.75	26.50
2	20	2	0	1	31.00	30.50	28.75	26.25
2	21	2	0	2	35.00	30.00	26.75	25.25
2	22	2	1	0	31.75	27.25	25.25	25.25
2	23	2	1	1	34.25	25.75	27.50	24.75
2	24	2	1	2	36.25	26.25	22.75	23.50
2	25	2	2	0	29.75	24.75	24.25	23.00
2	26	2	2	1	36.50	28.25	20.75	21.75
2	27	2	2	2	32.25	24.25	23.50	21.00

7. Data Input / Software Analysis: The experimental results (tables 3.6 & 3.7) were input into R-statistical software and the responses were individually analyzed. Mathematical models presented below, were generated for 25% experimental flux, 50% experimental flux, 75% experimental flux and 100% experimental flux (for both run 1 and run 2 respectively) and used for the optimization equations presented as follows:

Best fit equation based on Run 1

Best fit equation (25 % readings)

Coefficients:

(Intercept)	A [T.1]	A [T.2]	B [T.1]	B [T.2]	C [T.1]	C [T.2]
36.4630	-0.3056	-1.1389	-5.5000	2.2222	-1.8611	4.5833

$\hat{y} = 36.4630 - 0.306A_1 - 1.139A_2 - 5.500B_1 + 2.222\,B_2 - 1.861C_1 + 4.583C_2 \ldots\ldots\ldots$ (5)

Where,

$$A_1 = \begin{cases} 1 & if\ \ A = 1(Medium) \\ 0 & Otherwise \end{cases} \qquad A_2 = \begin{cases} 1 & if\ \ A = 2(High) \\ 0 & Otherwise \end{cases}$$

$$B_1 = \begin{cases} 1 & if\ \ B = 1(Medium) \\ 0 & Otherwise \end{cases} \qquad B_2 = \begin{cases} 1 & if\ \ B = 2(High) \\ 0 & Otherwise \end{cases}$$

$$C_1 = \begin{cases} 1 & if\ \ C = 1(Medium) \\ 0 & Otherwise \end{cases} \qquad C_2 = \begin{cases} 1 & if\ \ C = 2(High) \\ 0 & Otherwise \end{cases}$$

Best fit equation (50 % readings)

Coefficients:

(Intercept)	A [T.1]	A [T.2]	B [T.1]	B [T.2]	C [T.1]	C [T.2]
31.94259	-1.70556	-2.23333	-5.40000	1.96111	-0.03889	5.68333

$\hat{y} = 31.9426 - 1.706A_1 - 2.233\,A_2 - 5.400B_1 + 1.961B_2 - 0.039C_1 + 5.683C_2 \ldots\ldots\ldots\ldots$ 6

Where,

$$A_1 = \begin{cases} 1 & if\ \ A = 1(Medium) \\ 0 & Otherwise \end{cases} \qquad A_2 = \begin{cases} 1 & if\ \ A = 2(High) \\ 0 & Otherwise \end{cases}$$

$$B_1 = \begin{cases} 1 & if\ \ B = 1(Medium) \\ 0 & Otherwise \end{cases} \qquad B_2 = \begin{cases} 1 & if\ \ B = 2(High) \\ 0 & Otherwise \end{cases}$$

$$C_1 = \begin{cases} 1 & if\ \ C = 1(Medium) \\ 0 & Otherwise \end{cases} \qquad C_2 = \begin{cases} 1 & if\ \ C = 2(High) \\ 0 & Otherwise \end{cases}$$

Best fit equation (75 % readings)

Coefficients:

(Intercept)	A [T.1]	A [T.2]	B [T.1]	B [T.2]	C [T.1]	C [T.2]
27.21630	-1.52778	-0.32333	-4.41667	1.23222	0.07333	5.04556

$$\hat{y} = 27.2163 - 1.528A_1 - 0.323A_2 - 4.417B_1 + 1.232B_2 + 0.073C_1 + 5.046C_2 \quad \ldots\ldots\ldots\ldots\ldots \quad 7$$

Where,

$$A_1 = \begin{cases} 1 & if\ \ A = 1(Medium) \\ 0 & Otherwise \end{cases} \qquad A_2 = \begin{cases} 1 & if\ \ A = 2(High) \\ 0 & Otherwise \end{cases}$$

$$B_1 = \begin{cases} 1 & if\ \ B = 1(Medium) \\ 0 & Otherwise \end{cases} \qquad B_2 = \begin{cases} 1 & if\ \ B = 2(High) \\ 0 & Otherwise \end{cases}$$

$$C_1 = \begin{cases} 1 & if\ \ C = 1(Medium) \\ 0 & Otherwise \end{cases} \qquad C_2 = \begin{cases} 1 & if\ \ C = 2(High) \\ 0 & Otherwise \end{cases}$$

Best fit equation (100 % readings)

Coefficients:

(Intercept)	A [T.1]	A [T.2]	B [T.1]	B [T.2]	C [T.1]	C [T.2]
32.069	-6.250	-4.711	-5.878	1.750	-3.594	0.100

$$\hat{y} = 32.069 - 6.250\,A_1 - 4.711A_2 - 5.878B_1 + 1.750\,B_2 - 3.594C_1 + 0.100C_2 \quad \ldots\ldots\ldots\ldots\ldots \quad 8$$

Where,

$$A_1 = \begin{cases} 1 & if\ \ A = 1(Medium) \\ 0 & Otherwise \end{cases} \qquad A_2 = \begin{cases} 1 & if\ \ A = 2(High) \\ 0 & Otherwise \end{cases}$$

$$B_1 = \begin{cases} 1 & if\ \ B = 1(Medium) \\ 0 & Otherwise \end{cases} \qquad B_2 = \begin{cases} 1 & if\ \ B = 2(High) \\ 0 & Otherwise \end{cases}$$

$$C_1 = \begin{cases} 1 & if\ \ C = 1(Medium) \\ 0 & Otherwise \end{cases} \qquad C_2 = \begin{cases} 1 & if\ \ C = 2(High) \\ 0 & Otherwise \end{cases}$$

Best fit equation based on Run 2

Best fit equation (25% readings)

Coefficients:

(Intercept)	A [T.1]	A [T.2]	B [T.1]	B [T.2]	C [T.1]	C [T.2]
33.3733	-1.1689	-3.5578	2.2478	0.5256	2.1689	3.9444

$\hat{y} = 33.3733 - 1.169\,A_1 - 3.558A_2 + 2.248B_1 + 0.526\,B_2 + 2.169C_1 + 3.944C_2 \ldots\ldots\ldots\ldots$ 9

Where,

$$A_1 = \begin{cases} 1 & if\ \ A = 1(Medium) \\ 0 & Otherwise \end{cases} \qquad A_2 = \begin{cases} 1 & if\ \ A = 2(High) \\ 0 & Otherwise \end{cases}$$

$$B_1 = \begin{cases} 1 & if\ \ B = 1(Medium) \\ 0 & Otherwise \end{cases} \qquad B_2 = \begin{cases} 1 & if\ \ B = 2(High) \\ 0 & Otherwise \end{cases}$$

$$C_1 = \begin{cases} 1 & if\ \ C = 1(Medium) \\ 0 & Otherwise \end{cases} \qquad C_2 = \begin{cases} 1 & if\ \ C = 2(High) \\ 0 & Otherwise \end{cases}$$

Best fit equation (50% readings)

Coefficients:

(Intercept)	A [T.1]	A [T.2]	B [T.1]	B [T.2]	C [T.1]	C [T.2]
31.2778	0.8611	-3.4444	-1.3611	-3.2222	1.1389	2.0278

$\hat{y} = 31.2778 + 0.861\,A_1 - 3.444A_2 - 1.361B_1 - 3.222\,B_2 + 1.139C_1 + 2.028C_2 \ldots\ldots\ldots\ldots$ 10

Where,

$$A_1 = \begin{cases} 1 & if\ \ A = 1(Medium) \\ 0 & Otherwise \end{cases} \qquad A_2 = \begin{cases} 1 & if\ \ A = 2(High) \\ 0 & Otherwise \end{cases}$$

$$B_1 = \begin{cases} 1 & if\ \ B = 1(Medium) \\ 0 & Otherwise \end{cases} \qquad B_2 = \begin{cases} 1 & if\ \ B = 2(High) \\ 0 & Otherwise \end{cases}$$

$$C_1 = \begin{cases} 1 & if\ \ C = 1(Medium) \\ 0 & Otherwise \end{cases} \qquad C_2 = \begin{cases} 1 & if\ \ C = 2(High) \\ 0 & Otherwise \end{cases}$$

Best fit equation (75% readings)

Coefficients:

(Intercept)	A [T.1]	A [T.2]	B [T.1]	B [T.2]	C [T.1]	C [T.2]
28.1174	1.9078	-2.6056	-0.1244	-3.2967	1.3944	0.9078

$$\hat{y} = 28.1174 + 1.908\,A_1 - 2.606A_2 - 0.124B_1 - 3.297\,B_2 + 1.394C_1 + 0.908C_2 \ldots\ldots\ldots\ldots \quad 11$$

Where,

$$A_1 = \begin{cases} 1 & if\ \ A = 1(Medium) \\ 0 & Otherwise \end{cases} \qquad A_2 = \begin{cases} 1 & if\ \ A = 2(High) \\ 0 & Otherwise \end{cases}$$

$$B_1 = \begin{cases} 1 & if\ \ B = 1(Medium) \\ 0 & Otherwise \end{cases} \qquad B_2 = \begin{cases} 1 & if\ \ B = 2(High) \\ 0 & Otherwise \end{cases}$$

$$C_1 = \begin{cases} 1 & if\ \ C = 1(Medium) \\ 0 & Otherwise \end{cases} \qquad C_2 = \begin{cases} 1 & if\ \ C = 2(High) \\ 0 & Otherwise \end{cases}$$

Best fit equation (100% readings)

Coefficients:

(Intercept)	A [T.1]	A [T.2]	B [T.1]	B [T.2]	C [T.1]	C [T.2]
28.100	0.4611	-2.9830	+0.0001	-4.2390	0.7111	0.6000

$$\hat{y} = 28.100 + 0.461\,A_1 - 2.983A_2 + 0.0001B_1 - 4.239\,B_2 + 0.711C_1 + 0.600C_2 \ldots\ldots\ldots\ldots \quad 12$$

Where,

$$A_1 = \begin{cases} 1 & if\ \ A = 1(Medium) \\ 0 & Otherwise \end{cases} \qquad A_2 = \begin{cases} 1 & if\ \ A = 2(High) \\ 0 & Otherwise \end{cases}$$

$$B_1 = \begin{cases} 1 & if\ \ B = 1(Medium) \\ 0 & Otherwise \end{cases} \qquad B_2 = \begin{cases} 1 & if\ \ B = 2(High) \\ 0 & Otherwise \end{cases}$$

$$C_1 = \begin{cases} 1 & if\ \ C = 1(Medium) \\ 0 & Otherwise \end{cases} \qquad C_2 = \begin{cases} 1 & if\ \ C = 2(High) \\ 0 & Otherwise \end{cases}$$

8. Result confirmation: The DOE analysis was used to predict the ideal condition for the membrane fouling experiment. The results are presented as predicted results in the result section and were compared with the experimental results. The comparison which was presented as percentage deviation (Tables 4.3 and 4.4), measures the extent or degree to which the experimental results are far from the ideal condition (predicted results). The percentage deviations were estimated as follows:

$$Percentage\ deviation = \frac{Experimental\ flux - Predicted\ flux}{Predicted\ flux} * 100 \ldots\ldots\ldots \quad 13$$

These were used to validate the results of the membrane fouling experiment.

‘

4. RESULTS AND ANALYSIS

4.1. Fouling of the Non-Vibrated Membrane

A filtration experiment was conducted with no vibration of the membrane and a mass of 2grams of garden soil to 500grams of water was used with a fixed TMP of 5psi. The graph of the flux against time (fig. 4.1) shows that the membrane experienced significant decline in flux within the first 0.2hr of the filtration. This can be attributed to pore narrowing and blocking **[4]**. The flux reduction reduced slightly until 0.6hr after which cake filtration became the dominant fouling mechanism **[70]** that steadied the flux rate throughout the remaining filtration period. This cake filtration stage marked the period of minimal flux resulting in the drastic reduction of the permeate flow which remained steady until the end of the experiment.

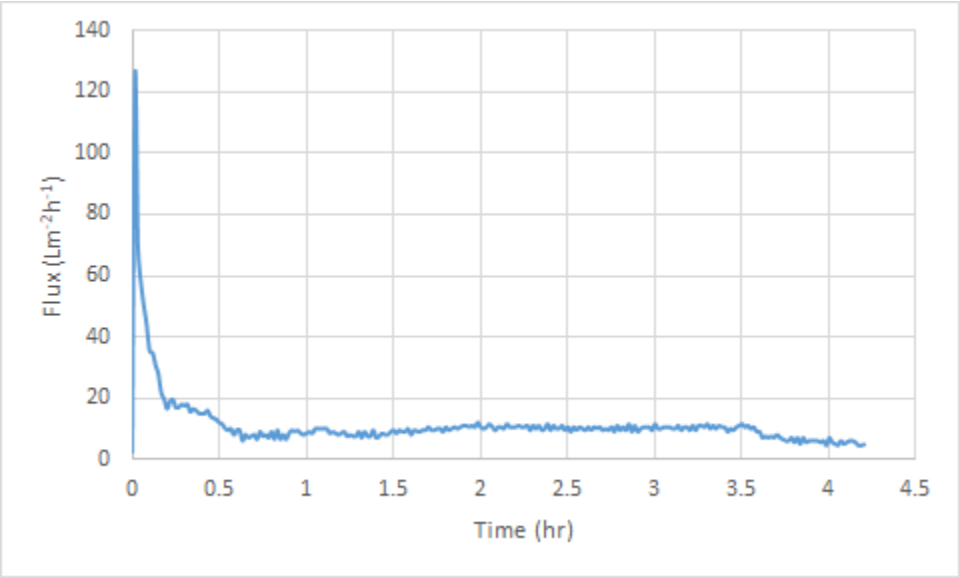

Figure 4.1. Filtration experiment for the non-vibrated membrane (base case)

This experiment with the non-vibrated membrane depicts the typical stages in fouling as stipulated by Ladewig et al, 2017 where the particles (at the beginning of the filtration) adsorbed into the pores resulting in concentration polarization which caused a drastic drop in flux that lasted for the first 0.6hrs of the filtration and was then followed by cake filtration, during which the flux became steady. The normalized flux (Fig. 4.2) also shows the same fouling trend.

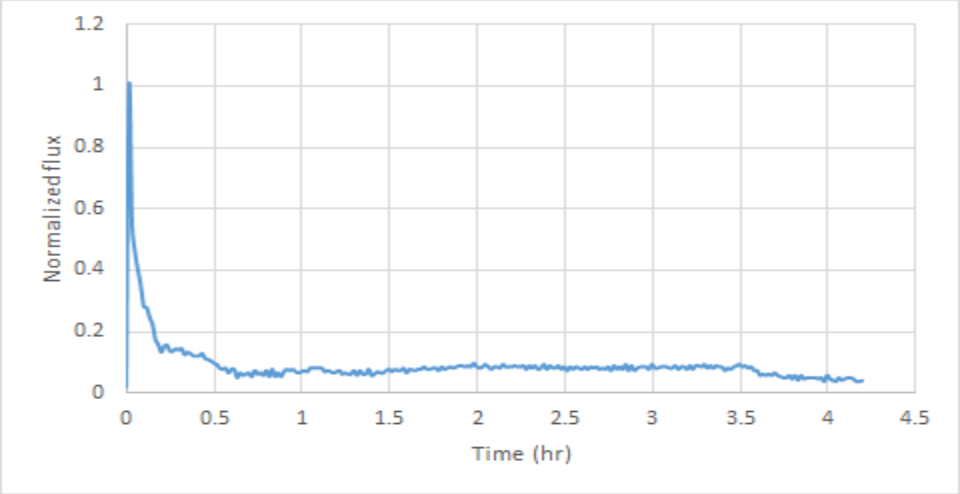

Figure 4.2. Normalized flux for the non-vibrated membrane

4.2 Membrane Surface Analysis

4.2.1 The non-vibrated membrane surface

Prior to the filtration experiment, a section of the fresh (unused) membrane was cut and observed using a Phenom XL G2 desktop Scanning Electron Microscope (SEM) as presented in Fig. 3.3. It should be noted that the white dots on the membrane are manufacturing defects and not the pores of the membrane. Because the pores are too tiny, they could not be captured by the microscope, however they are fresh and open.

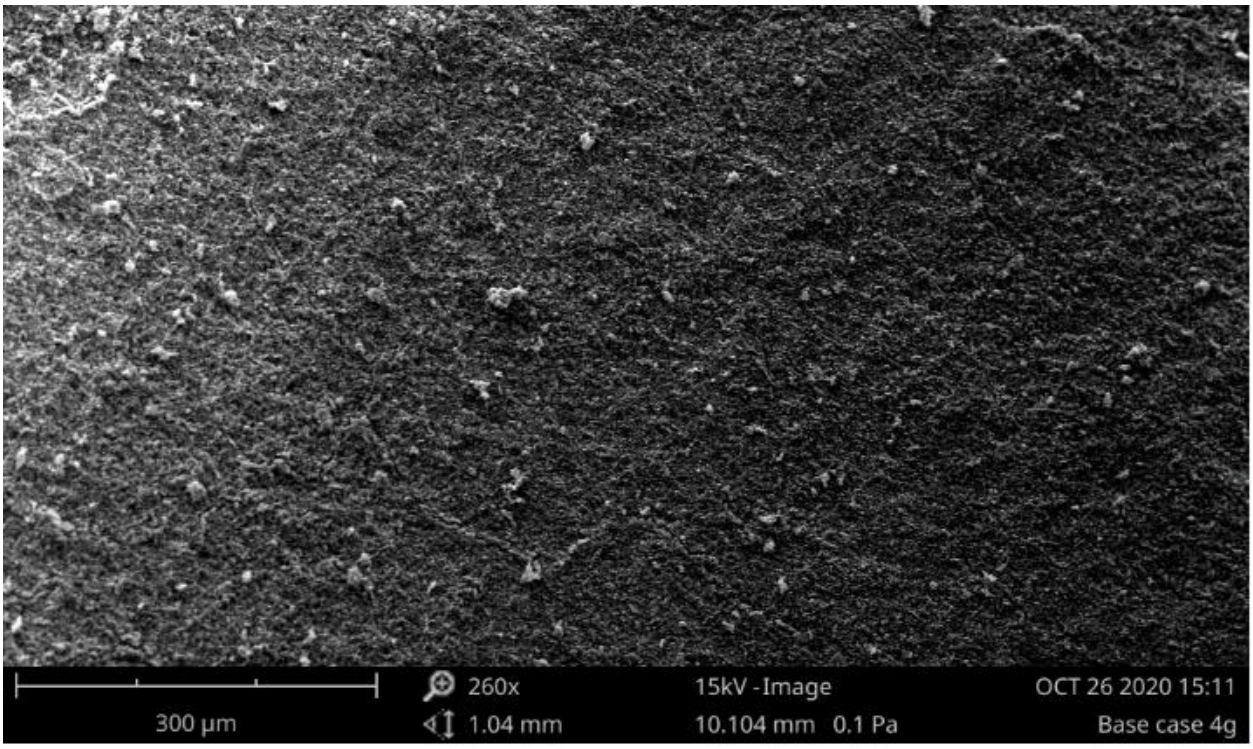

Figure 4.3. SEM image of the fouled (non-vibrated membrane)

Elemental analysis of the different constituents of the fresh membrane was accomplished using Energy Dispersive Spectroscopy (EDS) detector as presented in figure 3.4. With this the different elements present in the membrane were identified as carbon (C), Fluorine (F), Oxygen (O) and Sodium (Na) and with their percentage atomic concentration as 71.05%, 14.34%, 12.36%, 2.25% respectively and the percentage weight concentration as 62.05%, 19.81%, 14.38%, 3.76% respectively. These were recorded for comparison with the fouled membrane. The fouling of the membrane by the different constituents of the garden soil was also observed using SEM equipment. The fouled membrane was dried, and different sections of the membrane were cut for SEM observation and EDS analysis to ascertain the extent of fouling of the regions of the membrane, namely; the feed side, the middle part and the retentate side. The cut sections were inserted in a 22mm x 22mm square microscope slide and then observed in the SEM machine. One of such SEM images of the different regions is presented in figure 4.3. This reveals a surface whose pores are totally blocked due to formed cakes that made the surface impermeable to the feed water

resulting in the drastic reduction of the filtration flux leading to the reduction in the production of the permeate.

4.2.2 The vibrated membrane surface

Close study of the fouled vibrated membrane was conducted to determine the extent of fouling that occurred during water filtration. This was achieved by cutting the membrane into small parts for SEM observation.

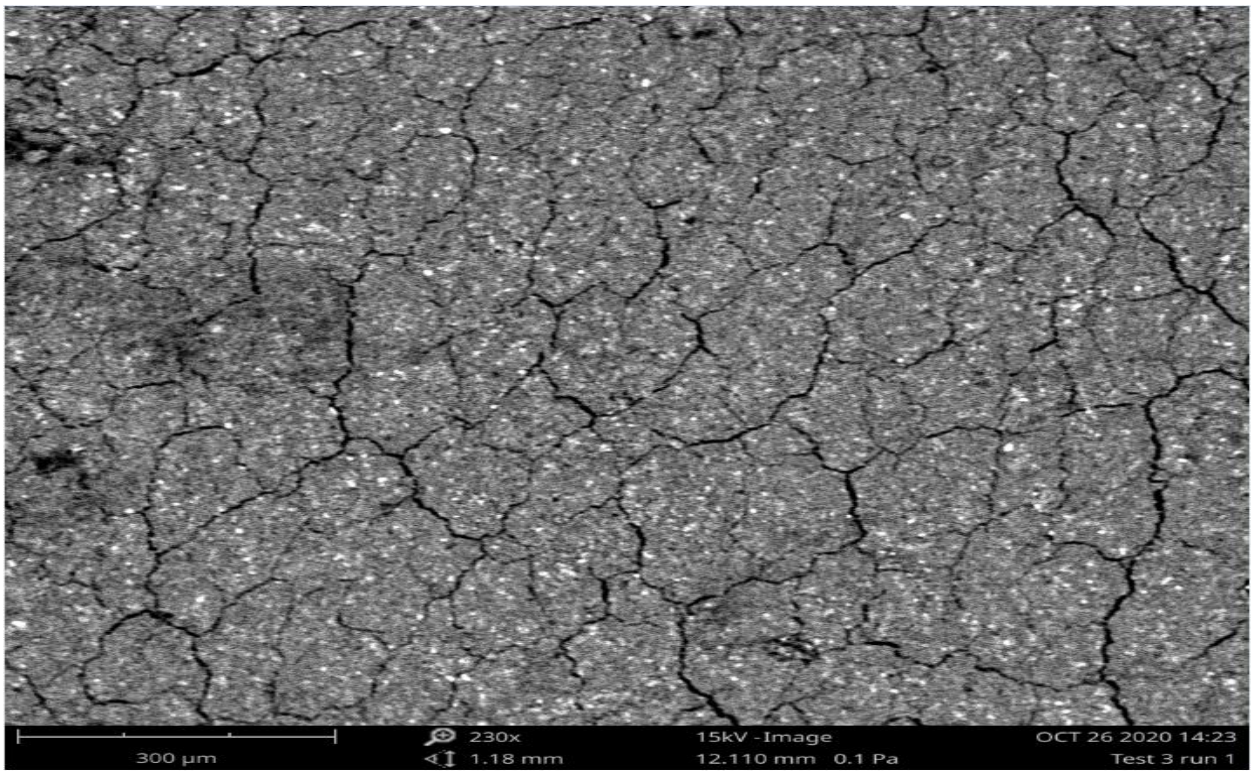

Figure 4.4. SEM image of the fouled (vibrated membrane)

The SEM observation (Fig.4.4) of one of the cut sections, revealed the complete blockage of the pores with interstitial cracks on the cakes formed on the surface of the membrane. These cracks were as a result of the vibratory action of the piezoelectrics. This is quite different from the SEM image of the non-vibrated membrane which unlike the vibrated membrane has no cracks on the cakes formed on the membrane. These cracks serve as the points through which the feed solution

passes through to get to the membrane surface where it gets filtered. Because of these cracks, the rate with which water passes through the cake was increased more than that of the non-vibrated membrane leading to a reduced fouling rate, higher permeate flux and higher volume flowrate. This also explains why the vibration was able to reduce the rate with which the membrane gets fouled while keeping the permeate production rate steady and not having a drastic reduction in flowrate.

4.2.3 Effect of Piezoelectrics

The filtration condition as used for the non-vibrated membrane was equally used for another fresh membrane (but this time) vibrated with 3 flat coin vibration motors all placed on the top surface of the membrane and connected to 2V d.c. Figure 4.5, shows a rapid drop in flux between 0-0.65hrs of the experiment. This is typical of filtration experiments since the fresh membrane whose pores were fully open before the experiment suddenly starts coming in contact with the feed water that contains a lot of particles. The particles tend to be adsorbed into the pores thereby narrowing them resulting to rapid drop in permeate flux as well as the

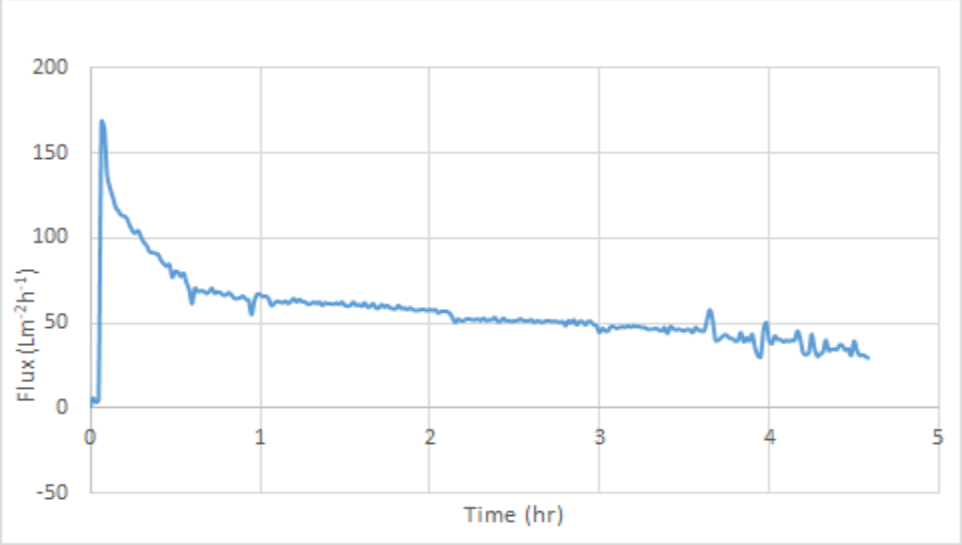

Figure 4.5. Reduction in flux for the vibrated membrane

flow rate. The drop in flux reduced between 1hr-2hrs after which another gradual reduction was experienced between 2.2hrs to 3hrs. From the 3rd hour to the 4th hour experienced considerable reduction in flux, this was basically as a result of the blocking of the pores of the membrane, leading to concentration polarization which increased the pressure on the membrane due to the accumulation of particles on the membrane surface. The further flux reduction from the 4th hour to the end of the filtration experiment can be attributed to the accumulation of fouling particles on top of the ones already blocking the pores leading to a buildup of particles otherwise known as cake filtration.

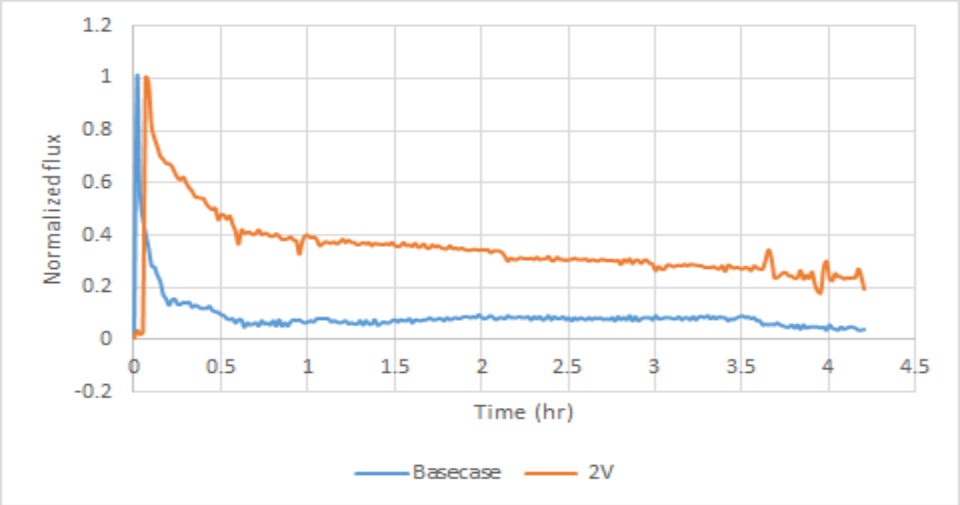

Figure 4.6. Normalized comparison between the base case and the 2V vibrated membrane

The normalized comparison of the reduction in flux between the base case (non-vibrated membrane) and the 2V vibrated membrane (Fig. 4.6) reveals the superior performance of the vibrated membrane over the base case. Both experienced the same pattern of flux drop between 0-0.6hrs of the fouling experiment but at different rates with that of vibrated membrane being lower than that of the base case.

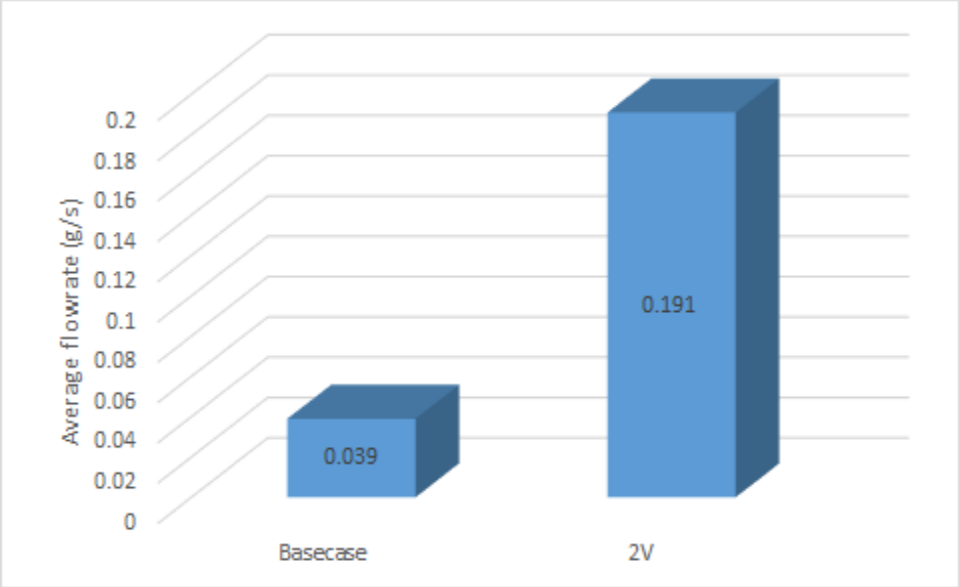

Figure 4.7. Average flow rate recorded for the 2 cases during the experiment

The superior effect of the piezoelectrics on the membrane was further investigated by determining the average flow rate (Fig. 4.7) recorded by the base case as well as the 2V-vibrated membrane. 0.039g/s average flow rate was recorded by the base case while 0.191g/s was recorded by 2V-vibrated membrane. This makes the flow rate produced (when the membrane is vibrated with piezoelectrics, 4.9 times that produced without vibration.

4.2.4 Effect of Vibration on the Different Piezoelectric Location

The effect of vibration on the different piezoelectric locations (namely; TTT, TSD and TBT) (Fig. 4.8) was investigated using 2 grams of foulant to 500 grams of water and 2V vibration voltage on the 3 piezoelectric crystals.

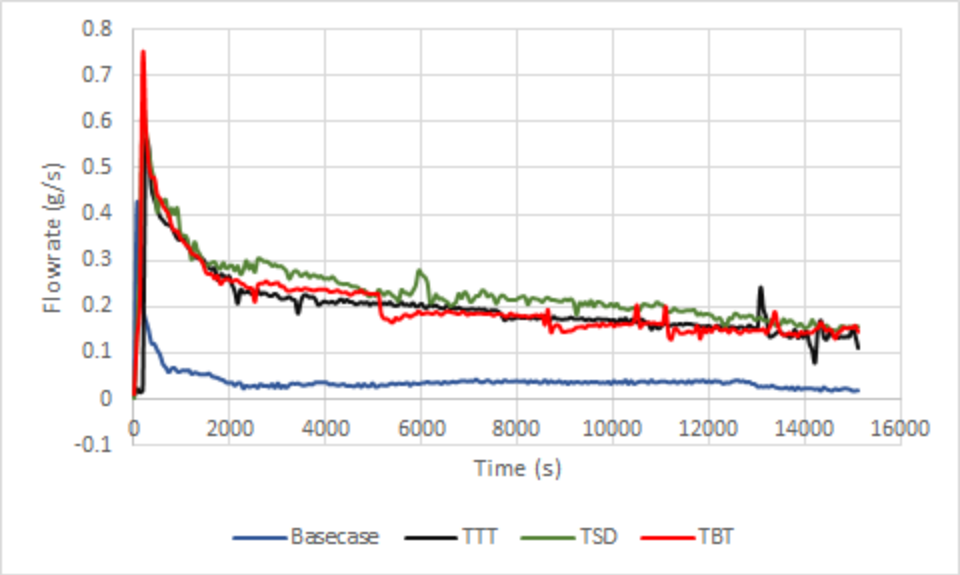

Figure 4.8. Location comparison for 2V-2g vibration

The difference in flow rate for the different locations is not very significant as can be observed from figure 4.8. However, the TSD location seems to have had a higher flow rate than the other two locations. The difference for the TTT and TBT is very vague, there is no distinctive difference in flow rate especially from 10,000s to the end of the filtration experiment. The base case still recorded the lowest flow rate. A clearer understanding of the different performance is presented as the average flow rate (Fig. 4.9) recorded by the individual location configuration.

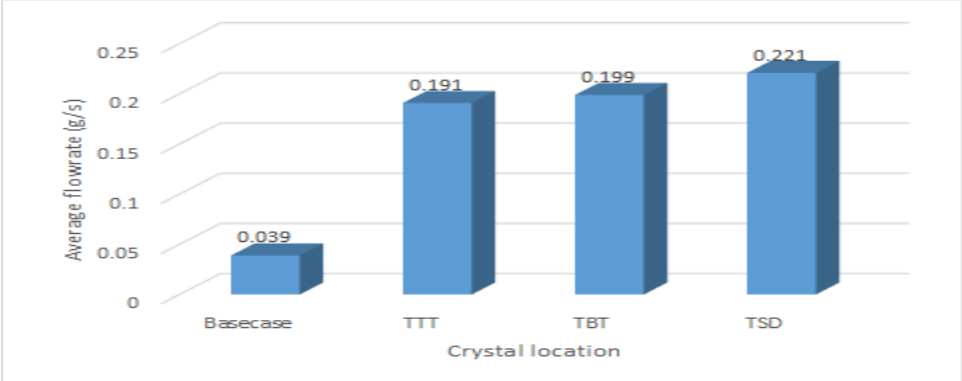

Figure 4.9. Average flow rate as recorded by the different crystal location configuration

As can be clearly observed from the above figure, the TSD location configuration with an average flow rate of 0.221g/s recorded the highest flow rate, the TBT location with an average flow rate of 0.199g/s performed better than the TTT location that recorded 0.191g/s. This makes the flow rates of the TSD, TBT and TTT locations respectively 5.7-, 5.1- and 4.9- times that of the base case.

4.2.5 Effect of Vibration Voltage

The effect of vibration voltage on fouling reduction was studied for the different piezoelectric locations (to determine the optimum voltage required at each location configuration to produce the highest flow rate) using 3 grams of the foulant to 500 grams of water i.e. the medium concentration. This was achieved by vibrating the membrane with 2V, 3V and 4V respectively while the crystals are appropriately placed on TTT, TSD and TBT locations while the filtration experiment was carried on.

4.2.5.1 Voltage Effect on TTT Location Configuration

Placing the crystals on the TTT locations and vibrating them with 2V, 3V and 4V respectively resulted in the observed flow rates as presented (Fig. 4.10). As can be clearly observed in the figure, 4V vibration produced the highest flow rate. The dip as observed between 6000s - 7800s was as a result of concentration polarization due to the accumulation of foulants on the membrane

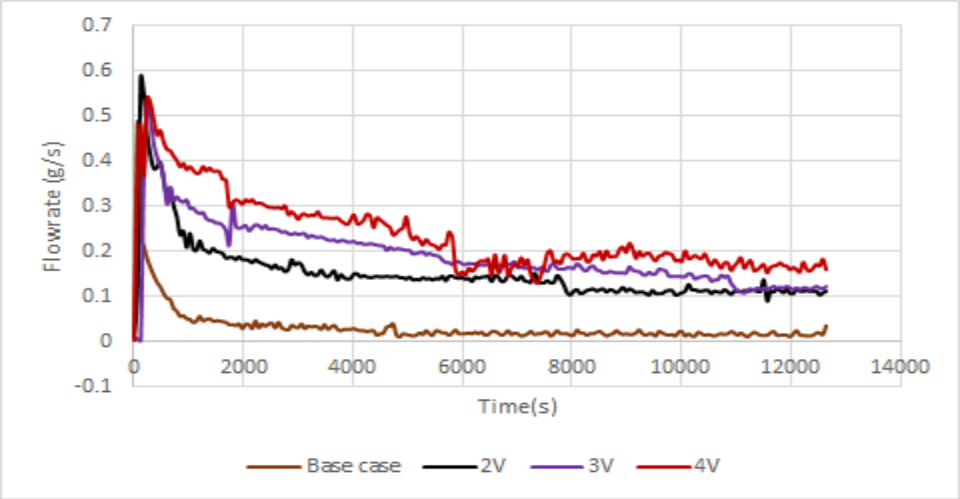

Figure 4.10. Voltage comparison for TTT location

surface resulting in higher transmembrane pressure and lower flow rate thereby causing the dip in flow rate. However, the 4V vibration was able to disperse the settled particles which led to the higher flow rate observed from 7800s to the end of the experiment. 3V vibration performed better than the 2V vibration, while the base case remained the most outperformed case. A better understanding of the different performance of the voltage is presented as the average flow rate (Fig. 4.11) recorded by the individual voltage. As observed from the figure, 4V vibration with an average flow rate of 0.237g/s recorded the highest flow rate, 3V vibration with an average flow rate of 0.192g/s performed better than 2V vibration which recorded a flow rate of 0.152g/s. This makes the flow rates of the 2V, 3V and 4V respectively 4.75-, 6.0- and 7.41 times that of the base case. From these results, it can be deduced that vibrating the membrane produced flow rates that were significantly higher than that of the base case. Also, increasing the voltage at this location configuration leads to a corresponding increase in flow rate.

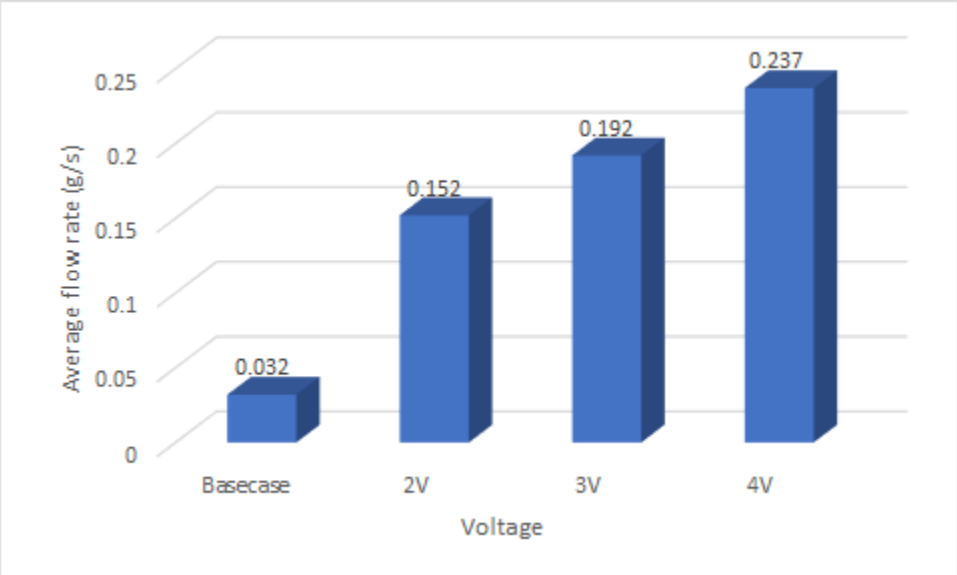

Figure 4.11. Average flow rate for different voltages on TTT location

4.2.5.2 Voltage Effect on TSD Location Configuration

Placing the crystals on the TSD location and vibrating with 2V, 3V and 4V respectively results in the observed flow rates (Fig. 4.12). 3V vibration produced the highest flow rate, which means that it was able to reduce membrane fouling more than 2V and 4V respectively. 2V vibration surprisingly performed better than 4V vibration. It can be deduced from this location that, 3V is the optimum voltage needed for maximum flow rate above which there would be a drastic reduction in flow rate.

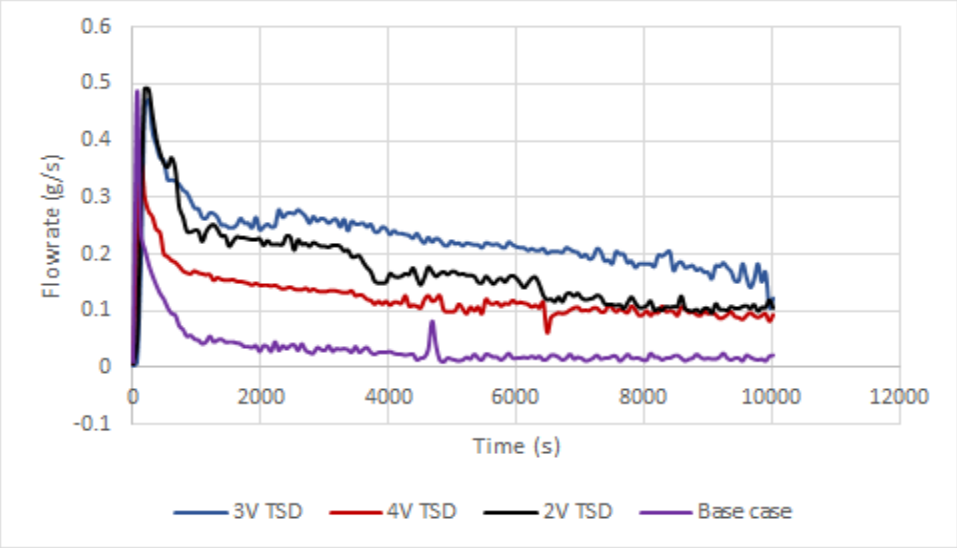

Figure 4.12. Voltage comparison for TSD location

This can be attributed to the fact that 3V vibration produced the maximum dispersal of the foulants on the membrane surface thereby preventing their accumulation and subsequent concentration polarization and cake formation. Beyond 3V (i.e. 4V), the kinetic energy impacted on the foulants by the crystals is so high that instead of dispersing the foulants, they tend to be compressed on one another and into the pores of the membrane thereby enhancing the buildup of these foulants on the surface of the membrane and into the pores of the membrane resulting in reduced permeate flux and reduction of flow rate.

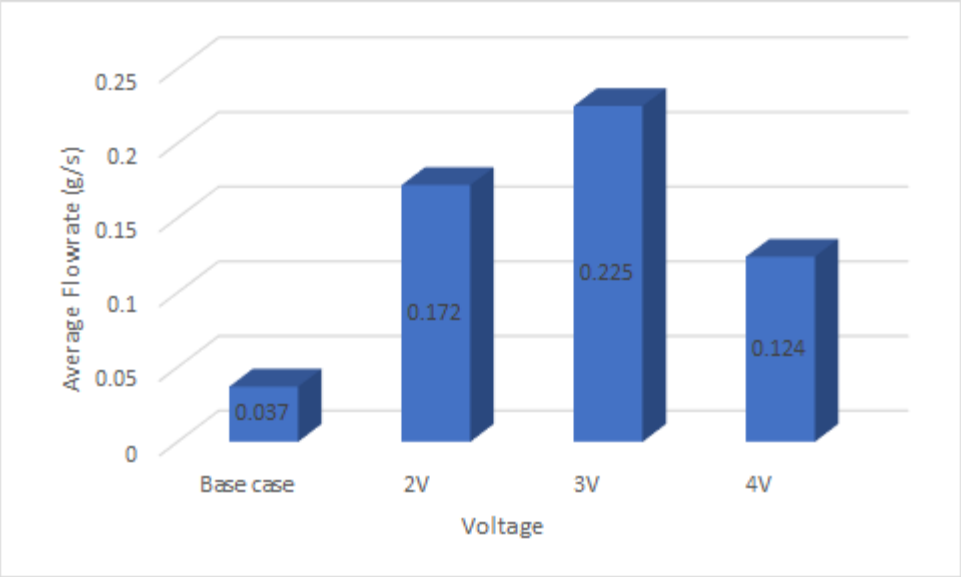

Figure 4.13. Average flow rate for different voltages on TSD location

The different performance of the voltages is better presented in the form of average flow rate (Fig. 4.13). 3V vibration with an average flow rate of 0.225g/s produced the highest average flow rate which is 6.1 times that of the base case. 2V vibration produced an average flow rate of 0.172g/s which is 4.6 times that of the base case while 4V vibration produced the lowest average flow rate of 0.124g/s which is 3.4 times greater than that of the base case. In all for this location, vibrating the membrane produced flow rates that were significantly higher than that of the base case. An increase in voltage leads to a corresponding increase in flow rate to a certain voltage (3V) beyond which further increase leads to a decrease in flow rate.

4.2.5.3 Voltage Effect on TBT Location Configuration

Like the previous voltage comparisons, the crystals were placed on TBT locations and vibrated with 2V, 3V and 4V respectively. A closely observed result (Fig. 4.14) is presented with 4V vibration maintaining the highest flow rate to the end of the filtration period. From 1000s to around 7000s, 3V vibration maintained a higher flow rate than 2V vibration. Beyond 7000s, both 2V and 3V maintained almost the same flow rate to the end of the filtration period.

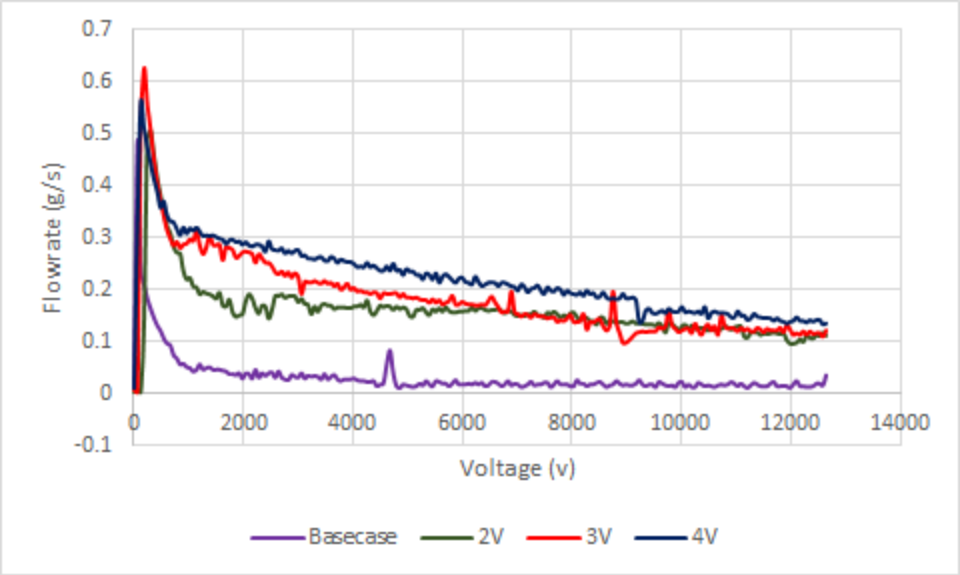

Figure 4.14. Voltage comparison for TBT location

A better understanding of their individual performance is created in terms of the average flow rate (Fig.4.15) recorded by each voltage in TBT location. 4V vibration produced an average flow rate of 0.223g/s which was the highest average flow rate which was 6.76 times that of the base case. 3V vibration, with an average flow rate of 0.186g/s (and 5.46 times higher than that of the base case) performed better than 2V vibration which recorded an average flow rate of 0.16 and was 4.85 times that of the base case. In all, for this location, the vibration of the membrane produced flow rates that were significantly higher than that of the base case. Also, an increment in voltage results in corresponding increase in flow rate.

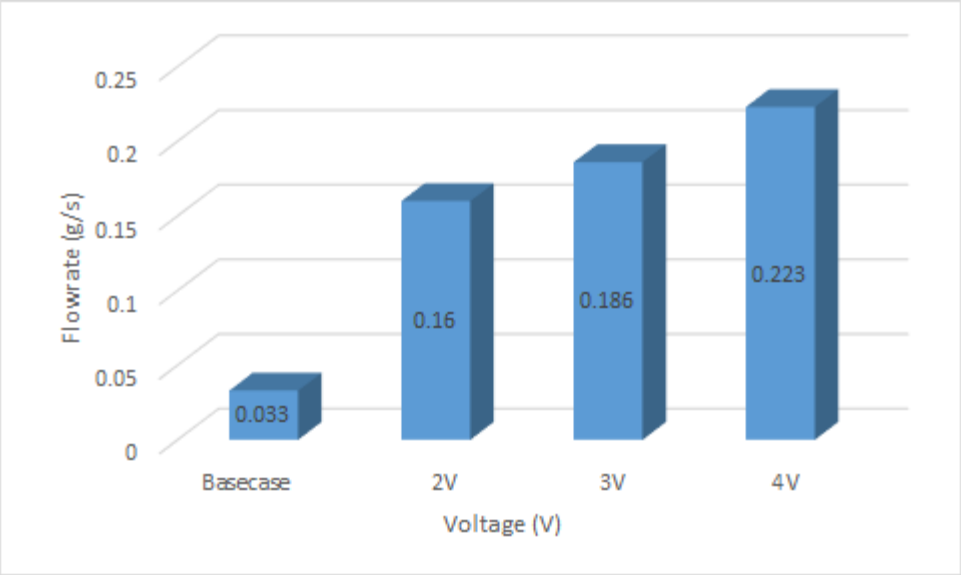

Figure 4.15. Average flow rate for different voltages on TBT location

4.2.6 The Predicted Results of the Experiment

The DOE best fit equations used on the 25% experimental flux, 50% experimental flux, 75% experimental flux and 100% experimental flux were used to develop equations 5 – 8 for run 1 and equations 9 – 12 for run 2. These equations were further used to estimate the predicted results or best fit results (Tables 4.1 and 4.2) for run 1 and run 2 respectively. These predicted results are the ideal conditions for the membrane fouling experiments and were arrived at by fitting least square fit lines before the steady state of the experimental results.

Table 4.1. Run 1 predicted/best fit results

Run	Test	Concentration (A)	Voltage (B)	Piezoelectric Location (C)	25% Predicted Flux ($Lm^{-2}h^{-1}$)	50% Predicted Flux ($Lm^{-2}h^{-1}$)	75% Predicted Flux ($Lm^{-2}h^{-1}$)	100% Predicted Flux ($Lm^{-2}h^{-1}$)
1	1	0	0	0	36.46	31.94	27.22	32.07
1	2	0	0	1	34.60	31.90	27.29	28.48
1	3	0	0	2	41.05	37.63	32.26	32.17
1	4	0	1	0	30.96	26.54	22.80	26.19
1	5	0	1	1	29.10	26.50	22.87	22.60
1	6	0	1	2	35.55	32.23	27.85	26.29
1	7	0	2	0	38.69	33.90	28.45	33.82
1	8	0	2	1	36.82	33.86	31.03	30.22
1	9	0	2	2	43.27	39.59	33.49	33.92
1	10	1	0	0	36.16	30.24	25.69	25.82
1	11	1	0	1	34.30	30.20	25.76	22.23
1	12	1	0	2	40.74	35.92	30.73	25.92
1	13	1	1	0	30.66	24.84	21.27	19.94
1	14	1	1	1	28.80	24.80	21.35	16.35
1	15	1	1	2	35.24	30.52	26.32	20.04
1	16	1	2	0	38.38	32.20	26.92	27.57
1	17	1	2	1	36.52	32.16	26.99	24.00
1	18	1	2	2	42.96	37.88	31.97	27.67
1	19	2	0	0	35.32	29.71	26.89	27.36
1	20	2	0	1	33.46	29.67	26.97	23.76
1	21	2	0	2	39.91	35.39	31.94	27.46
1	22	2	1	0	29.82	24.31	22.48	21.48
1	23	2	1	1	27.96	24.27	22.55	17.89
1	24	2	1	2	34.41	30.00	27.52	21.58
1	25	2	2	0	37.55	31.67	28.13	29.11
1	26	2	2	1	35.69	31.63	28.20	25.51
1	27	2	2	2	42.13	37.35	33.17	29.21

Table 4.2. Run 2 predicted/best fit results

Run	Test	Concentration (A)	Voltage (B)	Piezoelectric Location (C)	25% Predicted Flux ($Lm^{-2}h^{-1}$)	50% Predicted Flux ($Lm^{-2}h^{-1}$)	75% Predicted Flux ($Lm^{-2}h^{-1}$)	100% Predicted Flux ($Lm^{-2}h^{-1}$)
2	1	0	0	0	33.37	31.28	28.12	28.10
2	2	0	0	1	35.54	32.42	29.51	28.81
2	3	0	0	2	37.32	33.31	29.03	28.70
2	4	0	1	0	35.62	29.92	28.00	28.10
2	5	0	1	1	37.79	31.06	29.39	28.81
2	6	0	1	2	39.57	31.94	28.90	28.70
2	7	0	2	0	33.90	28.06	24.82	23.86
2	8	0	2	1	36.07	29.19	26.22	24.57
2	9	0	2	2	37.84	30.08	25.73	24.46
2	10	1	0	0	32.20	32.14	30.03	28.56
2	11	1	0	1	34.37	33.28	31.42	29.27
2	12	1	0	2	36.15	34.17	30.93	29.16
2	13	1	1	0	34.45	30.78	29.90	28.56
2	14	1	1	1	36.62	31.92	31.30	29.27
2	15	1	1	2	38.40	32.81	30.81	29.16
2	16	1	2	0	32.73	28.92	26.73	24.32
2	17	1	2	1	34.90	30.06	28.12	24.46
2	18	1	2	2	36.67	30.94	27.64	24.92
2	19	2	0	0	29.82	27.83	25.51	25.12
2	20	2	0	1	31.98	28.97	26.91	25.83
2	21	2	0	2	33.76	29.86	26.42	25.72
2	22	2	1	0	32.06	26.47	25.39	25.12
2	23	2	1	1	34.23	27.61	26.78	25.83
2	24	2	1	2	36.01	28.50	26.30	25.72
2	25	2	2	0	30.34	24.61	22.22	20.88
2	26	2	2	1	32.51	25.75	23.61	21.59
2	27	2	2	2	34.29	26.64	23.12	21.48

The term steady state is used to describe the period when there is no further or negligible change in flow rate. At this point the membrane has been fouled and there is no further change in flowrate to the end of the experiment. As has been earlier stated in section 3.6, it was observed that on the average, the steady state of the experiment was arrived at, after 2 hrs. of the experiment, the 25% experimental flux, 50% experimental flux, 75% experimental flux and 100% experimental flux readings for both run 1 and run 2, were taken within 2 hrs. of the experiment which is before the steady state. Percentage deviation (Tables 4.3 and 4.4), as estimated with equation 13, were used to measure the degree or the extent to which the experimental results of run1 and run 2 are far from the theoretical results of run 1 and run 2 respectively.

Table 4.3. Run 1 percentage deviation

Run	Test	Concentration (A)	Voltage (B)	Piezoelectric Location (C)	25% Flux ($Lm^{-2}h^{-1}$)	50% Flux ($Lm^{-2}h^{-1}$)	75% Flux ($Lm^{-2}h^{-1}$)	100% Flux ($Lm^{-2}h^{-1}$)
1	1	0	0	0	19.31	1.28	23.99	15.37
1	2	0	0	1	22.83	29.31	23.67	18.50
1	3	0	0	2	1.34	6.30	0.81	6.75
1	4	0	1	0	0.94	3.92	3.07	6.45
1	5	0	1	1	5.50	9.43	7.08	12.61
1	6	0	1	2	11.39	4.72	10.41	10.61
1	7	0	2	0	12.77	2.50	44.64	44.15
1	8	0	2	1	25.99	36.50	37.96	37.13
1	9	0	2	2	16.13	6.72	21.68	13.03
1	10	1	0	0	22.57	25.60	18.26	22.54
1	11	1	0	1	0.87	8.11	12.66	17.09
1	12	1	0	2	42.32	29.01	25.97	11.27
1	13	1	1	0	49.22	34.86	37.52	21.61
1	14	1	1	1	31.94	53.23	51.05	77.37
1	15	1	1	2	17.76	4.85	0.27	13.52
1	16	1	2	0	20.51	27.33	21.66	1.16
1	17	1	2	1	39.07	40.92	40.72	34.38
1	18	1	2	2	3.58	4.28	7.13	5.71
1	19	2	0	0	0.91	6.02	9.71	16.85
1	20	2	0	1	5.11	9.84	5.45	1.09
1	21	2	0	2	37.18	25.74	6.45	34.74
1	22	2	1	0	20.36	17.73	22.15	21.55
1	23	2	1	1	15.95	19.65	19.07	0.61
1	24	2	1	2	42.60	40.83	41.86	36.28
1	25	2	2	0	28.76	17.90	4.59	24.42
1	26	2	2	1	41.50	49.38	48.05	33.28
1	27	2	2	2	19.87	9.10	16.07	21.53

Table 4.4. Run 2 percentage deviation

Run	Test	Concentration (A)	Voltage (B)	Piezoelectric Location (C)	25% Flux ($Lm^{-2}h^{-1}$)	50% Flux ($Lm^{-2}h^{-1}$)	75% Flux ($Lm^{-2}h^{-1}$)	100% Flux ($Lm^{-2}h^{-1}$)
2	1	0	0	0	21.37	7.90	8.46	4.09
2	2	0	0	1	8.38	16.72	0.03	18.43
2	3	0	0	2	0.48	8.08	13.88	2.44
2	4	0	1	0	5.28	15.31	9.82	10.32
2	5	0	1	1	12.01	0.19	1.33	2.40
2	6	0	1	2	19.13	7.64	3.98	9.41
2	7	0	2	0	7.67	4.67	0.52	3.10
2	8	0	2	1	2.97	4.93	10.37	6.84
2	9	0	2	2	4.20	3.06	11.74	6.30
2	10	1	0	0	35.56	26.10	29.24	26.47
2	11	1	0	1	10.53	4.60	5.32	5.91
2	12	1	0	2	16.87	20.72	28.10	32.03
2	13	1	1	0	5.95	1.53	2.01	1.09
2	14	1	1	1	9.23	6.52	11.82	11.90
2	15	1	1	2	12.63	4.00	8.31	3.12
2	16	1	2	0	0.82	0.59	0.86	2.34
2	17	1	2	1	0.43	13.94	4.91	4.95
2	18	1	2	2	3.87	7.87	4.12	13.72
2	19	2	0	0	5.26	5.10	4.86	5.49
2	20	2	0	1	3.06	5.28	6.84	1.63
2	21	2	0	2	3.67	0.47	1.25	1.83
2	22	2	1	0	0.97	2.95	0.55	0.52
2	23	2	1	1	0.58	6.74	2.69	4.18
2	24	2	1	2	0.67	7.90	13.50	8.63
2	25	2	2	0	1.94	0.57	9.14	10.15
2	26	2	2	1	12.27	9.71	12.11	0.74
2	27	2	2	2	5.95	8.97	1.64	2.23

It was observed that in general, run 2 percentage deviations were lower than that of run 1. This in turn means that run 2 experimental flux is closer to the ideal condition (best fit/predicted flux) than that of run1.

4.2.6.1 High Flux Tests

High flux tests are generally considered as experimental tests that recorded 40 $Lm^{-2}h^{-1}$ and above at the beginning (i.e. 25% of the considered 2-hour time) of the experiment. The high flux tests for run 1 are presented in Table 4.5 while figures 4.16– 4.26 present the graphical representations of the experimental and predicted fluxes in single graphs. Run 1 produced more tests with high flux than run 2. It has to be noted that what is meant by theoretical flux in the graph is the predicted or best fit flux.

Table 4.5. Run 1 high flux tests

Run	Test	Concentration (A)	Voltage (B)	Piezo Location (C)	25% Experimental Flux ($Lm^{-2}h^{-1}$)	50% Experimental Flux ($Lm^{-2}h^{-1}$)	75% Experimental Flux ($Lm^{-2}h^{-1}$)	100% Experimental Flux ($Lm^{-2}h^{-1}$)
1	1	0	0	0	43.50	32.35	33.75	37.00
1	2	0	0	1	42.50	41.25	33.75	33.75
1	3	0	0	2	40.50	40.00	32.00	30.00
1	9	0	2	2	50.25	42.25	40.75	29.50
1	13	1	1	0	45.75	33.50	29.25	24.25
1	15	1	1	2	41.50	32.00	26.25	22.75
1	16	1	2	0	46.25	41.00	32.75	27.25
1	18	1	2	2	44.50	39.50	34.25	29.25
1	21	2	0	2	54.75	44.50	34.00	37.00
1	26	2	2	1	50.50	47.25	41.75	34.00
1	27	2	2	2	50.50	40.75	38.50	35.50

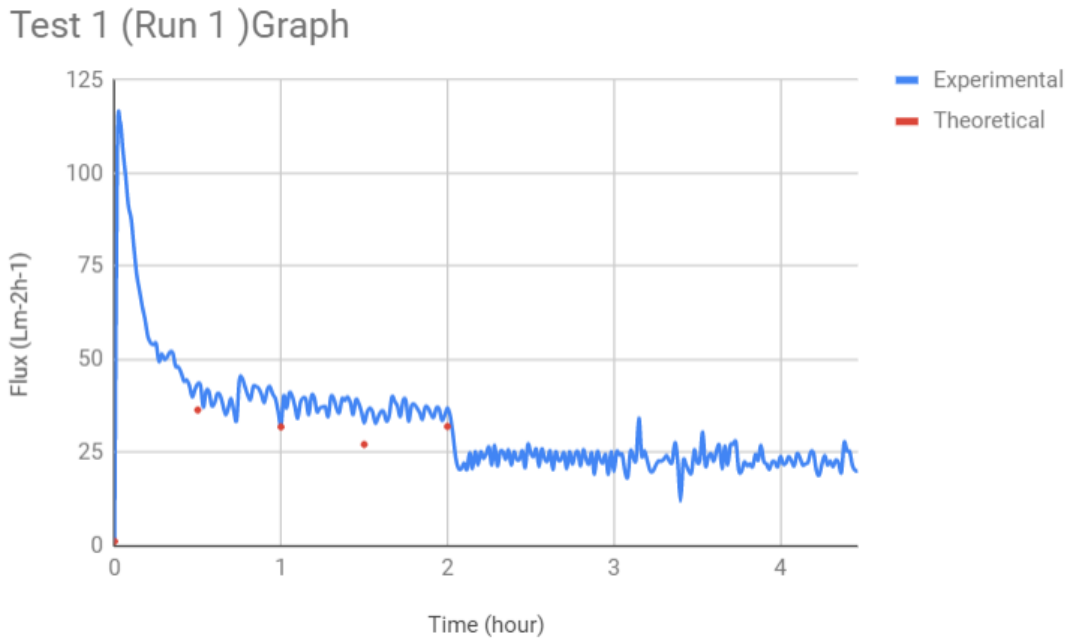

Figure 4.16. Experimental and best fit graphs of test 1 (Run 1) against time

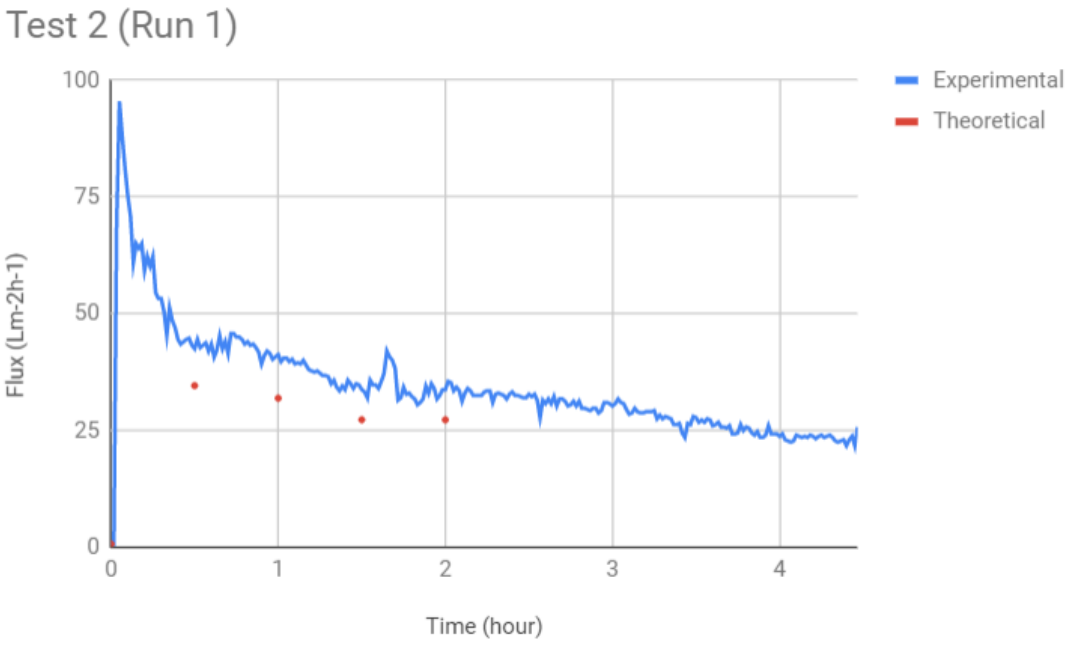

Figure 4.17. Experimental and best fit graphs of Test 2 (Run 1) against time

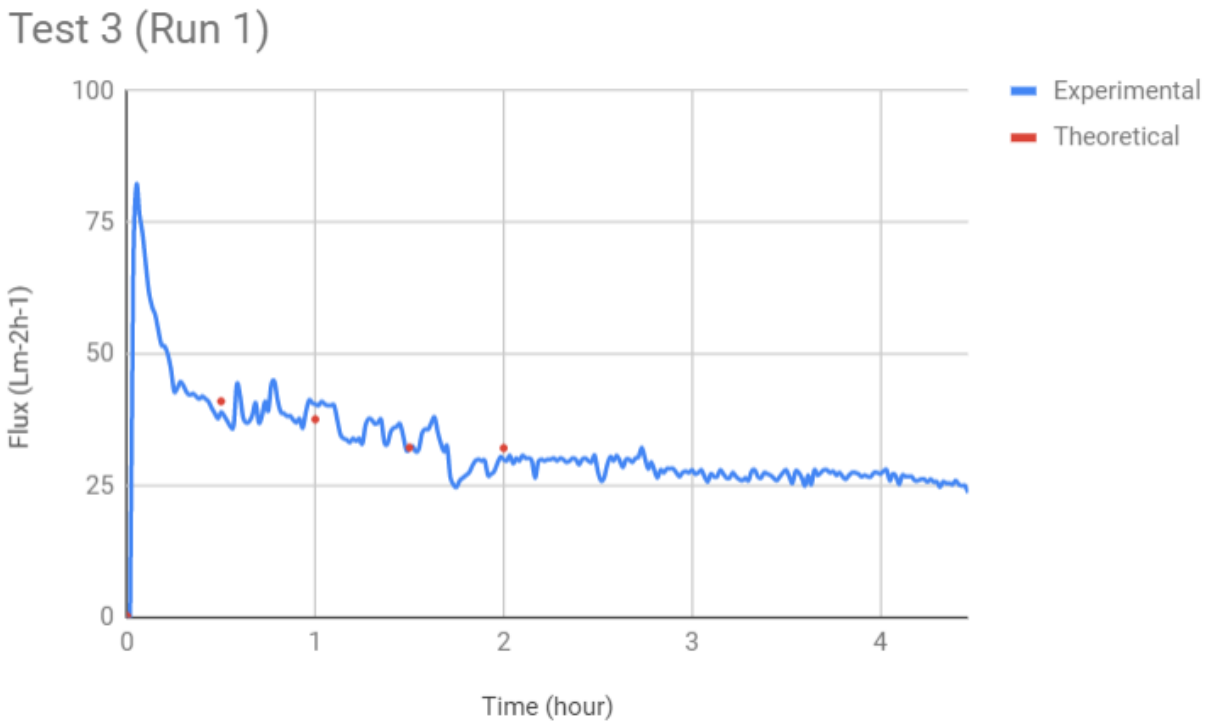

Figure 4.18. Experimental and best fit graphs of Test 3 (Run 1) against time

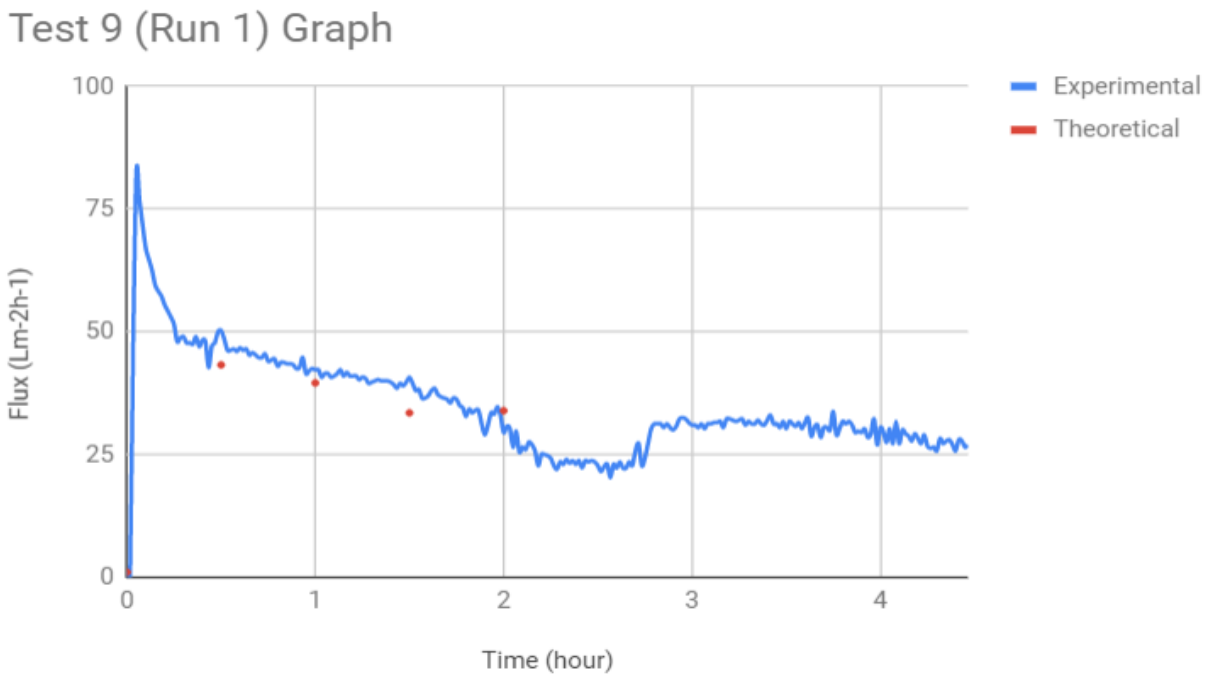

Figure 4.19. Experimental and best fit graphs of Test 9 (Run 1) against time

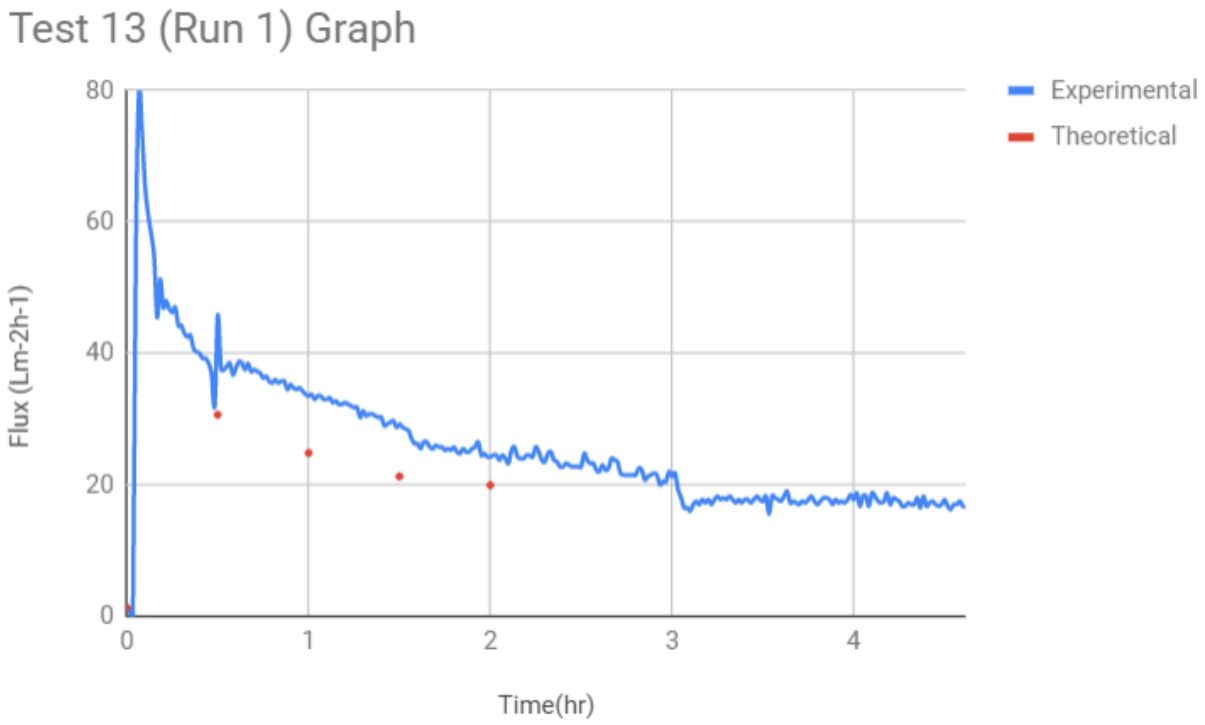

Figure 4.20. Experimental and best fit graphs of Test 13 (Run 1) against time

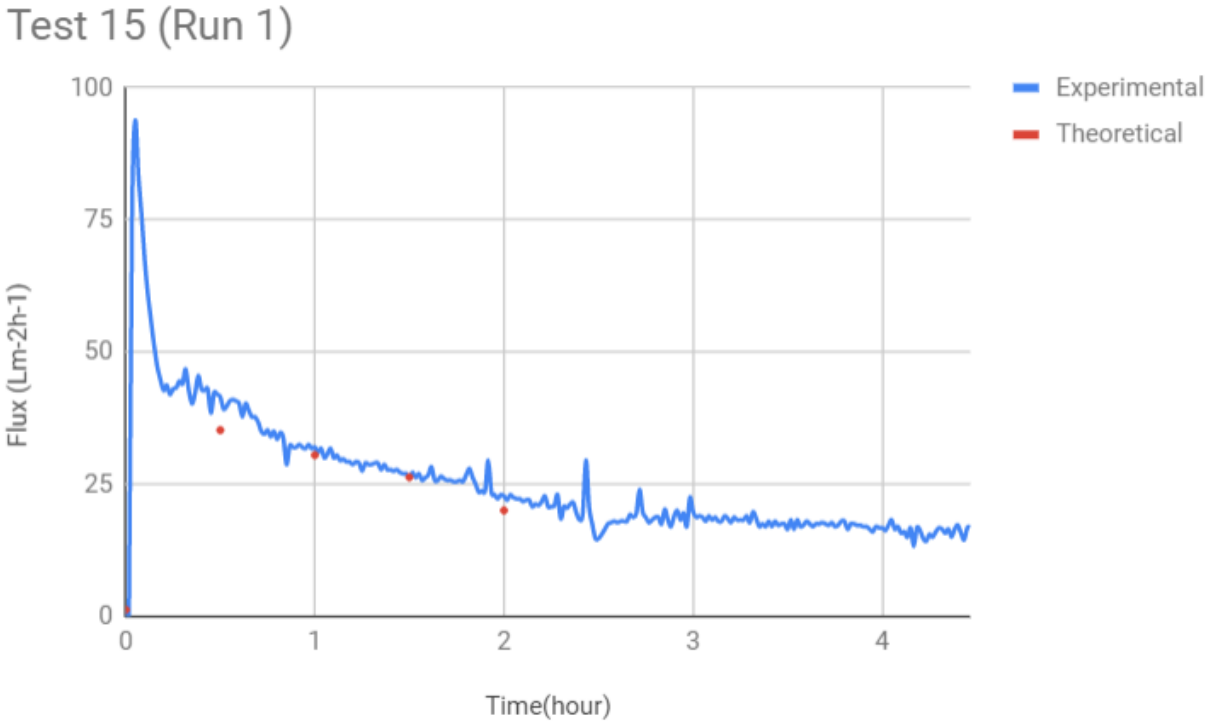

Figure 4.21. Experimental and best fit graphs of Test 15 (Run 1) against time

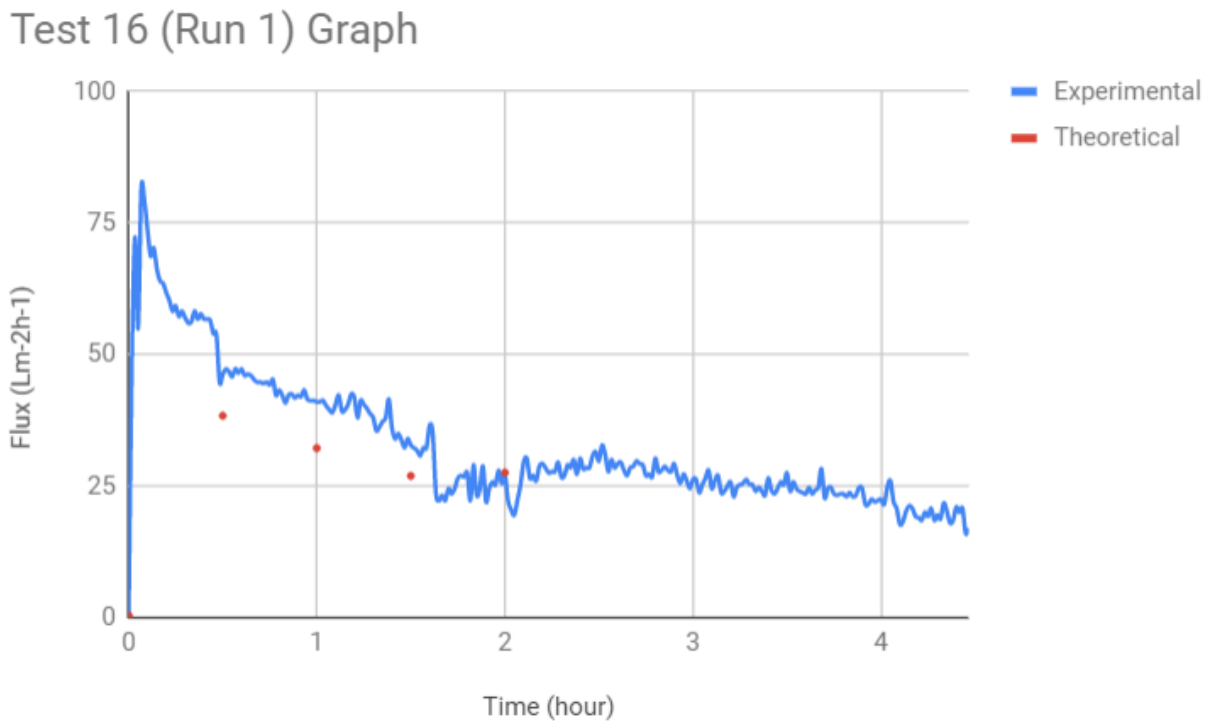

Figure 4.22. Experimental and best fit graphs of Test 16 (Run 1) against time

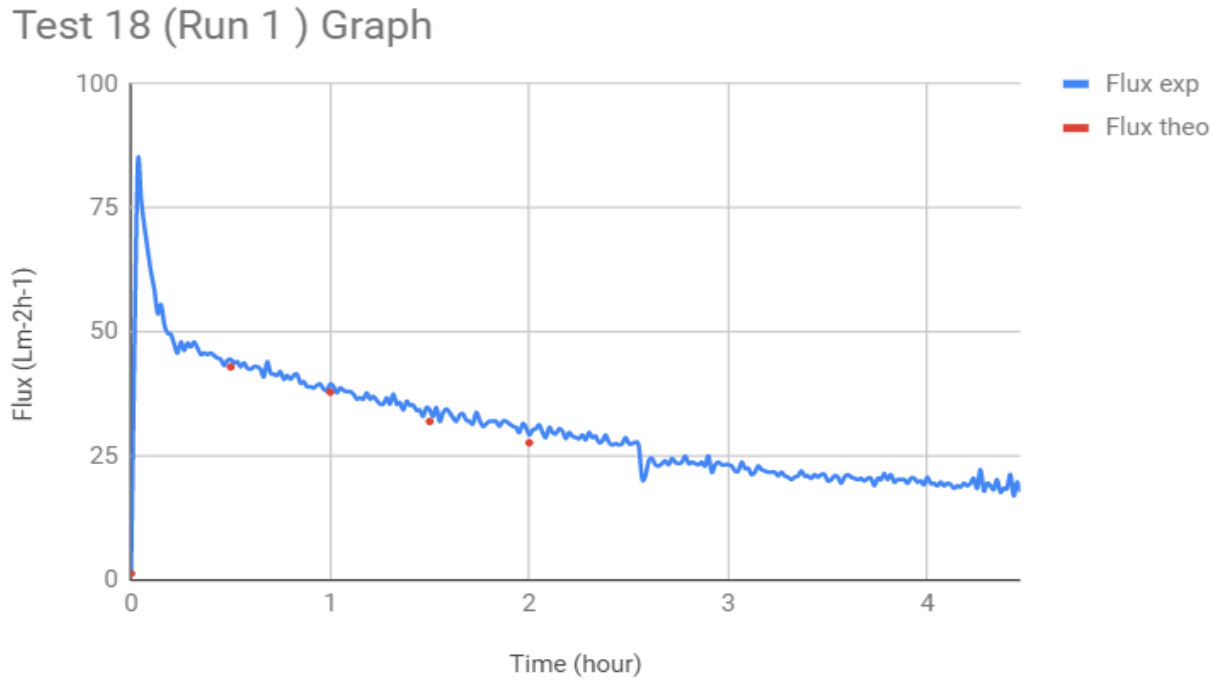

Figure 4.23. Experimental and best fit graphs of Test 18 (Run 1) against time

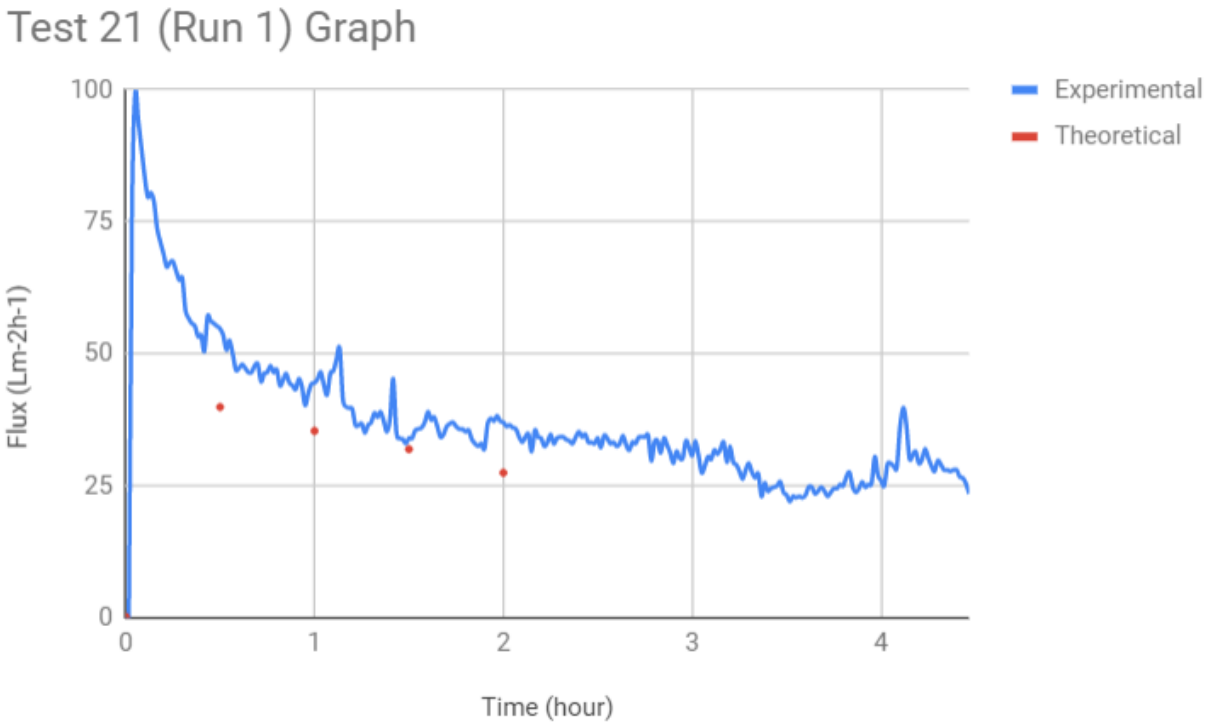

Figure 4.24. Experimental and best fit graphs of Test 21 (Run 1) against time

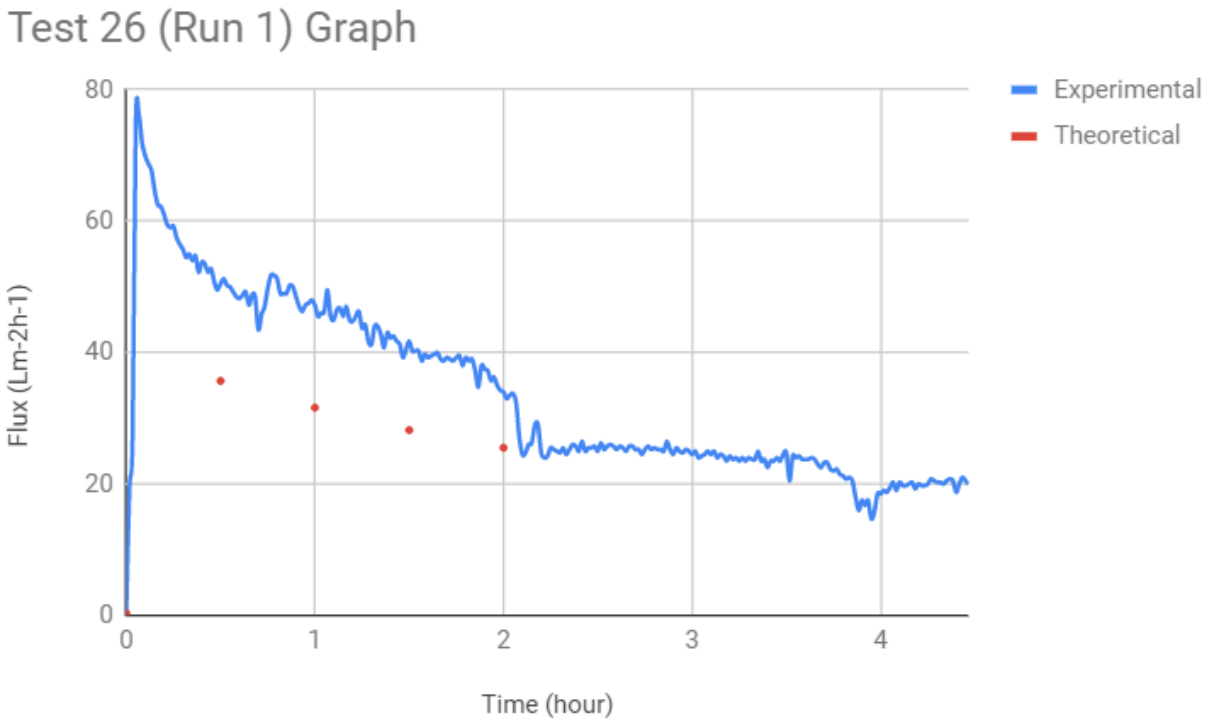

Figure 4.25. Experimental and best fit graphs of Test 26 (Run 1) against time

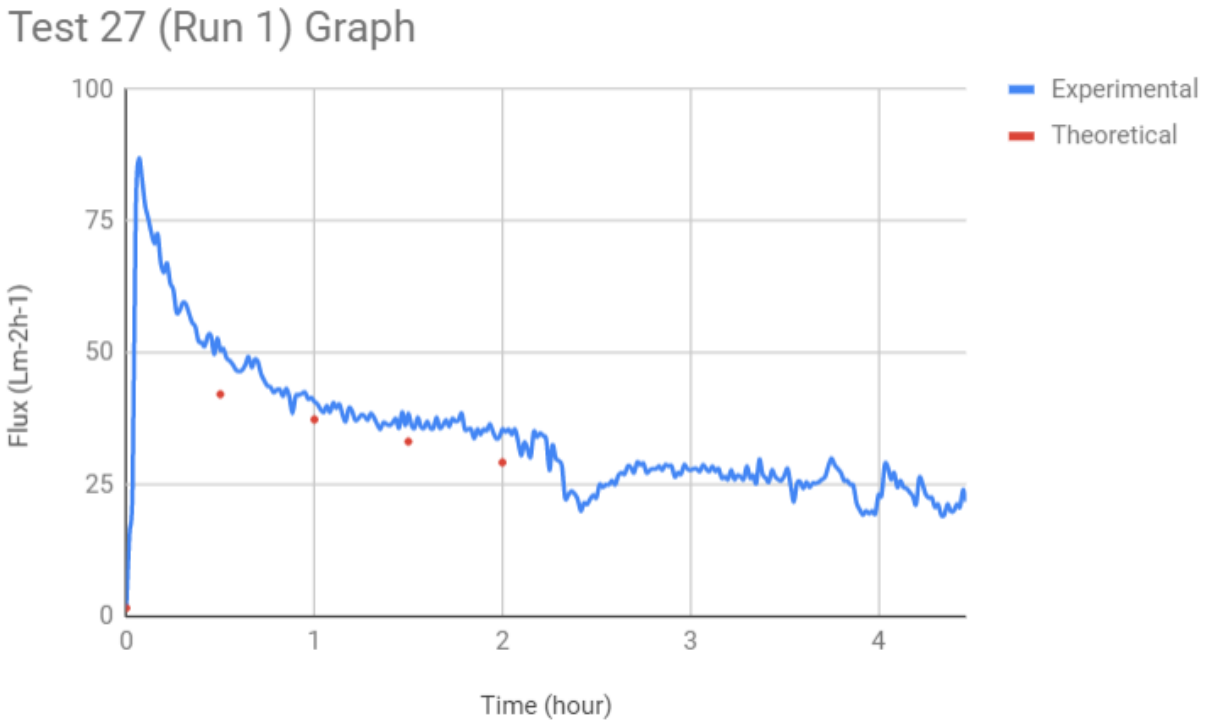

Figure 4.26. Experimental and best fit graphs of Test 27 (Run 1) against time

Of all the high flux tests of run 1, the experimental flux of Test 26 (run 1) with [2 2 0] configuration i.e. [high concentration, high voltage, TTT crystal location] deviated most from the normal condition (predicted flux) with the deviations respectively; 41.50% deviation of the experimental flux from the normal condition (predicted flux) for 25% flux , 49.38% deviation of the experimental flux from the normal condition (predicted flux) for 50% flux, 48.05% deviation of the experimental flux from the normal condition (predicted flux) for 75% flux and 33.28% deviation of the experimental flux from the normal condition (predicted flux) for 100% flux while the least deviation of experimental flux from the normal condition was recorded by test 18 having [1 2 2] configuration i.e. [medium concentration, high voltage, TBT crystal location] with 3.58% deviation of the experimental flux from the normal condition (predicted flux) for 25% flux, 4.28% deviation of the experimental flux from the normal condition (predicted flux) for 50% flux, 7.13% deviation of the experimental flux from the normal condition (predicted flux) for 75% flux and 5.71% deviation of the experimental flux from the normal condition (predicted flux) for 100% flux. On the other hand, fewer high flux tests were recorded by run 2. However, these high experimental flux tests were closer to their ideal conditions (predicted flux) than those of run 1.

Considering all the conducted experiments of run 1, the experimental flux of Test 14 (run 1) with [1 1 1] configuration i.e. [medium concentration, medium voltage, TSD crystal location] deviated most from the normal condition (predicted flux) with the deviations respectively; 31.94% deviation of the experimental flux from the normal condition (predicted flux) for 25% flux , 53.23% deviation of the experimental flux from the normal condition (predicted flux) for 50% flux, 51.05% deviation of the experimental flux from the normal condition (predicted flux) for 75% flux and 77.37% deviation of the experimental flux from the normal condition (predicted flux) for 100% flux. While the least deviation of experimental flux from the normal condition was recorded by test 4 having [0 1 0] configuration i.e. [low concentration, medium voltage, TTT crystal location] with 0.94% deviation of the experimental flux from the normal condition (predicted flux) for 25% flux, 3.92% deviation of the experimental flux from the normal condition (predicted flux) for 50% flux, 3.07% deviation of the experimental flux from the normal condition (predicted flux) for 75% flux and 6.45% deviation of the experimental flux from the normal condition (predicted flux) for 100% flux. All these deviations are presented in Table 4.3.

Table 4.6. Run 2 high flux tests

Run	Test	Concentration (A)	Voltage (B)	Piezo Location (C)	25% Experimental Flux ($Lm^{-2}h^{-1}$)	50% Experimental Flux ($Lm^{-2}h^{-1}$)	75% Experimental Flux ($Lm^{-2}h^{-1}$)	100% Experimental Flux ($Lm^{-2}h^{-1}$)
2	1	0	0	0	40.50	33.75	30.50	29.25
2	12	1	0	2	42.25	41.25	39.62	38.50
2	14	1	1	1	40.00	34.00	35.00	32.75
2	15	1	1	2	43.25	31.50	28.25	28.25

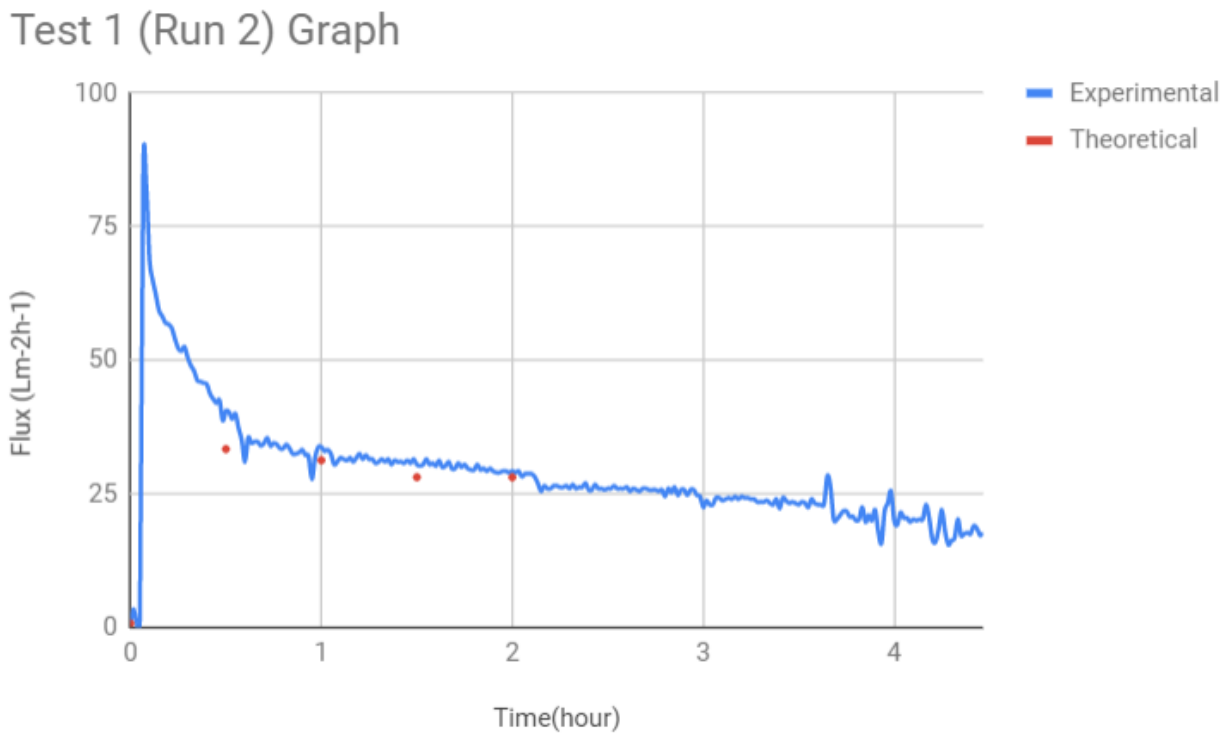

Figure 4.27. Experimental and best fit graphs of Test 1 (Run 2) against time

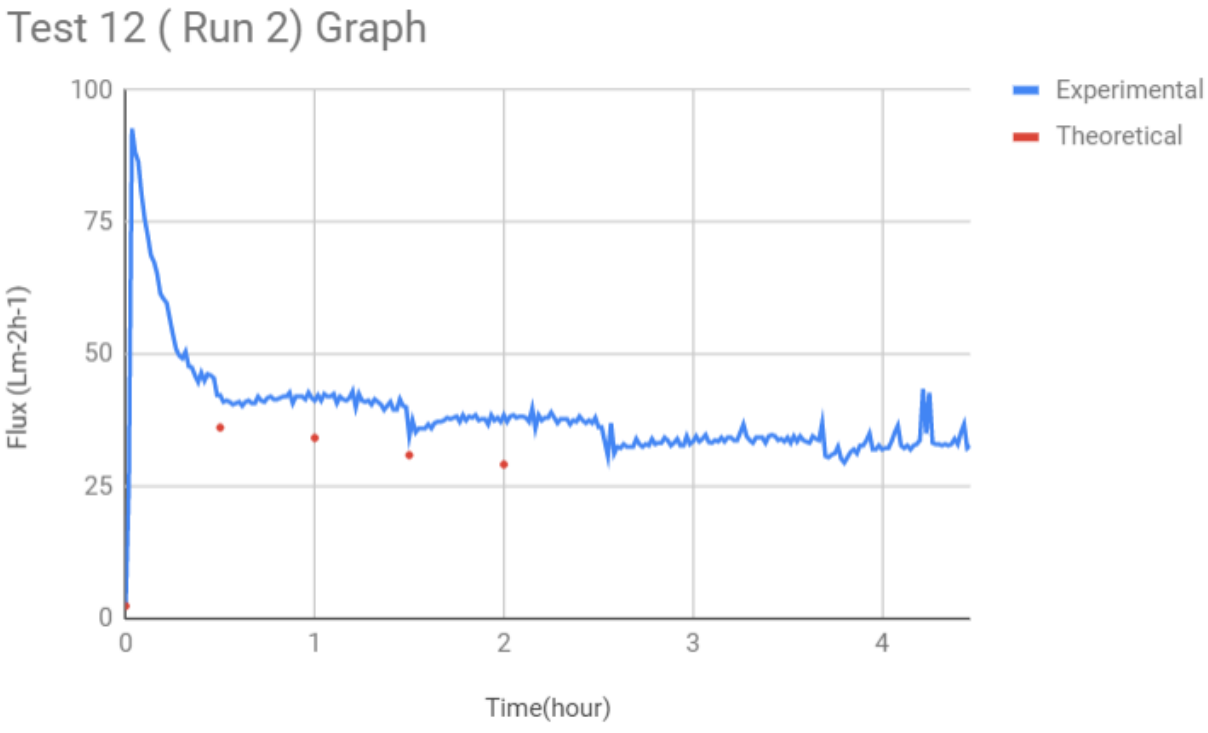

Figure 4.28. Experimental and best fit graphs of Test 12 (Run 2) against time

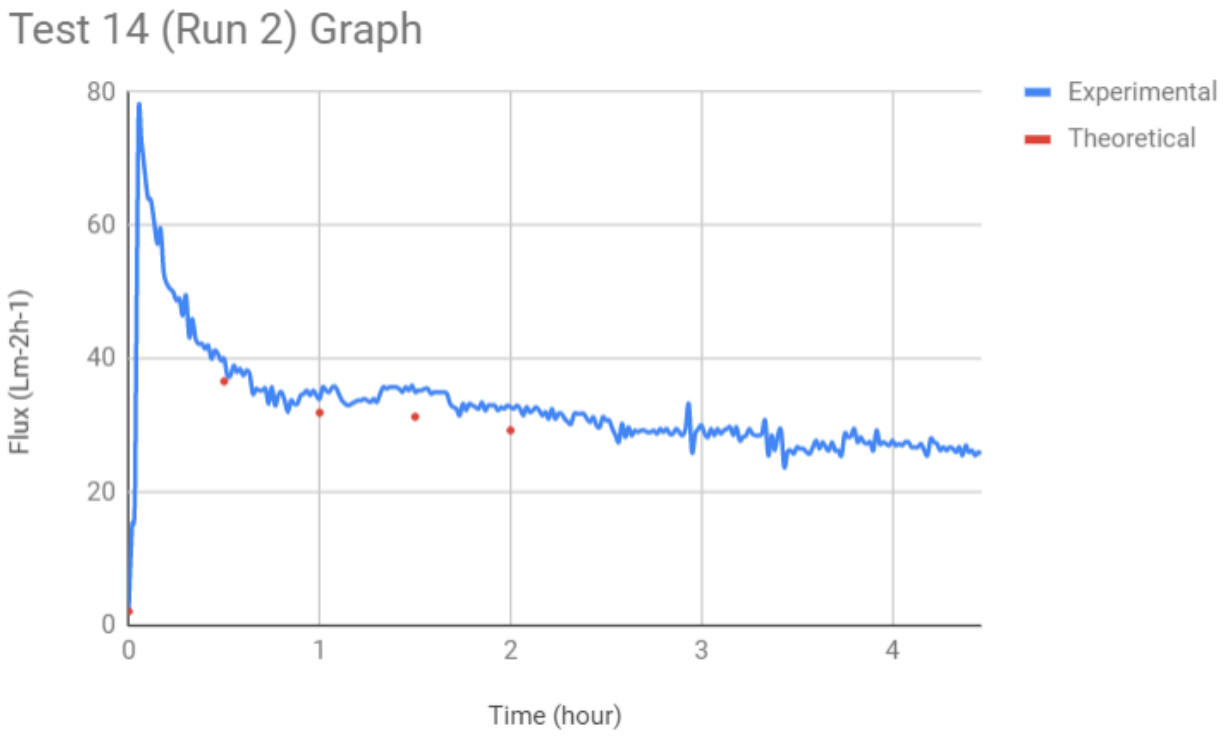

Figure 4.29. Experimental and best fit graphs of Test 14 (Run 2) against time

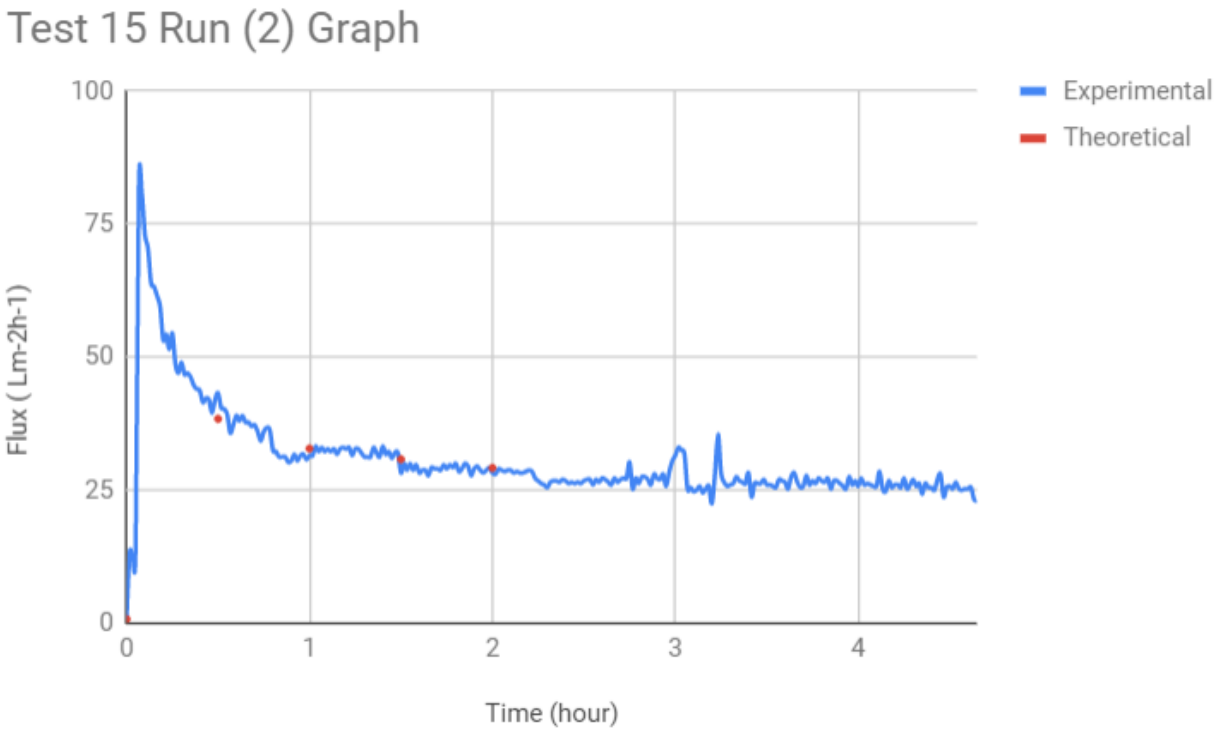

Figure 4.30. Experimental and best fit graphs of Test 15 (Run 2) against time

The high flux tests for run 2 are presented in Table 4.6 while figures 4.27 – 4.30 present the graphical representations of the experimental and predicted fluxes in single graphs.

Of all the high flux tests of run 2, the experimental flux of Test 12 with [1 0 2] configuration i.e. [medium concentration, low voltage, TBT crystal location] deviated most from the normal condition (predicted flux) with 16.87% deviation of the experimental flux from the normal condition (predicted flux) for 25% flux, 20.72% deviation of the experimental flux from the normal condition (predicted flux) for 50% flux, 28.10% deviation of the experimental flux from the normal condition (predicted flux) for 75% flux and 32.03 % deviation of the experimental flux from the normal condition (predicted flux) for 100% flux while the least deviation of experimental flux from the normal condition was recorded by test 15 having [1 1 2] configuration i.e. [medium concentration, medium voltage, TBT crystal location], with 12.63 % deviation of the experimental flux from the normal condition (predicted flux) for 25% flux, 4% deviation of the experimental flux from the normal condition (predicted flux) for 50% flux, 8.31% deviation of the experimental flux from the normal condition (predicted flux) for 75% flux and 3.12% deviation of the experimental flux from the normal condition (predicted flux) for 100% flux.

Considering all the conducted experiments of run 2, the experimental flux of Test 10 (run 2) with [1 0 0] configuration i.e. [medium concentration, low voltage, TTT crystal location] deviated most from the normal condition (predicted flux) with the deviations respectively; 35.56% deviation of the experimental flux from the normal condition (predicted flux) for 25% flux , 26.10% deviation of the experimental flux from the normal condition (predicted flux) for 50% flux, 29.24% deviation of the experimental flux from the normal condition (predicted flux) for 75% flux and 26.47% deviation of the experimental flux from the normal condition (predicted flux) for 100% flux. While the least deviation of experimental flux from the normal condition was recorded by Test 22 having [2 1 0] configuration i.e. [high concentration, medium voltage, TTT crystal location] with 0.97% deviation of the experimental flux from the normal condition (predicted flux) for 25% flux, 2.95% deviation of the experimental flux from the normal condition (predicted flux) for 50% flux, 0.55% deviation of the experimental flux from the normal condition (predicted flux) for 75% flux and 0.52% deviation of the experimental flux from the normal condition (predicted flux) for 100% flux. All these deviations are recorded in Table 4.4.

Table 4.7. Error range for Run 1 and Run 2 high flux tests

Error Range	25% Best Fit	50% Best Fit	75% Best Fit	100% Best Fit
Run 1 Error Range	1.34 - 41.50	6.30 - 49.38	0.81 - 48.05	6.75 - 33.28
Run 1 Average Error	21.42	27.84	24.43	20.02
Run 2 Error Range	12.63 - 16.87	4 - 20.72	8.31 - 28.10	3.12 - 32.02
Run 2 Average Error	14.75	12.36	18.21	17.57

The error range (Table 4.7) shows that the experimental high flux tests of run 1 are more deviated from the normal condition (predicted flux) than that of run 2 even though run 1 produced more tests with high flux than run 2. While the lowest average error for run 1 was 20.02, that for run 2 was found to be 12.36.

5. DISCUSSION AND CONCLUSION

5.1 Discussion

The objectives of this research have been to effectively reduce the rate with which particles clog up the pores on the membrane and optimize its permeate flux production which in turn could eliminate back wash as often used in industries (like water treatment plants) that utilize membrane in their production processes. The first approach towards the objectives was a comprehensive review of most of the past work done on this area. With this review, different research questions were generated in order to help strengthen the knowledge needed for the research. The research questions are as listed below:

RQ 1. What are the most important variables for reducing membrane fouling in UF system incorporating piezoelectrics for vibration?
RQ 2. What range of the variables should be tested?
RQ 3. What combination of the level of the variables will optimize the permeate flux?

In seeking answers to these research questions, membrane fouling experiments were conducted in two runs, run 1 and run 2 respectively. The design of experiment (DOE) approach was adopted to determine the different combinations of the factors under study. These combinations are the different experiments that are needed to be conducted in order to fully investigate the issue at hand. The DOE approach yielded 3^3 (i.e. 27) experiments. The experimental results obtained from the experiments were used to generate the different best fit equations for 25%, 50%, 75% and 100% experimental fluxes. These served as the basis used for the 25%, 50%, 75% and 100% predicted results used for the result analysis. Scanning Electron Microscope (SEM) imaging was used to understand the different constituents of the neutral membrane before the experiments. This was used to compare the images of the membrane obtained at the end of the different experiments. Energy Dispersive Spectroscopy (EDS) was used to identify the different elements and their respective proportion by mass present in the neutral membrane as well as that present after each experiment was conducted. The following answers were provided for the research questions during the research.

RQ 1. What are the most important variables for reducing membrane fouling in UF system incorporating piezoelectrics for vibration?

Having studied the different stages of membrane fouling and having looked at different factors affecting the fouling of membrane, the important variables for membrane fouling in UF system incorporating piezoelectrics for vibration are grouped into two categories:

i. Piezoelectrics: Under this category, the important factors are; Type of piezoelectrics crystal, Size of piezoelectrics crystal, Number of piezoelectrics crystals, Location of Piezoelectric crystal and the Applied voltage. Of all these variables, the type, size and number of crystals were fixed while location of piezoelectrics and the applied voltage were varied accordingly in this work.

ii. The Feed water: Under this category, the important factors are; Foulant type and the concentration of the foulant. The foulant type was fixed while the concentration of the foulant was varied.

RQ 2. What range of the variables should be tested?

i. The location of the piezoelectric crystals

As has been earlier mentioned in section 3.6, three positions were investigated in this research. They are namely: (a) Placing the three crystals on top of the membrane equally spaced out from one another i.e. top-top-top denoted as TTT. (b) Placing the three crystals in such a way that one is on top, one is by the side while the last one is at the bottom i.e. top-side-down denoted as TSD. (c) Placing the crystals in such a way that one is on top, one is at the bottom while the last is on top i.e. top-bottom-top denoted as TBT. This choice was due to the three-level factorial design adopted for the research. TTT position was assigned low level, TSD position was assigned medium level while TBT was assigned high level. The corresponding effects of these location are measured by their respective permeate flux production. The considered locations are the locations that produced high flux in run 1 and run 2 respectively.

ii. The voltage with which the piezoelectric is vibrated

Since 3-level factorial design was adopted for this research, 3 levels of voltage were used. The low voltage (2V dc), the medium voltage (3V dc) and the high voltage (4V dc). These different voltages had different and unique effects on the produced flux for run 1 and run 2.

iii. The concentration of the foulant

The fouling medium as used in the experiments was garden soil. The garden soil was collected in 3 stages: the low concentration, the medium concentration and high concentration. This was due to the 3- level factorial design adopted for the DOE as stated earlier in section 3.6. This led to the categorization of each of the factors understudy into 3: low, medium and high. The low concentration of the fouling medium used was 2g of soil to 500grams of water. The medium concentration of fouling medium used was 3g of soil to 500grams of water while the high concentration used was 4grams of soil to 500grams of water. It however, has to be noted that as the filtration time increases, the concentration of the foulant in the feed suspension continually increases, this is due to the fact that as the filtration continues and the permeate is collected, the quantity of the feed suspension continues decreasing while the foulants are being trapped in the filtration system (the membrane). The trapped foulants continue their journey into the feed water and gets circulated throughout the system, leading to a more concentrated feed suspension. The effect of this more concentrated suspension on the fouling of the membrane is beyond the scope of this research and thus was not considered. This is left as future work for this research and has to be investigated.

RQ 3. What combination of the level of the variables will optimize the permeate flux?

The combination of the level of the variables that will optimize the permeate flux was obtained from tests that recorded high flux. These high flux tests satisfy the following conditions:

i. 40 $Lm^{-2}h^{-1}$ flux cutoffs for 25% best fit for all runs
ii. 30 $Lm^{-2}h^{-1}$ flux cutoffs for 75% best fit for all runs
iii. 25 $Lm^{-2}h^{-1}$ flux cutoffs for 100% best fit for all runs

For better understanding and clarity, the comparison was not made for only run 1 and run 2. Best fit equations were also generated for both runs and their results were also incorporated in this comparison. The 50% best fit was not included in this comparison because there was no single flux cutoff that could fit all the runs thereby giving no basis for a level comparison among all the runs. The different crystal location, voltage and feedwater concentration involved were respectively analyzed as follows:

i. Performance by crystal location analysis

The performance by piezoelectric crystal location was carefully analyzed and presented in figures 5.1 (a) – (i) as follows:

25% best fit with 40 $Lm^{-2}h^{-1}$ for all runs:

Run 1 Run 2 Both runs

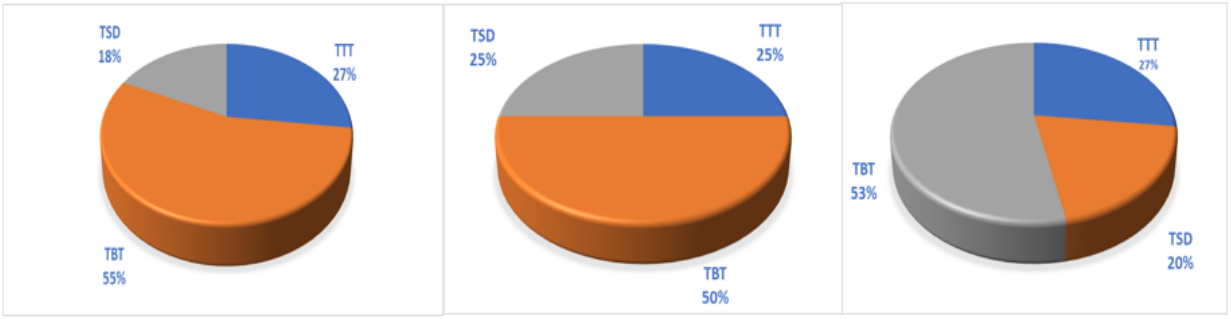

(a) (b) (c)

75% best fit with 30 $Lm^{-2}h^{-1}$ for all runs:

Run 1 Run 2 Both runs

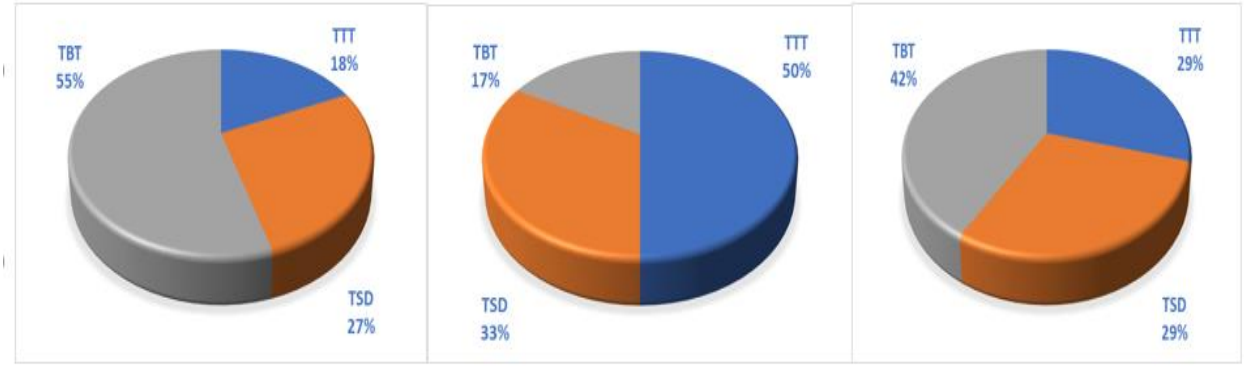

(d) (e) (f)

Figure 5.1(a) Run 1 high flux tests' performance by crystal location for 25% best fit (b) Run 2 high flux tests' performance by crystal location for 25% best fit (c) Both runs high flux tests' performance by crystal location for 25% best fit (d) Run 1 high flux tests' performance by crystal location for 75% best fit (e) Run 2 high flux tests' performance by crystal location for 75% best fit (f) Both runs high flux tests' performance by crystal location for 75% best fit (g) Run 1 high flux tests' performance by crystal location for 100% best fit (h) Run 2 high flux tests' performance by location for 100% (i) Both runs high flux performance by location for 100%

100% best fit with 25 $Lm^{-2}h^{-1}$ for all runs:

..Figure 5.1. cont'd

Run 1 Run 2 Both runs

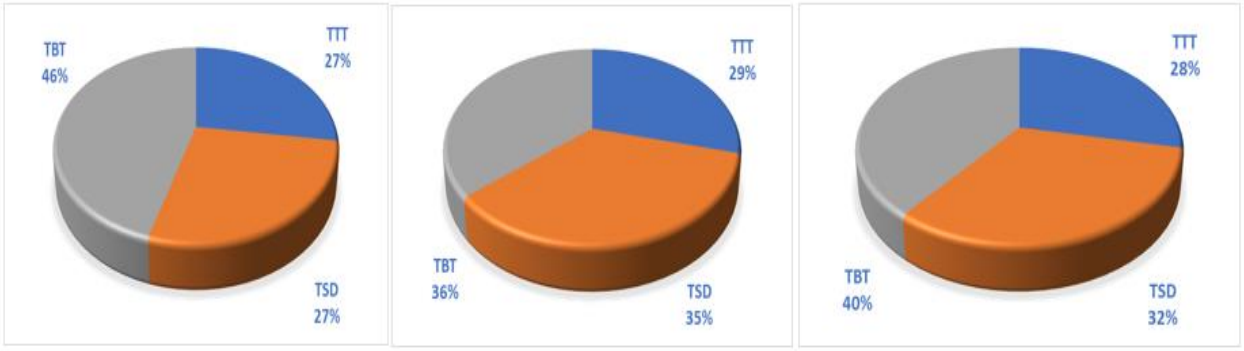

(g) (h) (i)

With 55%, 50% and 53% of all the high flux tests of run 1, run 2 and Both runs respectively coming from the TBT location; TBT location becomes the most important location for high flux production for all the runs for 25% best fit. 75% best fit has TBT location performing well in Run 1 and Both runs with respectively 55% and 42% of all high flux tests coming from this location. However, TBT location did not perform so well in Run 2. With 17% of all high flux tests coming from the TBT location; this location recorded the lowest number of high flux tests in Run 2. 46%, 36% and 40% of all high flux tests of Run 1, Run 2 and Both runs respectively for 100% best fit were recorded by the TBT location.

ii. Performance by voltage level analysis

The performance by voltage level was carefully analyzed and presented in figures 5.2 (a) – (i) as follows:

25% best fit with 40 $Lm^{-2}h^{-1}$ cutoffs for all runs:

Run 1 Run 2 Both runs

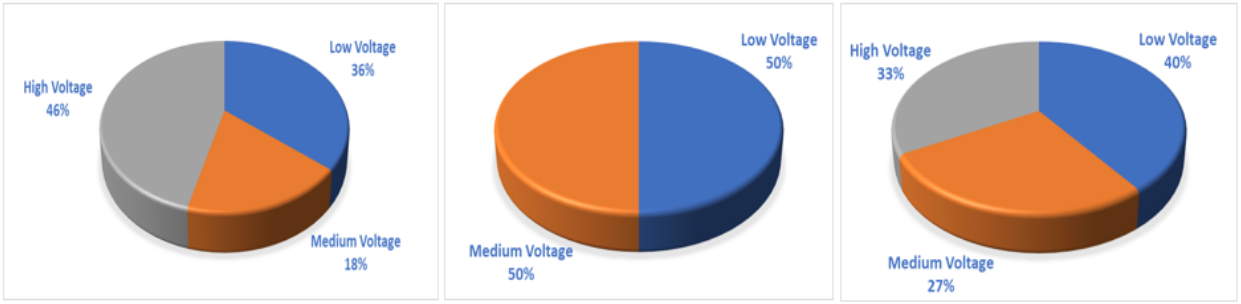

(a) (b) (c)

75% best fit with 30 $Lm^{-2}h^{-1}$ cutoffs for all runs:

Run 1 Run 2 Both runs

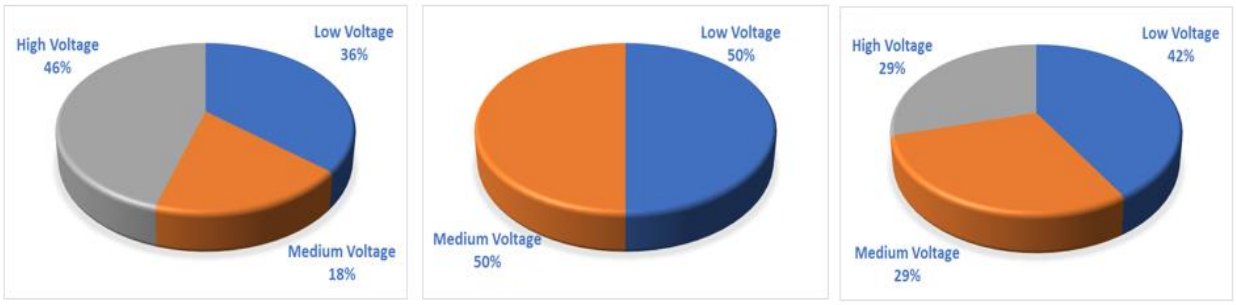

(d) (e) (f)

Figure 5.2 (a) Run 1 high flux tests' performance by voltage level for 25% best fit (b) Run 2 high flux tests' performance by voltage level for 25% best fit (c) Both runs high flux tests' performance by voltage level for 25% best fit (d) Run 1 high flux tests' performance by voltage level for 75% best fit (e) Run 2 high flux tests' performance by voltage level for 75% best fit (f) Both runs high flux tests' performance by voltage level for 75% best fit (g) Run 1 high flux tests' performance by voltage level for 100% best fit (h) Run 2 high flux tests' performance by voltage level for 100% best fit (i) Both runs high flux tests' performance by voltage level for 100% best fit

Figure 5.2 cont'd

100% best fit with 25 $Lm^{-2}h^{-1}$ for all runs:

Run 1 Run 2 Both runs

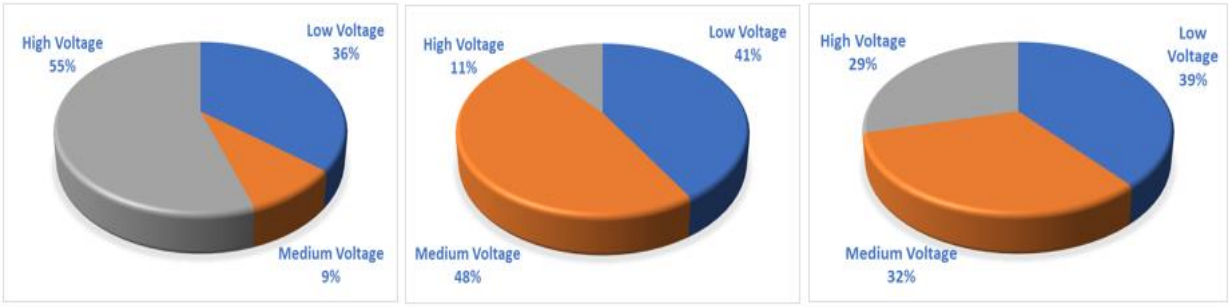

(g) (h) (i)

With 50% and 40% of all the high flux tests for Run 2 and Both runs coming from low voltage; low voltage performed best in these runs while high voltage performed best in run 1 after having 46% of all high flux tests for 25% best fit. The scenario played out for 75% best fit while for 100% best fit, low voltage did not perform outstandingly well because it continually recorded the second-best results in Run 1 and Run 2. But, taking a close look at the general performance of the voltage level reveals that it performed better than the others at this stage.

iii. Performance by feed water concentration level analysis

25% best fit with 40 $Lm^{-2}h^{-1}$ cutoffs for all runs:

The performance by feed water concentration level was carefully analyzed and presented in figures 5.3 (a) - (i) as follows:

Run 1 Run 2 Both runs

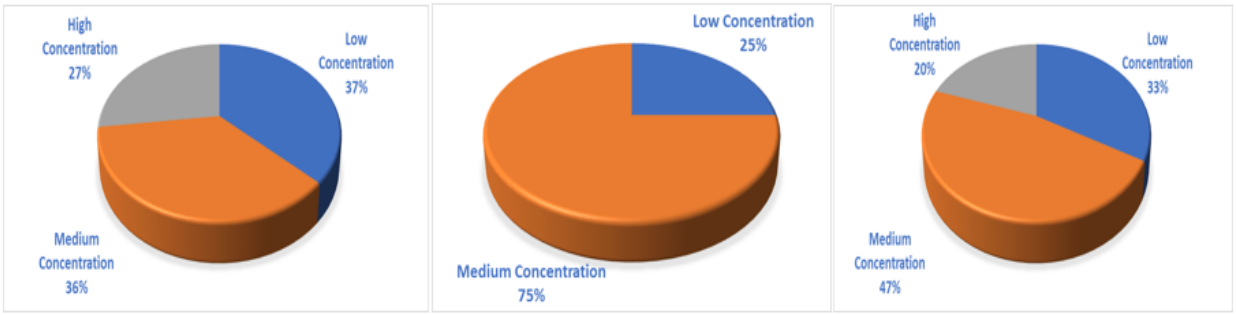

(a) (b) (c)

75% best fit with 30 $Lm^{-2}h^{-1}$ cutoffs for all runs:

Run 1 Run 2 Both runs

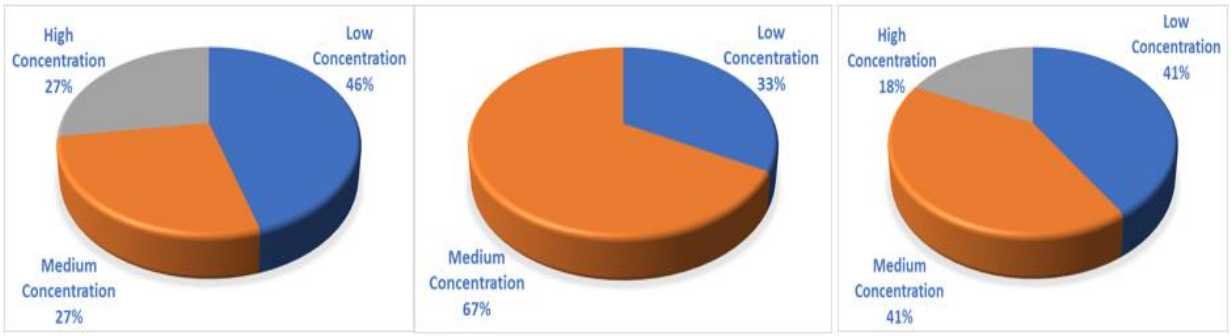

(d) (e) (f)

100% best fit with 25 $Lm^{-2}h^{-1}$ for all runs:

Run 1 Run 2 Both runs

Figure 5.3 (a) Run 1 high flux tests' performance by feedwater concentration level for 25% best fit (b) Run 2 high flux tests' performance by feedwater concentration level for 25% best fit (c) Both runs high flux tests' performance by feedwater concentration level for 25% best fit (d) Run 1 high flux tests' performance by feedwater concentration level for 75% best fit (e) Run 2 high flux tests' performance by feedwater concentration level for 75% best fit (f) Both runs high flux tests' performance by feedwater concentration level for 75% best fit (g) Run 1 high flux tests' performance by feedwater concentration level for 100% best fit (h) Run 2 high flux tests' performance by feedwater concentration level for 100% best fit (i) Both runs high flux tests' performance by feedwater concentration level for 100% best fit

Figure 5.3 cont'd

100% best fit with 25 $Lm^{-2}h^{-1}$ for all runs:

Run 1 Run 2 Both runs

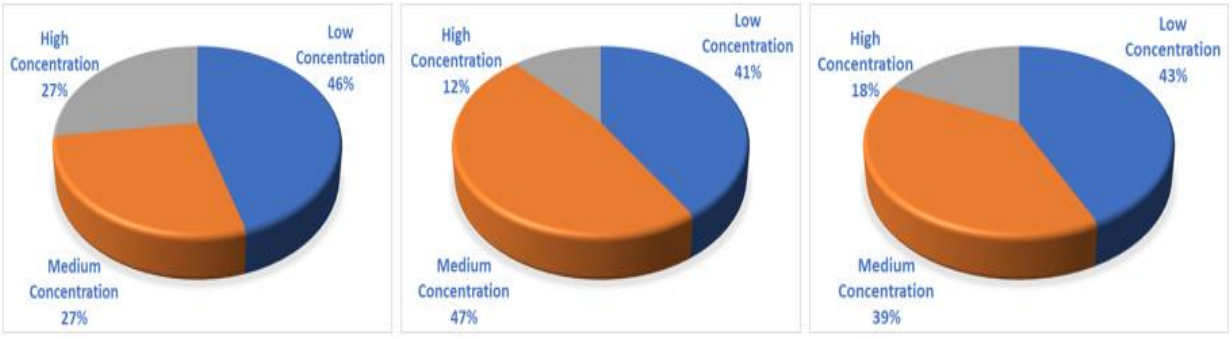

(g) (h) (i)

For 25% best fit, medium concentration performed best for all runs, having recorded respectively 36%, 75% and 47% of all high flux tests at this stage. Medium and low concentrations performed equally at 75% best fit stage while for 100% best fit stage, low voltage constantly outperformed every other concentration level for all runs; having recorded 46%, 41% and 43% of all high flux test respectively for Run 1, Run 2 and Both runs.

5.2. Conclusion

In this thesis, thorough literature review was conducted on membrane and the different works done on the use of membrane for water filtration. Piezoelectrics was also reviewed together with the work done on using membrane and piezoelectrics for water purification. Membrane surface analysis was also carried to determine the extent of fouling of the vibrated and non-vibrated membranes. Three factors (involved in membrane fouling) namely vibration voltage of the piezoelectrics, concentration of the feed water and location of piezoelectrics were also extensively studied to understand the most important factor for membrane fouling reduction. A design of experiment approach (DOE) was adopted to obtain the different experimental combinations for the variables being investigated. With the DOE approach, 3^3 number of experiments were needed to be conducted to fully investigate the three important variables that would be optimized in order to reduce membrane fouling which in turn could help to eliminate backwash in industries that

utilize membrane in their production process. These 27 experiments were carried out in two runs; namely Run 1 and Run 2. Different best fit / predicted equations and results were developed for both runs from 25%, 50%, 75% and 100% experimental results of run 1 and run 2. The deviation which was a measure of how far the experimental results are from the predicted results was also determined for both runs of the experiments.

The obtained results from the membrane surface analysis revealed that the drastic reduction in flux experienced by the non-vibrated membrane was due to the total surface covering by a cake layer while for the vibrated surface, the reduced rate of flux reduction was due to the interstitial cracks introduced between the cake layers by the vibratory action of the piezoelectrics.
That from the variables revealed that, vibrating the membrane with low voltage (level 0), keeping the feed water concentration at low level (Level 0) or medium level (level 1) and placing the crystals at TBT locations (level 2) could yield the highest permeate flux. Although the fluxes are different for the individual runs, they are not that different in terms of the level that seems the best. TBT location recorded the most consistent high flux test for all runs, hence a very important variable.

5.2.1 Recommendations/Future Work

The major source of inconsistency in the obtained results for run 1 and run 2 could be due to the two different pumps used differently for run 1 and run 2 respectively in the course of this research. The pump used for run 1 became faulty and was replaced with another similar pump. This new pump was used for run 2. To ensure a consistency in the results and optimize the flux production, one pump is recommended for both runs.

As was mentioned earlier in this work, the feed water gets more concentrated as the filtration continues. The effect of this on fouling rate was not considered in this research and is beyond the scope of this work. Further study is recommended on this effect and how it affects fouling rate
Finally, a study is recommended for an outside-in-flow system to investigate how the fouling reduction will be affected when the outer part of the membrane is exposed to the feed water.

REFERENCES

[1] Kuscer, D., Rojac, T., Belavič, D., Santo Zarnik, M., Bradeško, A., Kos, T., ... & Faccini, M. (2017). Integrated piezoelectric vibration system for fouling mitigation in ceramic filtration membranes. *Journal of membrane science*, *540*, 277-284.

[2] Li, K., Liang, H., Qu, F., Shao, S., Yu, H., Han, Z. S., ... & Li, G. (2014). Control of natural organic matter fouling of ultrafiltration membrane by adsorption pretreatment: Comparison of mesoporous adsorbent resin and powdered activated carbon. *Journal of membrane science*, *471*, 94-102.

[3] Ma, Z., Lu, X., Wu, C., Gao, Q., Zhao, L., Zhang, H., & Liu, Z. (2017). Functional surface modification of PVDF membrane for chemical pulse cleaning. *Journal of membrane science*, *524*, 389-399.

[4] Abid, H. S., Johnson, D. J., Hashaikeh, R., & Hilal, N. (2017). A review of efforts to reduce membrane fouling by control of feed spacer characteristics. *Desalination*, *420*, 384-402.

[5] Bae, J., Baek, I., & Choi, H. (2017). Efficacy of piezoelectric electrospun nanofiber membrane for water treatment. *Chemical Engineering Journal*, *307*, 670-678.

[6] Koo, C. H., Mohammad, A. W., & Talib, M. Z. M. (2012). Review of the effect of selected physicochemical factors on membrane fouling propensity based on fouling indices. *Desalination*, *287*, 167-177.

[7] Cai, M., Zhao, S., & Liang, H. (2010). Mechanisms for the enhancement of ultrafiltration and membrane cleaning by different ultrasonic frequencies. *Desalination*, *263*(1-3), 133-138.

[8] Shi, X., Tal, G., Hankins, N. P., & Gitis, V. (2014). Fouling and cleaning of ultrafiltration membranes: A review. *Journal of Water Process Engineering*, *1*, 121-138.

[9] Mohammad, A. W., & Hankins, N. (2014). The Journal of Water Process Engineering.

[10] Krinks, J. K., Qiu, M., Mergos, I. A., Weavers, L. K., Mouser, P. J., & Verweij, H. (2015). Piezoceramic membrane with built-in ultrasonic defouling. *Journal of Membrane Science*, *494*, 130-135.

[11] Sands, T. and Kenny, T., 2017. Experimental piezoelectric system identification. *Journal of Mechanical Engineering and Automation*, *7*, pp.179- 195.

[12] Li, H., Tian, C., & Deng, Z. D. (2014). Energy harvesting from low frequency applications using piezoelectric materials. *Applied physics reviews*, *1*(4), 041301.

[13] Coster, H.G.L., Farahani, T.D. and Chilcott, T.C., 2011. Production and characterization of piezo-electric membranes. *Desalination*, *283*, pp.52-57.

[14] Kuscer, D., Rojac, T., Belavič, D., Santo Zarnik, M., Bradeško, A., Kos, T., ... & Faccini, M. (2017). Integrated piezoelectric vibration system for fouling mitigation in ceramic filtration membranes. *Journal of membrane science*, *540*, 277-284.

[15] Darestani, M. T., Coster, H. G. L., & Chilcott, T. C. (2013). Piezoelectric membranes for separation processes: Operating conditions and filtration performance. *Journal of membrane science*, *435*, 226-232.

[16] T. Gaede, H., Patel and J. Patel., 2017. *Water filtration system using piezoelectric crystals.* Senior design project, 2017. Purdue University Northwest.

[17] Aronu, O., Abramowitz, H., & Nnanna, A. G. (2019, November). Membrane Fouling Mitigation in Water Filtration Using Piezoelectrics. In *ASME International Mechanical Engineering Congress and Exposition* (Vol. 59452, p. V008T09A006). American Society of Mechanical Engineers.

[18] Jhaveri, J. H., & Murthy, Z. V. P. (2016). A comprehensive review on anti-fouling nanocomposite membranes for pressure driven membrane separation processes. *Desalination*, *379*, 137-154.

[19] Voittonen, S. (2018). Minimization of Fouling for Treatment of Municipal Wastewater with Membrane Filtration.

[20] Singh, R. (2006). *Hybrid membrane systems for water purification: technology, systems design and operations*. Elsevier.

[21] Shamsuddin, N., Das, D. B., & Starov, V. M. (2015). Filtration of natural organic matter using ultrafiltration membranes for drinking water purposes: Circular cross-flow compared with stirred dead-end flow. *Chemical Engineering Journal*, *276*, 331-339.

[22] Membrane Based Separation, "2020". [Online]. Available at https://www.researchgate.net/figure/Membrane-based-separation-process_fig1_46253982 [Accessed 6 December 2020].

[23] Ladewig, B., & Al-Shaeli, M. N. Z. (2017). Fundamentals of membrane bioreactors. *Springer Transactions in Civil and Environmental Engineering*.

[24] Dick, G. H. (2015). Direct Membrane Filtration of Domestic Wastewater: Implications for Coupling with Anaerobic Membrane Bioreactor (DF-AnMBR) for Wastewater Resource Recovery.

[25] Basic facts about separation membranes, Spiral Wound Membranes, "2020". [Online] Available at: http://www.muro-chem.co.jp/en/en_business/en_knowledge.html [Accessed 6 December 2020].

[26] SynderFiltration,"HollowFiberMembranes,"2018.[Online]. Availableat:http://synderfiltration.com/learning-center/articles/module-configurations-process/hollowfiber-membranes/. [Accessed 22 December 2018].

[27] SynderFiltration, 'Tubular Membranes", 2019 [online]. Available at: https://synderfiltration.com/learning-center/articles/module-configurations-process/tubular-membranes/

[28] "Membrane classification based on size exclusion", 2020 [online]. Available at: types of water filtration membranes - Bing images [Accessed 2 December, 2020].

[29] Wankat, P. C. (2006). *Separation process engineering*. Pearson Education.

[30] Kang, G. D., & Cao, Y. M. (2014). Application and modification of poly (vinylidene fluoride) (PVDF) membranes–a review. *Journal of Membrane Science*, *463*, 145-165.

[31] Liu, F., Hashim, N.A., Liu, Y., Abed, M.M. and Li, K., 2011. Progress in the production and modification of PVDF membranes. *Journal of membrane science*, *375*(1-2), pp.1-27

[32] Chang, X., Wang, Z., Quan, S., Xu, Y., Jiang, Z., & Shao, L. (2014). Exploring the synergetic effects of graphene oxide (GO) and polyvinylpyrrodione (PVP) on poly (vinylylidenefluoride)(PVDF) ultrafiltration membrane performance. *Applied Surface Science*, *316*, 537-548.

[33] Oh, S. J., Kim, N., & Lee, Y. T. (2009). Preparation and characterization of PVDF/TiO2 organic–inorganic composite membranes for fouling resistance improvement. *Journal of Membrane Science*, *345*(1-2), 13-20.

[34] Hester, J. F., Banerjee, P., Won, Y. Y., Akthakul, A., Acar, A. M., & Mayes, A. M. (2002). ATRP of amphiphilic graft copolymers based on PVDF and their use as membrane additives. *Macromolecules*, *35*(20), 7652-7661.

[35] Mistry, V. V., & Maubois, J. L. (2017). Application of membrane separation technology to cheese production. In *Cheese* (pp. 677-697). Academic Press.

[36] Urtiaga, A. M., Pérez, G., Ibáñez, R., & Ortiz, I. (2013). Removal of pharmaceuticals from a WWTP secondary effluent by ultrafiltration/reverse osmosis followed by electrochemical oxidation of the RO concentrate. *Desalination*, *331*, 26-34.

[37] Zhang, W., Huang, G., Wei, J., & Yan, D. (2013). Gemini micellar enhanced ultrafiltration (GMEUF) process for the treatment of phenol wastewater. *Desalination*, *311*, 31-36.

[38] Eren, E., Sarihan, A., Eren, B., Gumus, H., & Kocak, F. O. (2015). Preparation, characterization and performance enhancement of polysulfone ultrafiltration membrane using PBI as hydrophilic modifier. *Journal of Membrane Science*, *475*, 1-8.

[39] Bae, J., Baek, I., & Choi, H. (2017). Efficacy of piezoelectric electrospun nanofiber membrane for water treatment. *Chemical Engineering Journal*, *307*, 670-678.

[40] Jiang, S., Li, Y., & Ladewig, B. P. (2017). A review of reverse osmosis membrane fouling and control strategies. *Science of the Total Environment*, *595*, 567-583.

[41] Pourbozorg, M., Li, T., & Law, A. W. K. (2017). Fouling of submerged hollow fiber membrane filtration in turbulence: Statistical dependence and cost-benefit analysis. *Journal of Membrane Science*, *521*, 43-52.

[42] Radaei, E., Liu, X., Tng, K. H., Wang, Y., Trujillo, F. J., & Leslie, G. (2018). Insights on pulsed bubble control of membrane fouling: Effect of bubble size and frequency. *Journal of Membrane Science*, *554*, 59-70.

[43] Rana, D., & Matsuura, T. (2010). Surface modifications for antifouling membranes. *Chemical reviews*, *110*(4), 2448-2471.

[44] Tu, S. C., Ravindran, V., & Pirbazari, M. (2005). A pore diffusion transport model for forecasting the performance of membrane processes. *Journal of Membrane Science*, *265*(1-2), 29-50.

[45] Vanysacker, L., Declerck, P., & Vankelecom, I. (2013). Development of a high throughput cross-flow filtration system for detailed investigation of fouling processes. *Journal of membrane science*, *442*, 168-176.

[46] Liu, Y., Liu, H., Cui, L., & Zhang, K. (2012). The ratio of food-to-microorganism (F/M) on membrane fouling of anaerobic membrane bioreactors treating low-strength wastewater. *Desalination*, *297*, 97-103.

[47] Ladewig, B., & Al-Shaeli, M. N. Z. (2017). Fundamentals of membrane bioreactors. *Springer Transactions in Civil and Environmental Engineering*.

[48] Kimura, K., Hane, Y., Watanabe, Y., Amy, G., & Ohkuma, N. (2004). Irreversible membrane fouling during ultrafiltration of surface water. *Water research*, *38*(14-15), 3431-3441.

[49] Katsoufidou, K., Yiantsios, S.G. and Karabelas, A.J., 2007. Experimental study of ultrafiltration membrane fouling by sodium alginate and flux recovery by backwashing. *Journal of Membrane Science*, *300*(1-2), pp.137-146.

[50] Huyskens, C., Brauns, E., Van Hoof, E., & De Wever, H. (2008). A new method for the evaluation of the reversible and irreversible fouling propensity of MBR mixed liquor. *Journal of membrane science*, *323*(1), 185-192.

[51] Meng, F., Chae, S. R., Drews, A., Kraume, M., Shin, H. S., & Yang, F. (2009). Recent advances in membrane bioreactors (MBRs): membrane fouling and membrane material. *Water research*, *43*(6), 1489-1512.

[52] Huang, J., Arthanareeswaran, G., & Zhang, K. (2012). Effect of silver loaded sodium zirconium phosphate (nanoAgZ) nanoparticles incorporation on PES membrane performance. *Desalination*, *285*, 100-107.

[53] Judd, S. (2008). The status of membrane bioreactor technology. *Trends in biotechnology*, *26*(2), 109-116.

[54] Ravazzini, A. M., Van Nieuwenhuijzen, A. F., & Van der Graaf, J. H. M. J. (2005). Direct ultrafiltration of municipal wastewater: comparison between filtration of raw sewage and primary clarifier effluent. *Desalination*, *178*(1-3), 51-62.

[55] Curie, J., & Curie, P. (1880). Développement par compression de l'électricité polaire dans les cristaux hémièdres à faces inclinées. *Bulletin de minéralogie*, *3*(4), 90-93.

[56] De Jong, M., Chen, W., Geerlings, H., Asta, M., & Persson, K. A. (2015). A database to enable discovery and design of piezoelectric materials. *Scientific data*, *2*(1), 1-13.

[57] Zou, L., Ge, C., Wang, Z. J., Cretu, E., & Li, X. (2017). Novel tactile sensor technology and smart tactile sensing systems: A review. *Sensors*, *17*(11), 2653.

[58] Piezoelectric effect "2014" [Online]. Available at https://www.cosmic-energy.org/?page_id=771 [Accessed 20 December 2018]

[59] Bansevičius, R., Telksnytė, S., Janušas, G., & Palevičius, A. (2011). Hybrid numerical-experimental investigation of two-degree-of-freedom piezoelectric positioning actuator. *Mechanics*, *17*(2), 182-186.

[60] Ahner, N., Gottschlich, D., Narang, S., Roberts, D., Sharma, S., & Ventura, S. (1993). Piezoelectrically assisted ultrafiltration. *Separation science and technology*, *28*(1-3), 895-908.

[61] N. Politis, S., Colombo, P., Colombo, G. and M. Rekkas, D., 2017. Design of experiments (DoE) in pharmaceutical development. *Drug development and industrial pharmacy*, *43*(6), pp.889-901.

[62] Hald, A., 1998. *A History of Mathematical Statistics from 1750 to 1930* (Vol. 2, No. 4). New York: Wiley.

[63] Fisher, R.A., 1992. The arrangement of field experiments. In *Breakthroughs in statistics* (pp. 82-91). Springer, New York, NY.

[64] Fischer, R.A., 1935. The design of experiments. 1st edn. New York: Hafner Publishing Company.

[65] Edwards, A.W., 2005. RA Fischer, statistical methods for research workers, (1925). In *Landmark Writings in Western Mathematics 1640-1940* (pp. 856-870). Elsevier Science.

[66] Weissman, S. A., & Anderson, N. G. (2015). Design of experiments (DoE) and process optimization. A review of recent publications. *Organic Process Research & Development*, *19*(11), 1605-1633.

[67] Mills, J. E. (2003). Design of experiments in pharmaceutical process research and development.

[68] Mullin, R., 2013. Design of Experiments Makes A Comeback. *Chem. Eng. News*, (April 1), pp.25-28.

[69] Pilipauskas, D. R. (1999). *Using Factorial Experiments in the Development of Process Chemistry* (pp. 411-428). Dekker: New York.

[70] Iritani, E. (2013). A review on modeling of pore-blocking behaviors of membranes during pressurized membrane filtration. *Drying technology*, *31*(2), 146-162.

APPENDIX A. RUN 1 GRAPHS

All the experiments carried out in Run 1 are presented in this section.

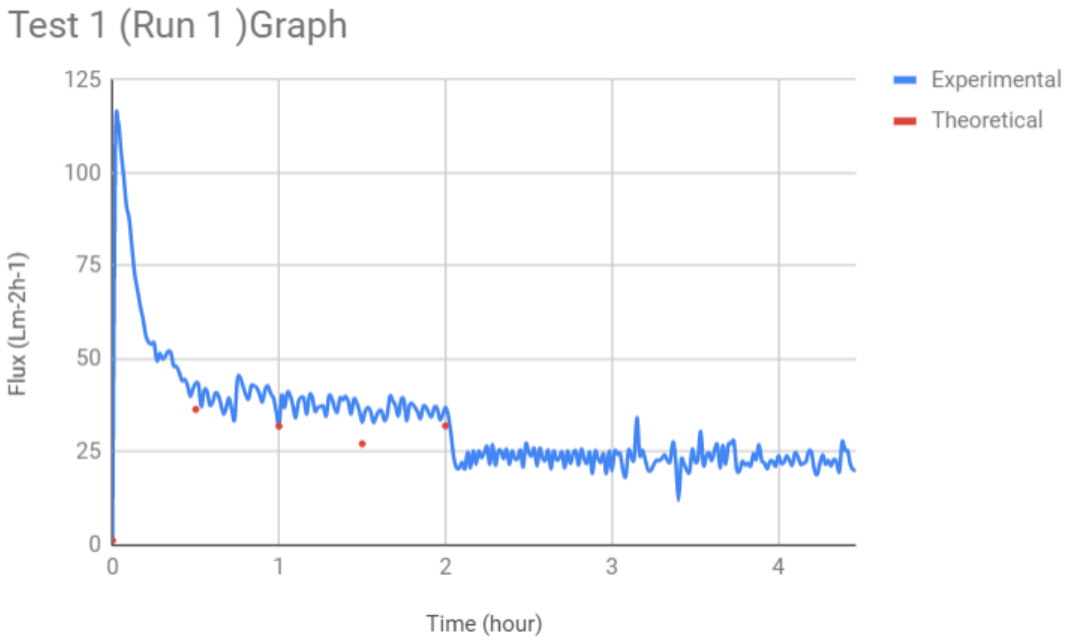

Experimental and best fit graphs of test 1 (Run 1) against time

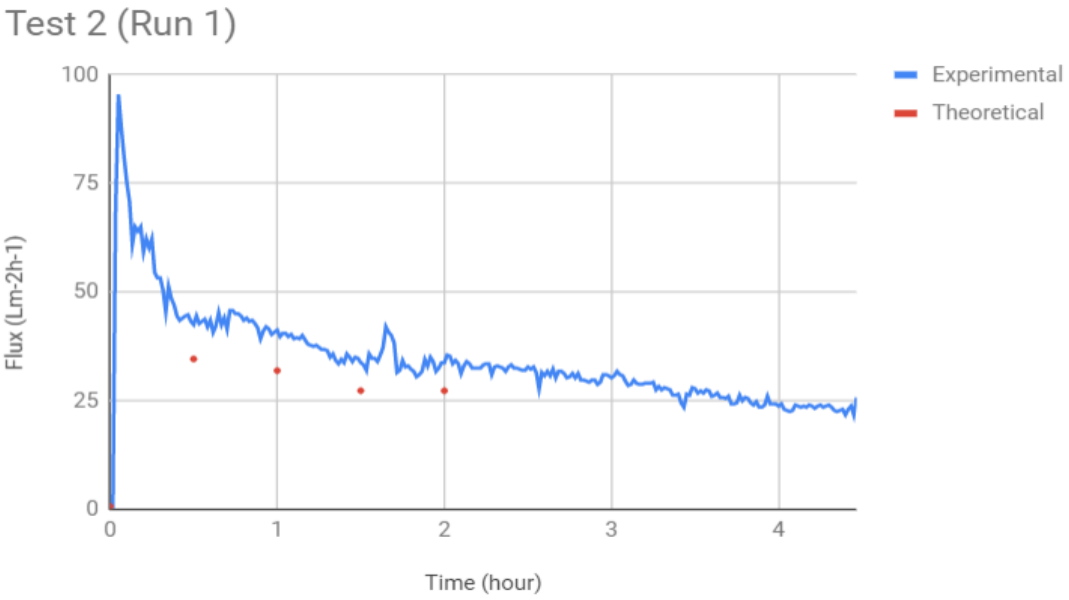

Experimental and best fit graphs of test 2 (Run 1) against time

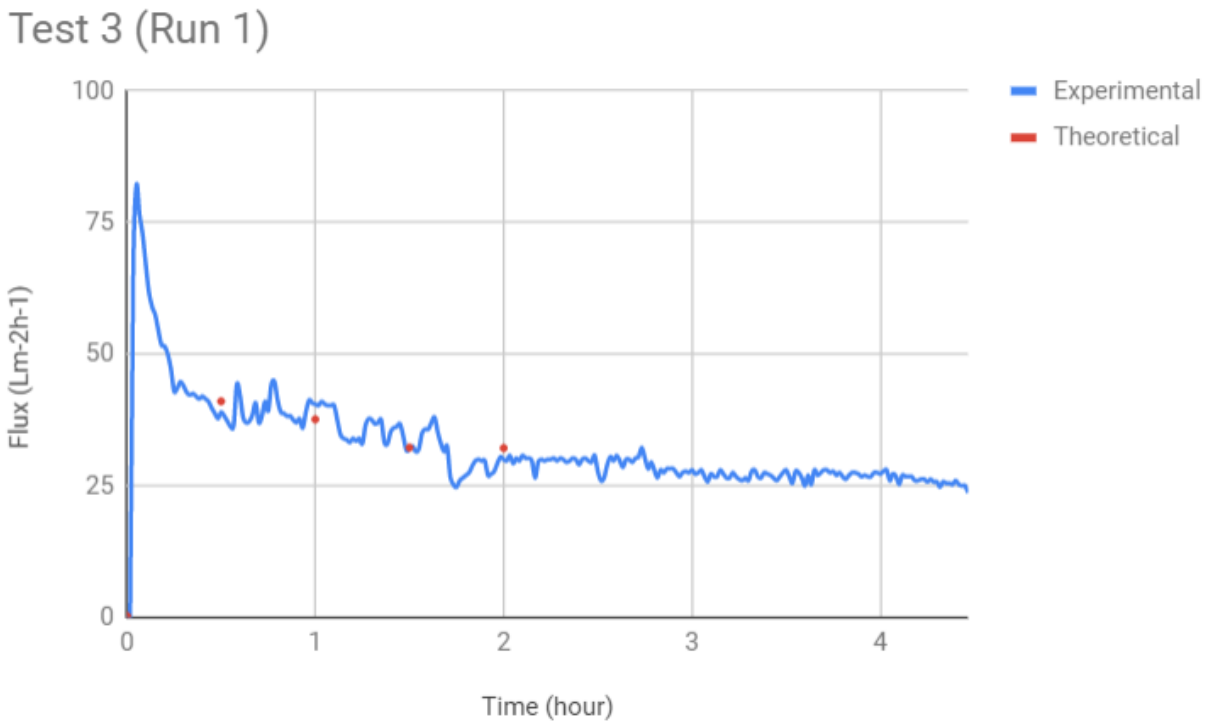

Experimental and best fit graphs of test 2 (Run 1) against time

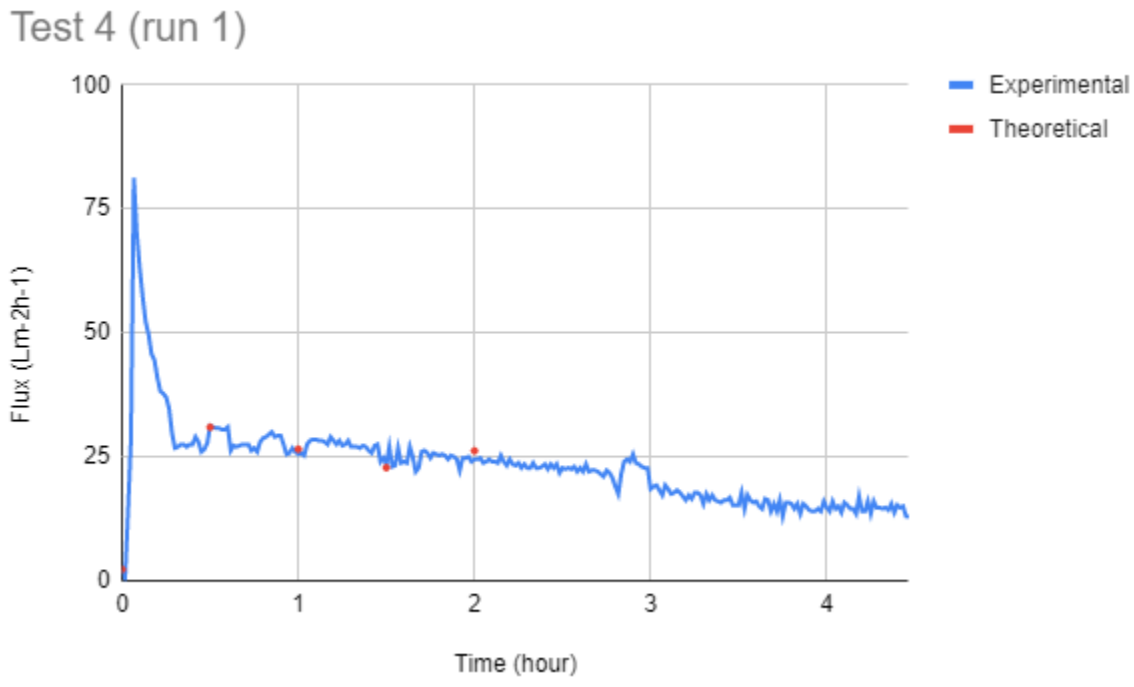

Experimental and best fit graphs of test 4 (Run 1) against time

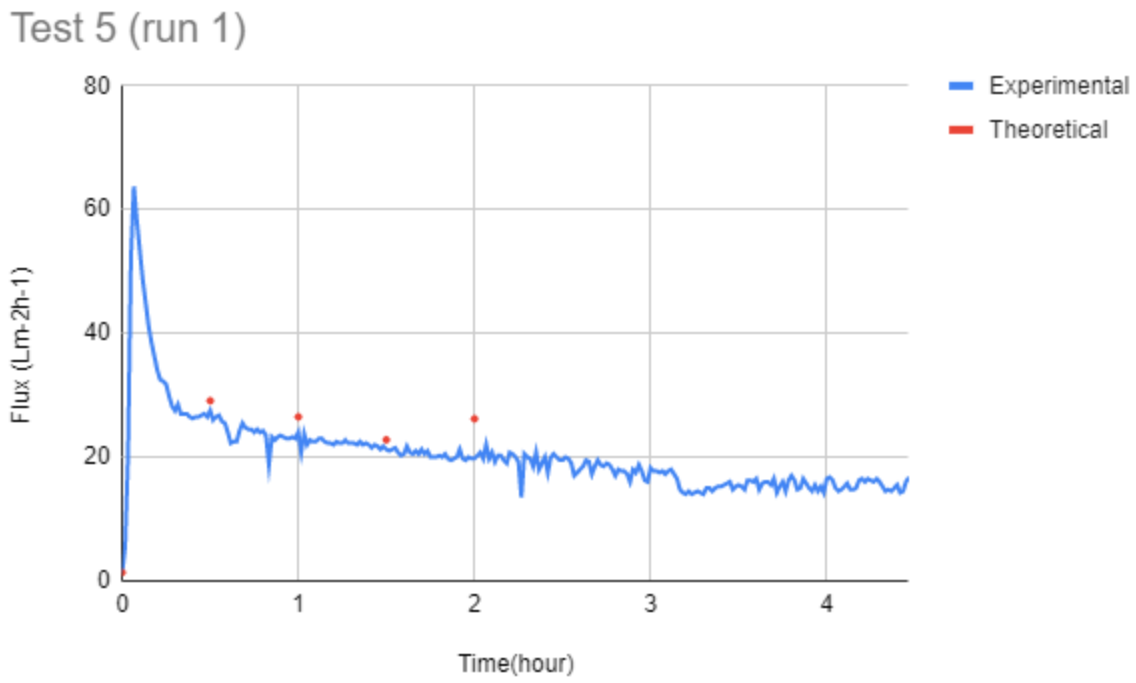

Experimental and best fit graphs of test 5 (Run 1) against time

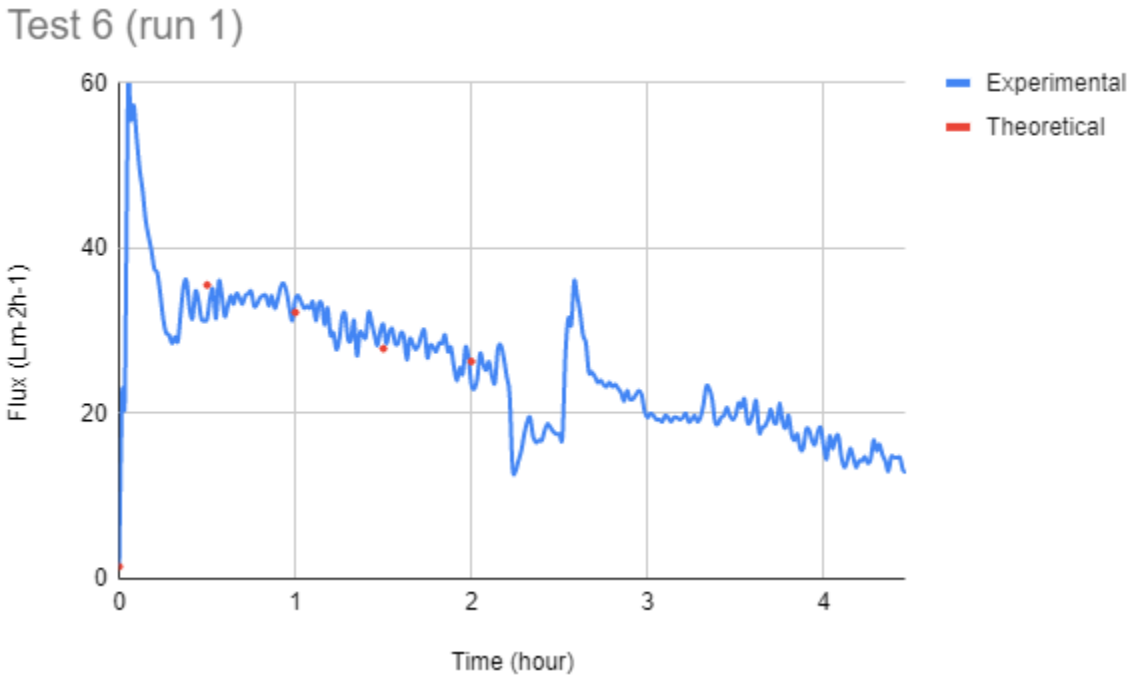

Experimental and best fit graphs of test 6 (Run 1) against time

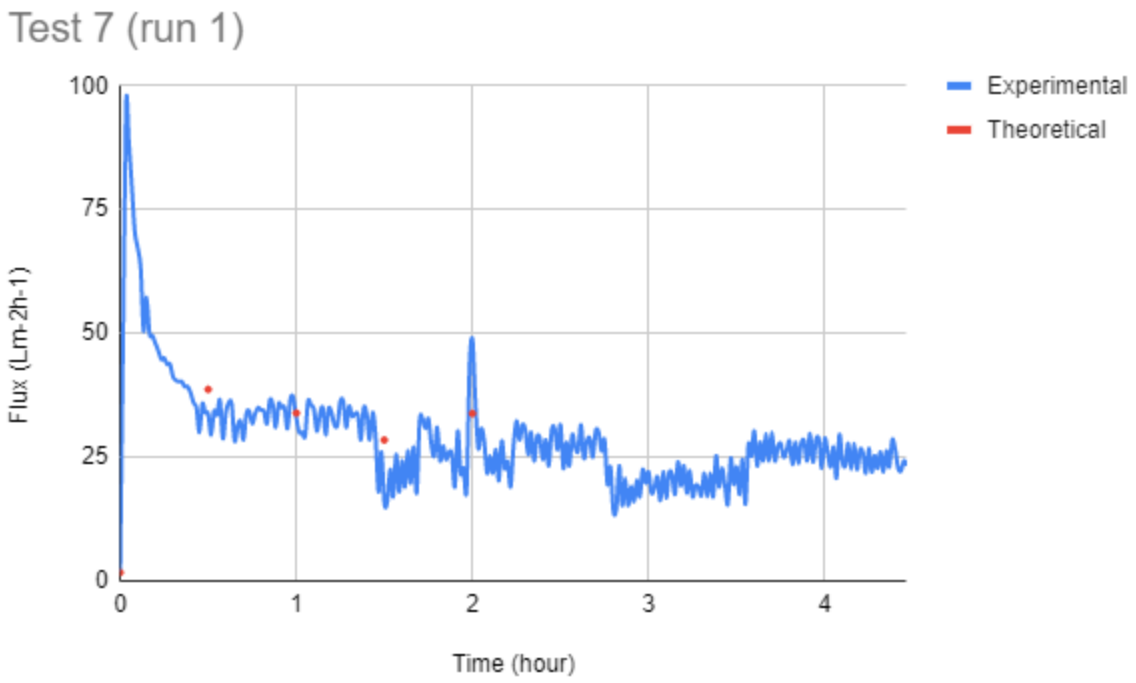

Experimental and best fit graphs of test 7 (Run 1) against time

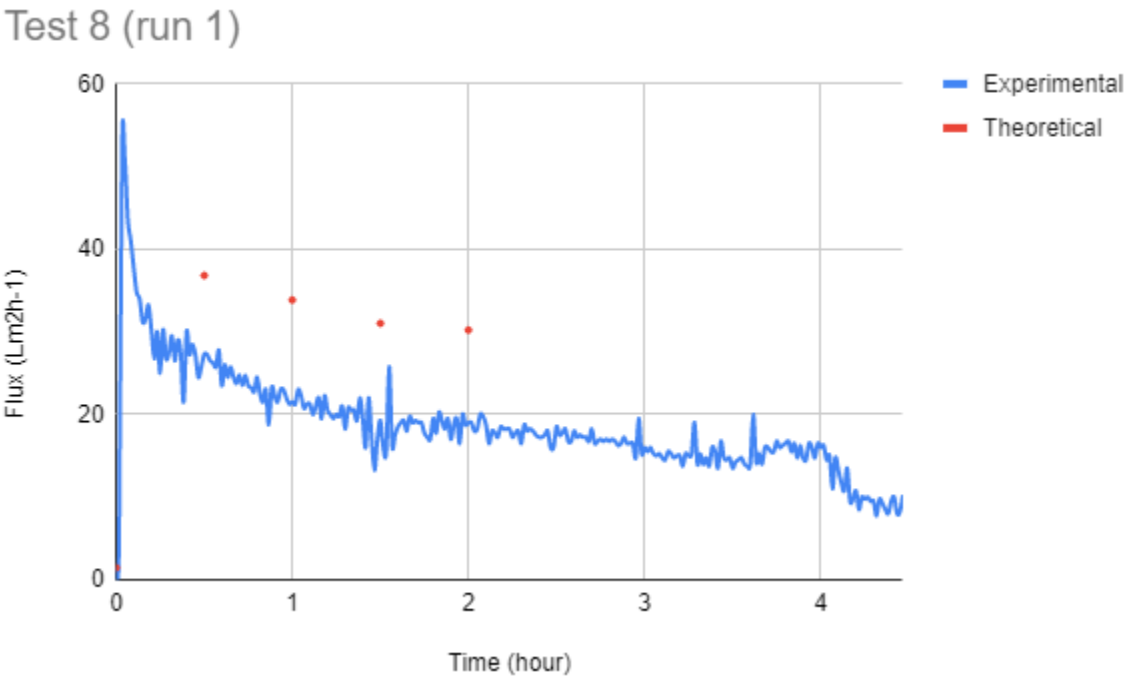

Experimental and best fit graphs of test 8 (Run 1) against time

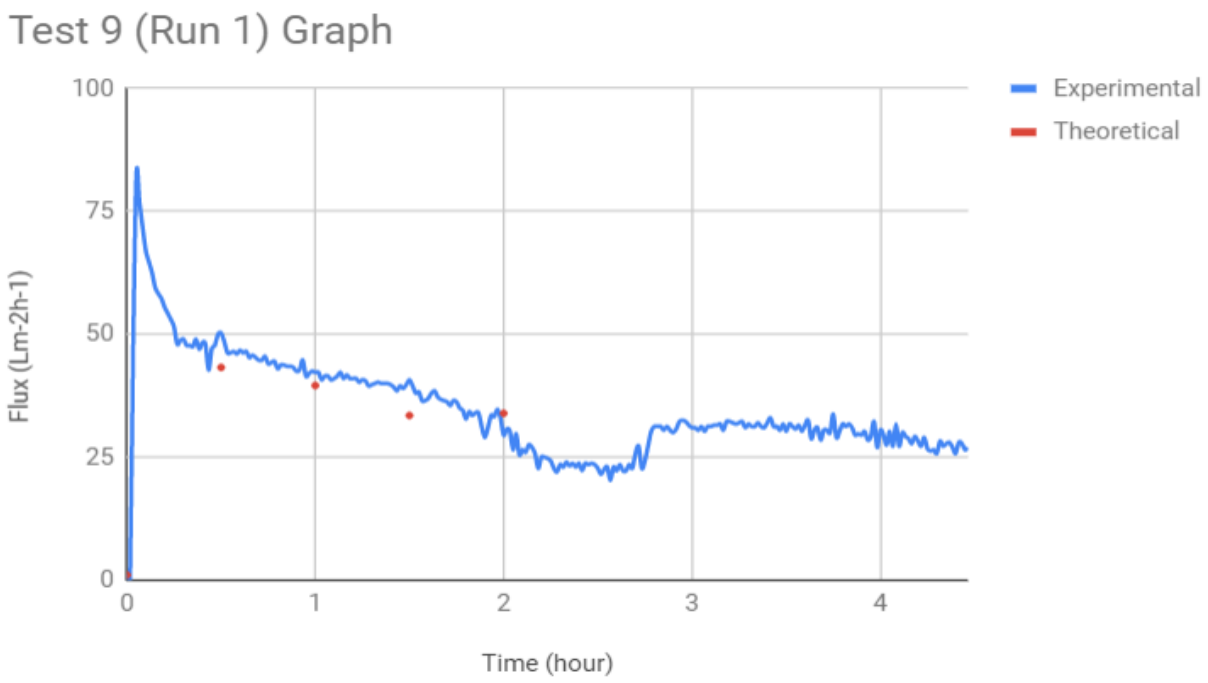

Experimental and best fit graphs of test 9 (Run 1) against time

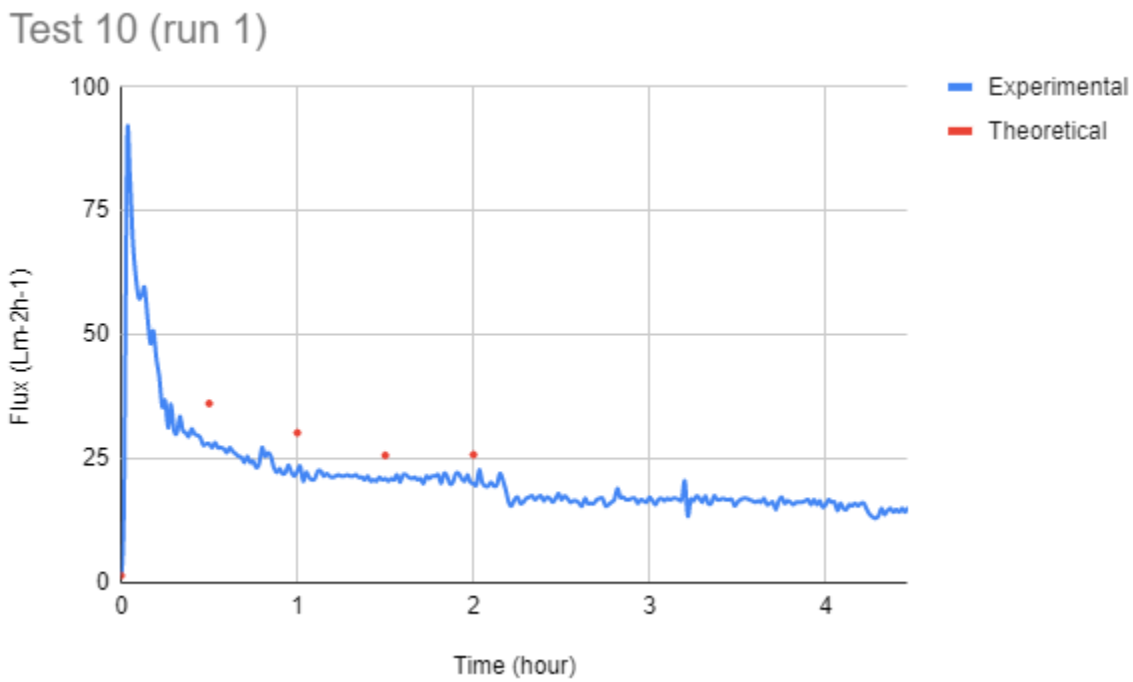

Experimental and best fit graphs of test 10 (Run 1) against time

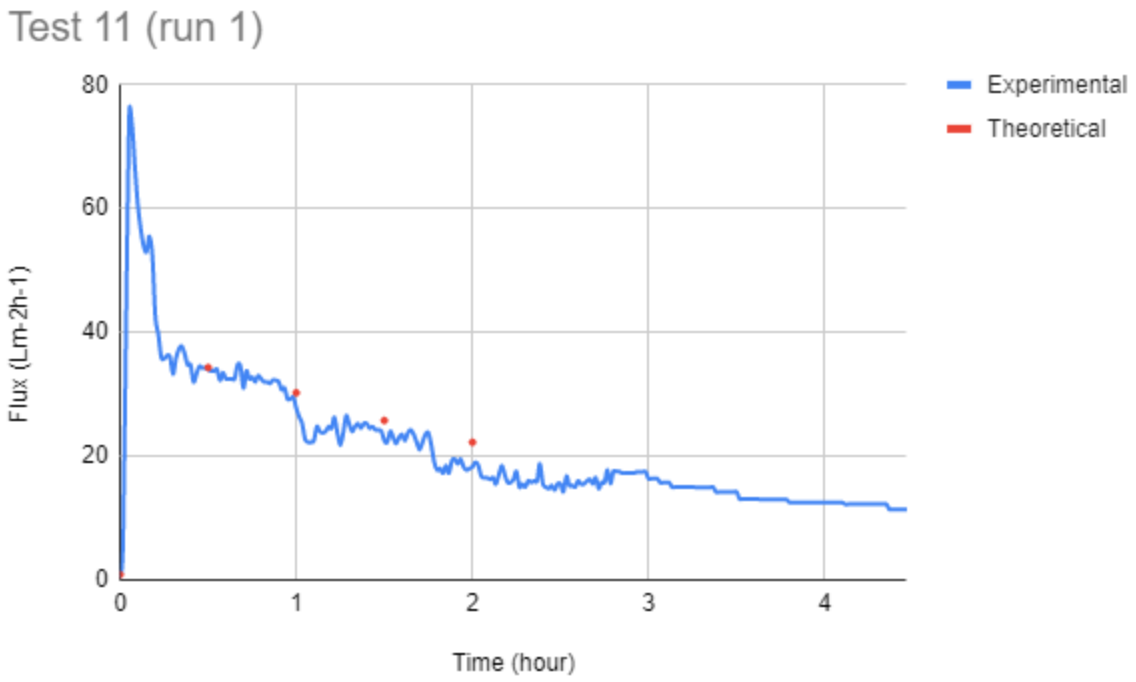

Experimental and best fit graphs of test 5 (Run 1) against time

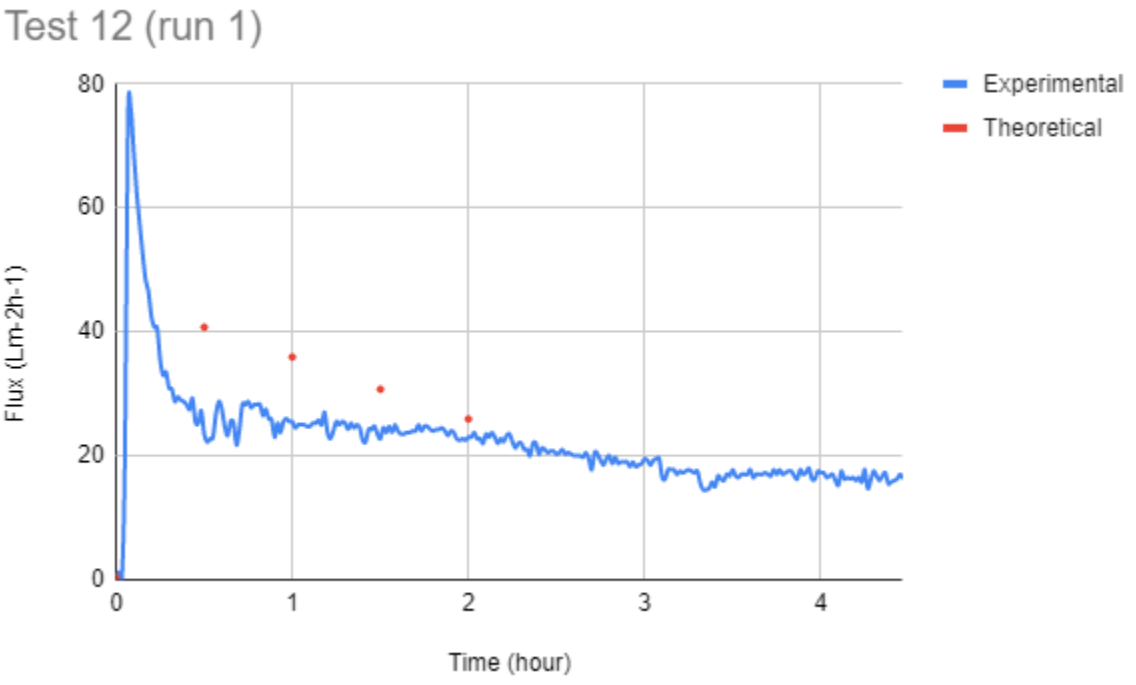

Experimental and best fit graphs of test 12 (Run 1) against time

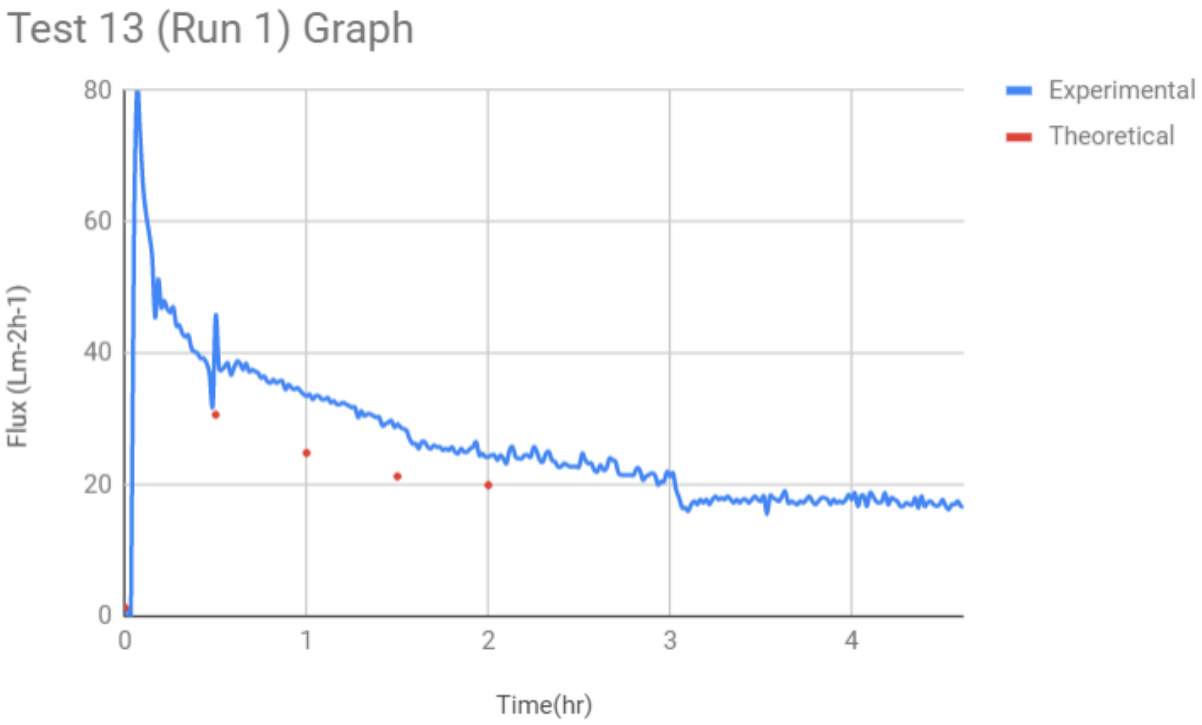

Experimental and best fit graphs of test 13 (Run 1) against time

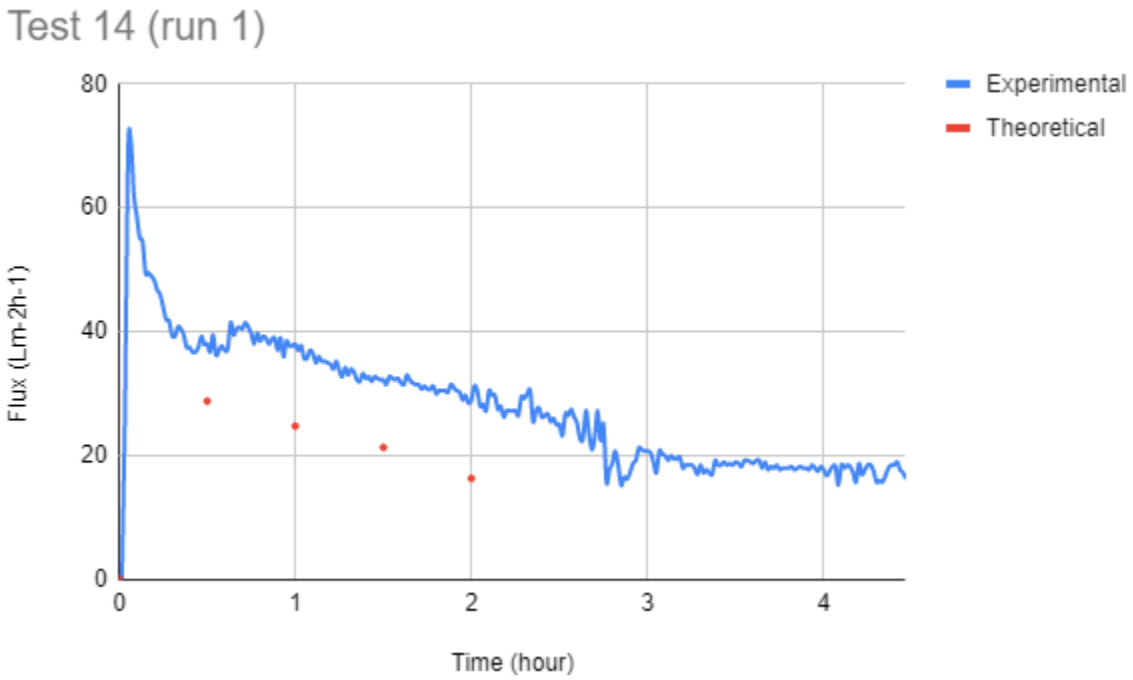

Experimental and best fit graphs of test 14 (Run 1) against time

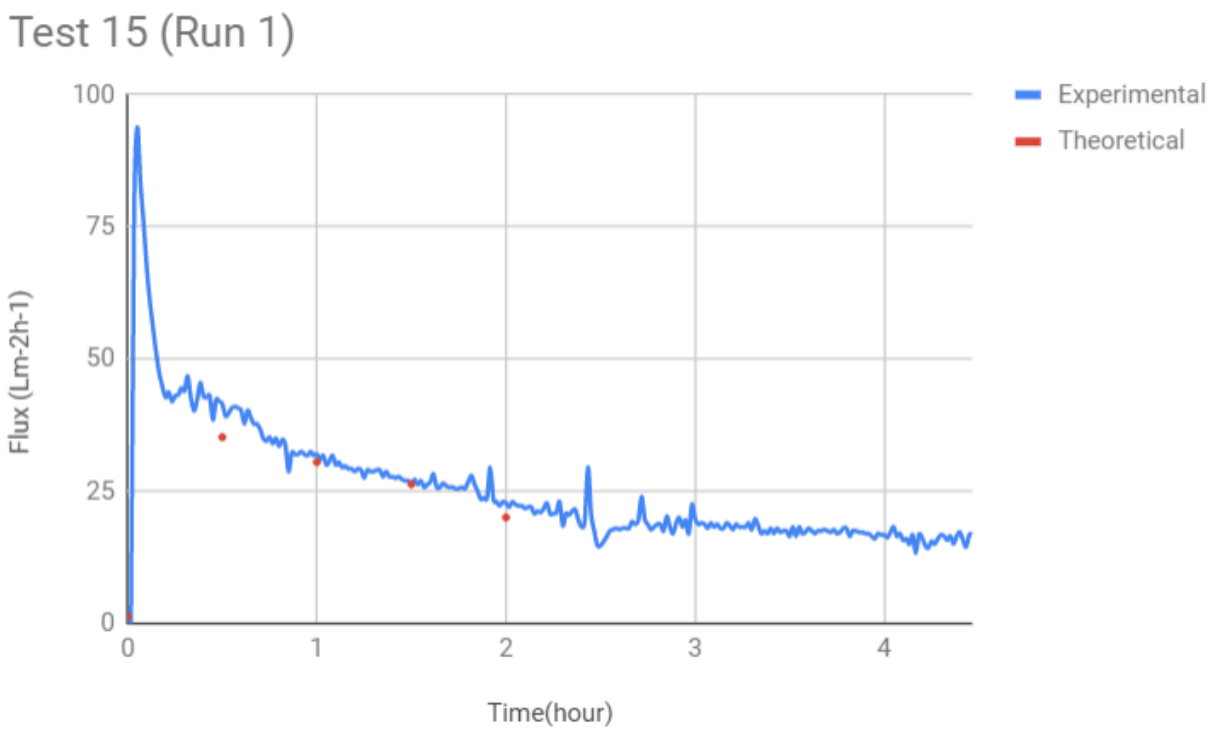

Experimental and best fit graphs of test 15 (Run 1) against time

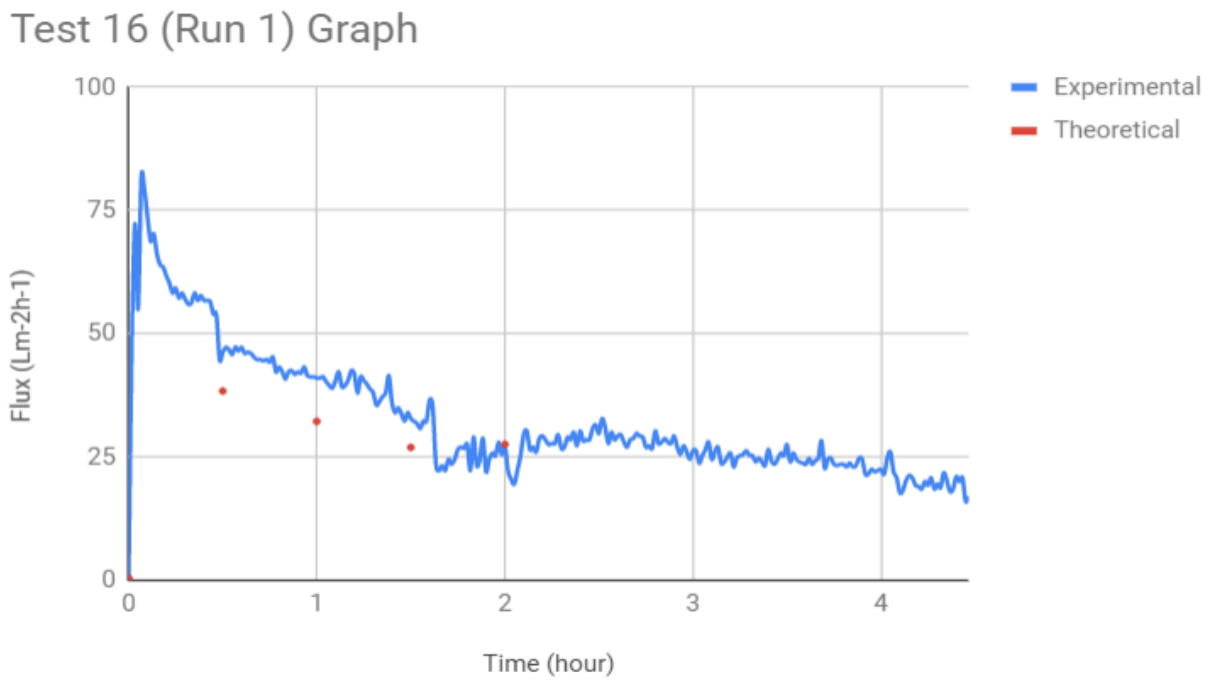

Experimental and best fit graphs of test 16 (Run 1) against time

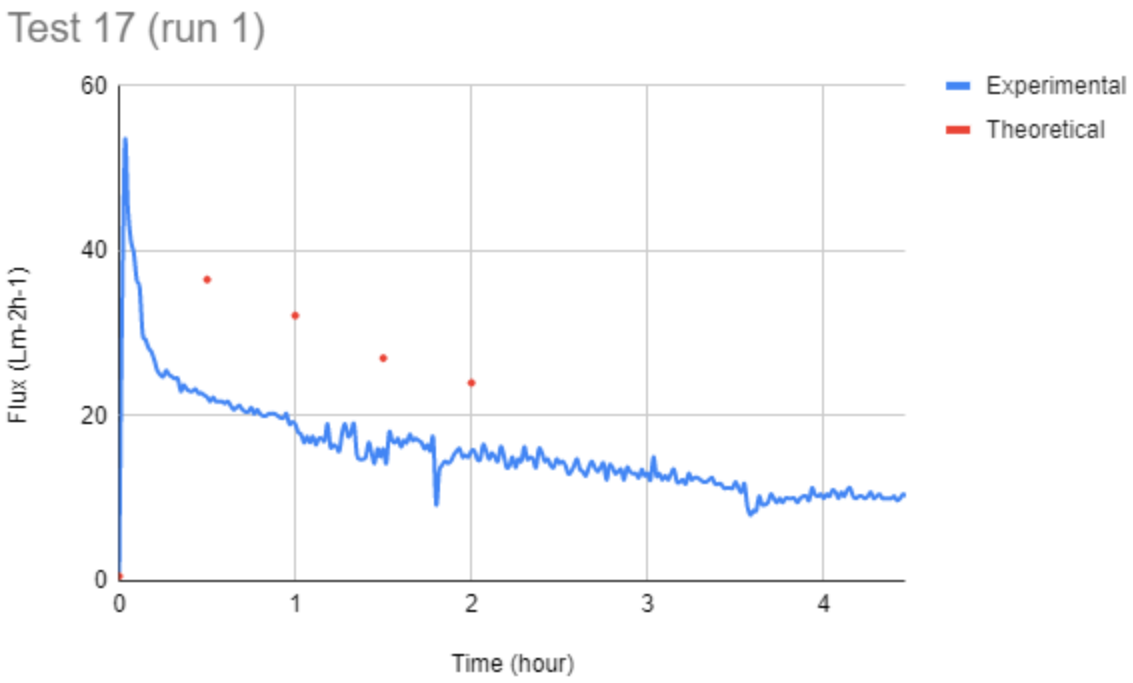

Experimental and best fit graphs of test 17 (Run 1) against time

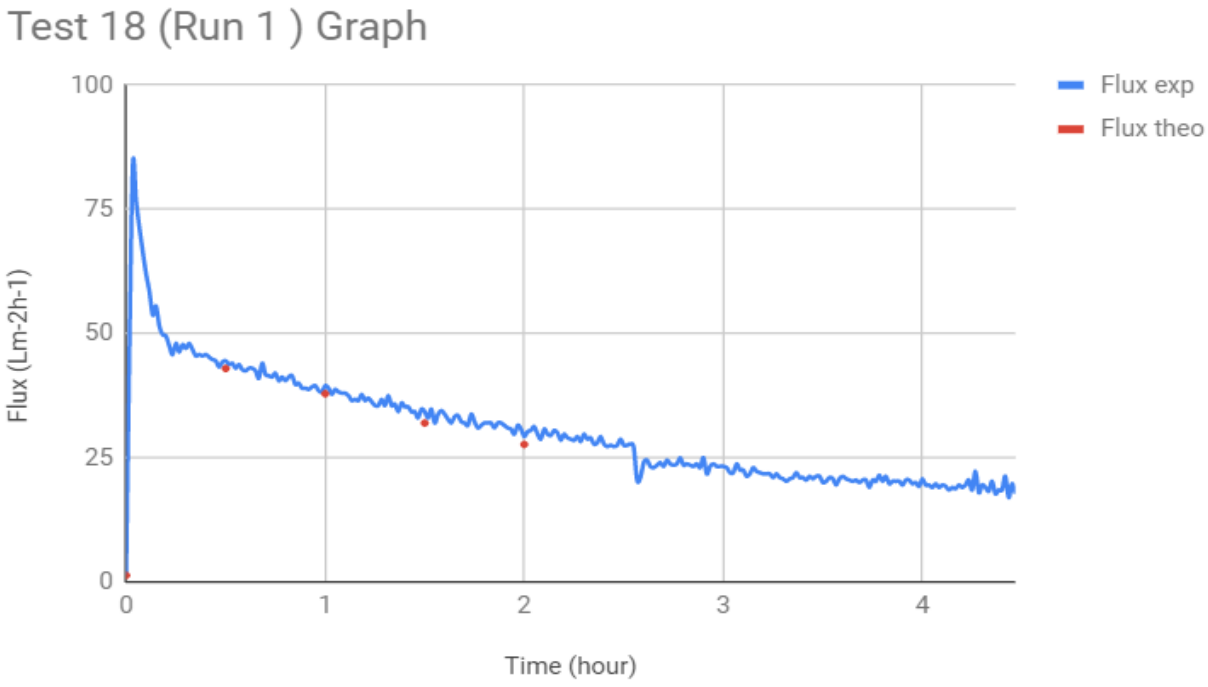

Experimental and best fit graphs of test 18 (Run 1) against time

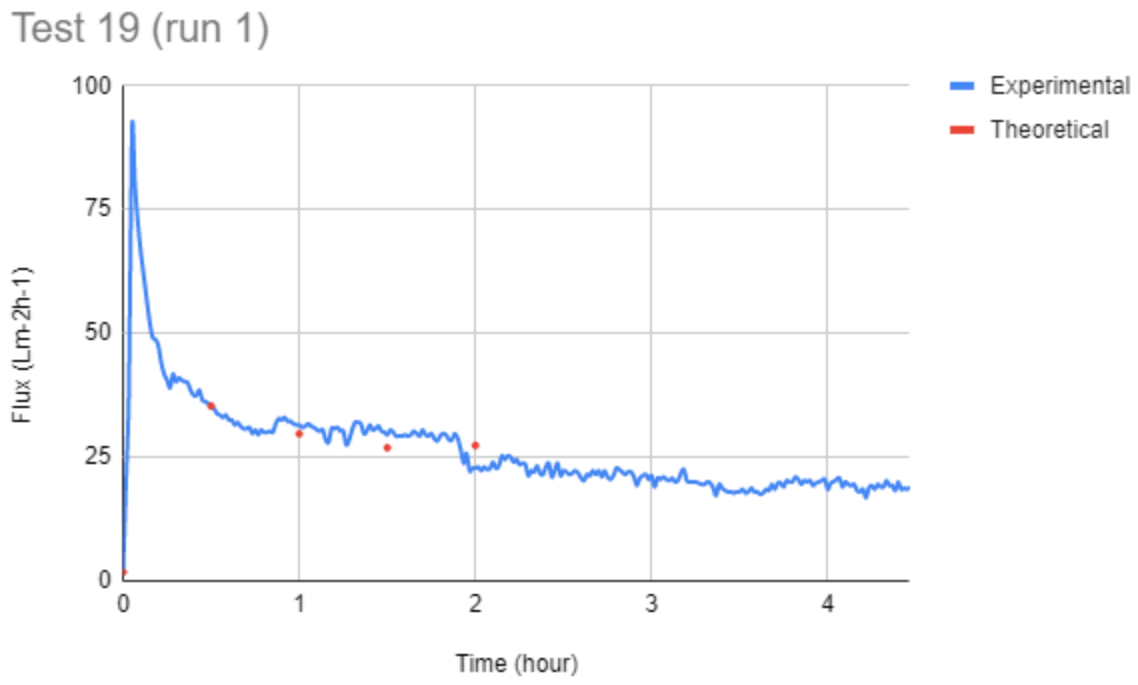

Experimental and best fit graphs of test 19 (Run 1) against time

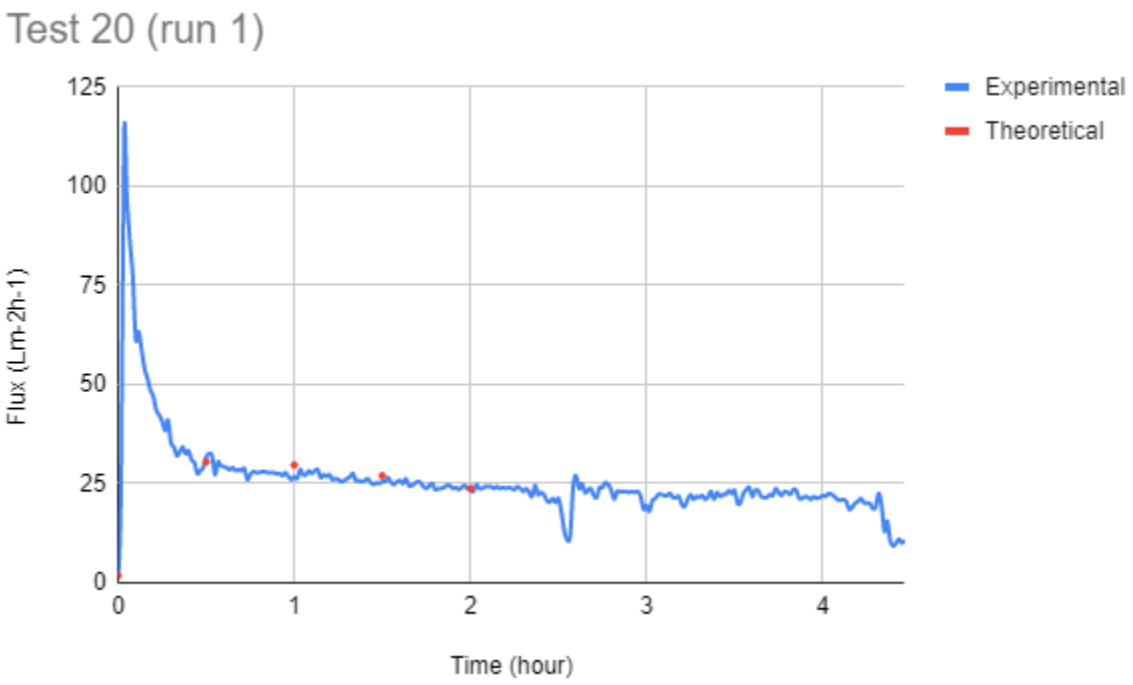

Experimental and best fit graphs of test 20 (Run 1) against time

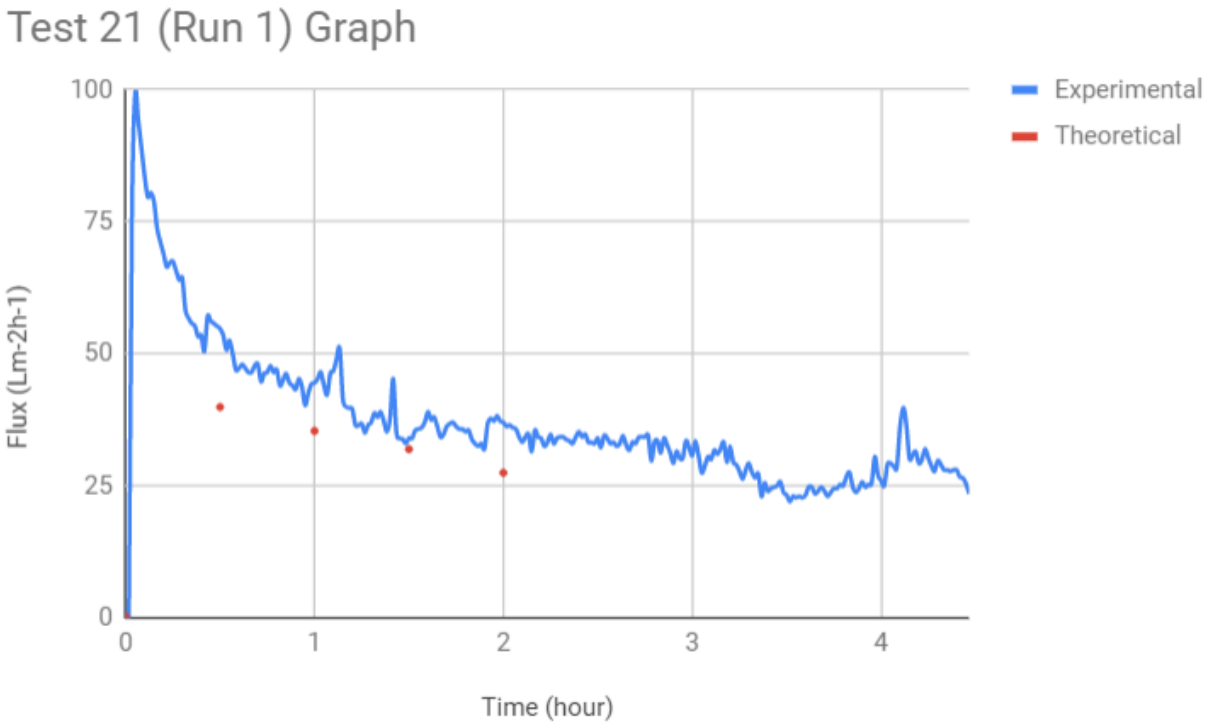

Experimental and best fit graphs of test 21 (Run 1) against time

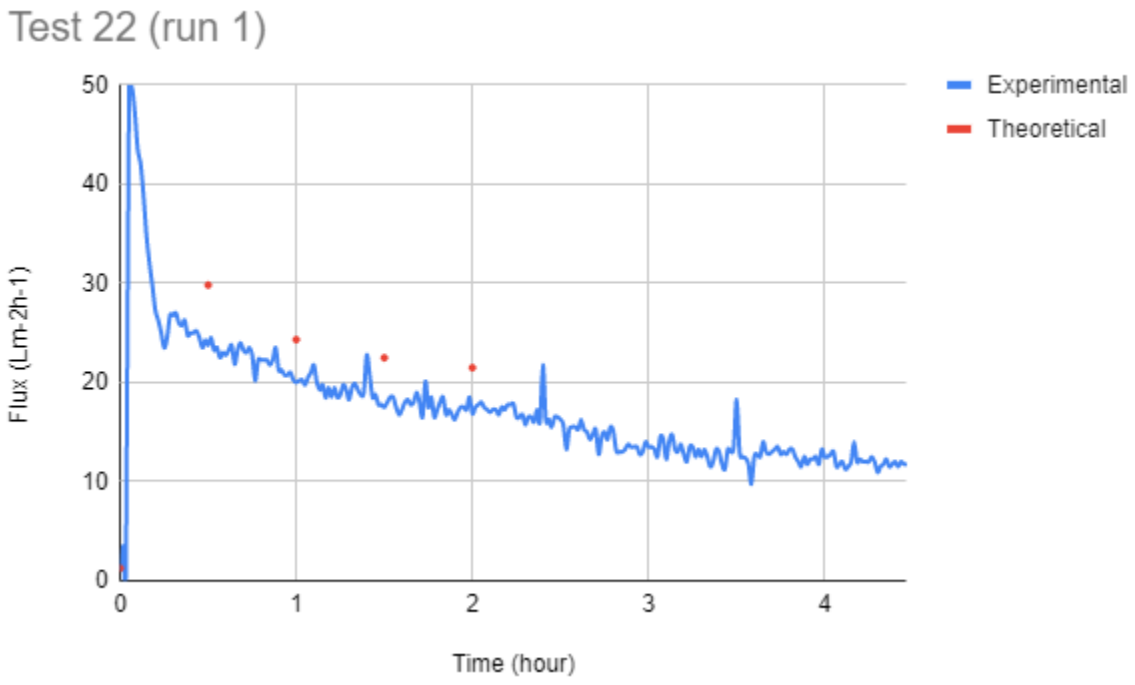

Experimental and best fit graphs of test 22 (Run 1) against time

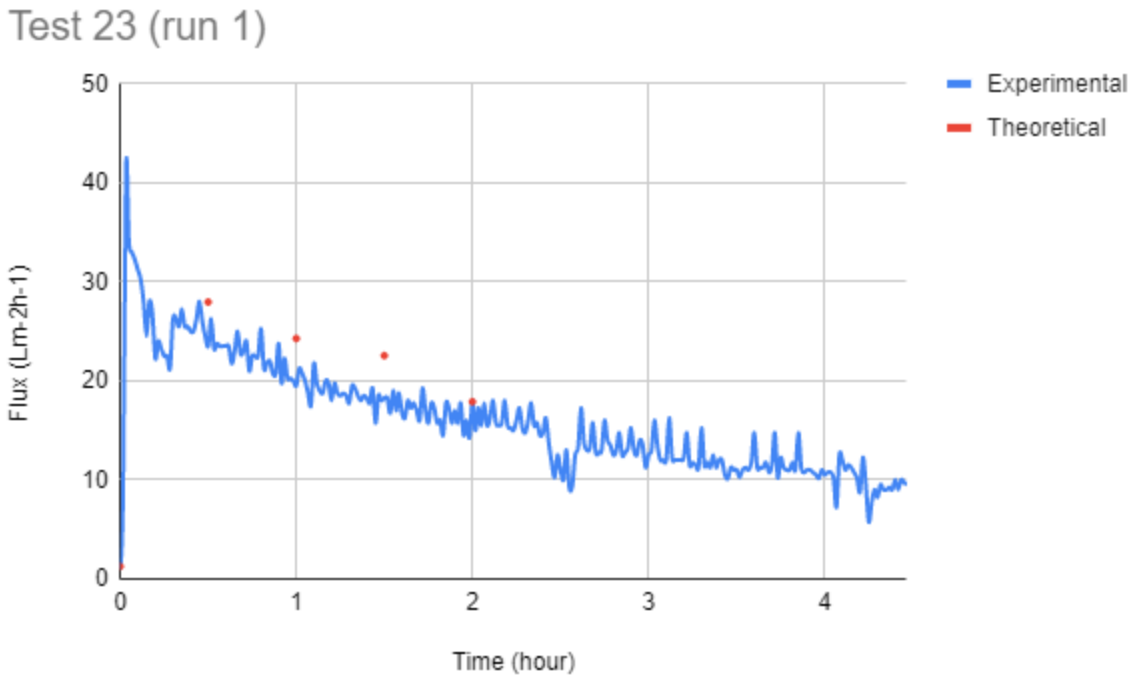

Experimental and best fit graphs of test 23 (Run 1) against time

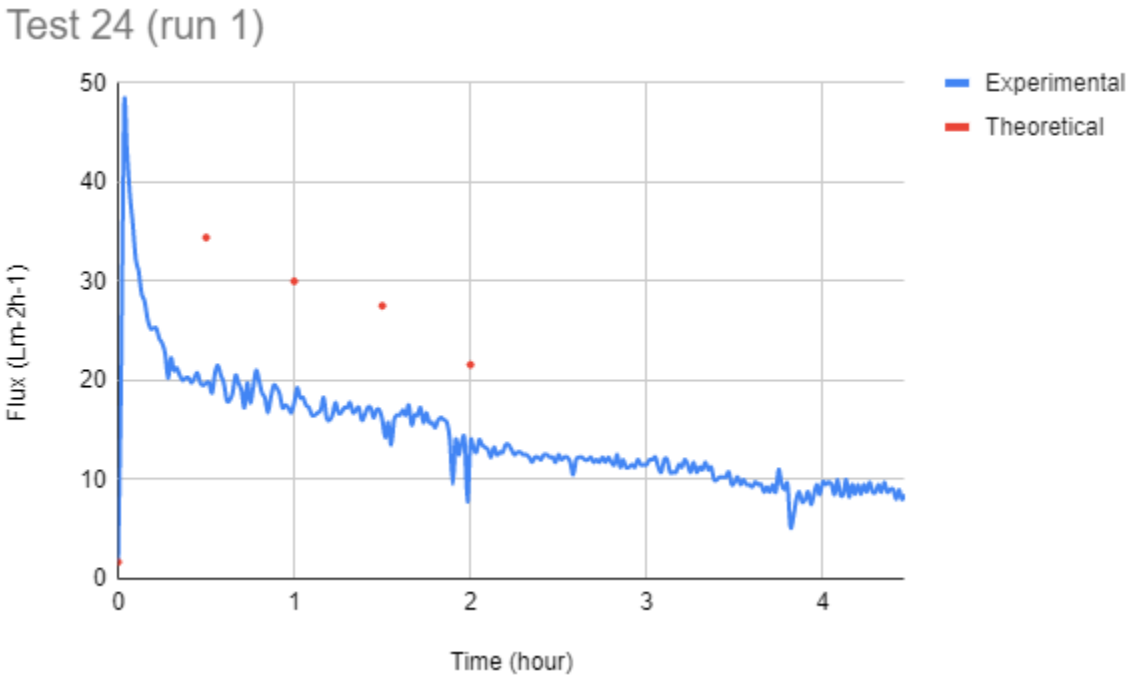

Experimental and best fit graphs of test 24 (Run 1) against time

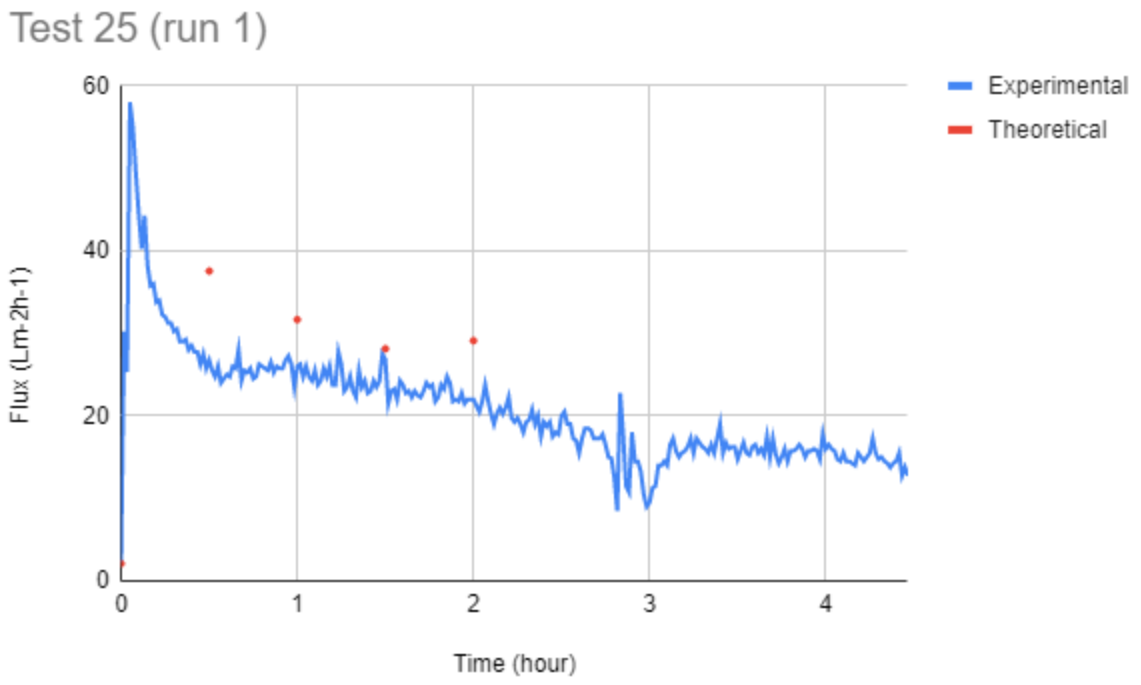

Experimental and best fit graphs of test 25 (Run 1) against time

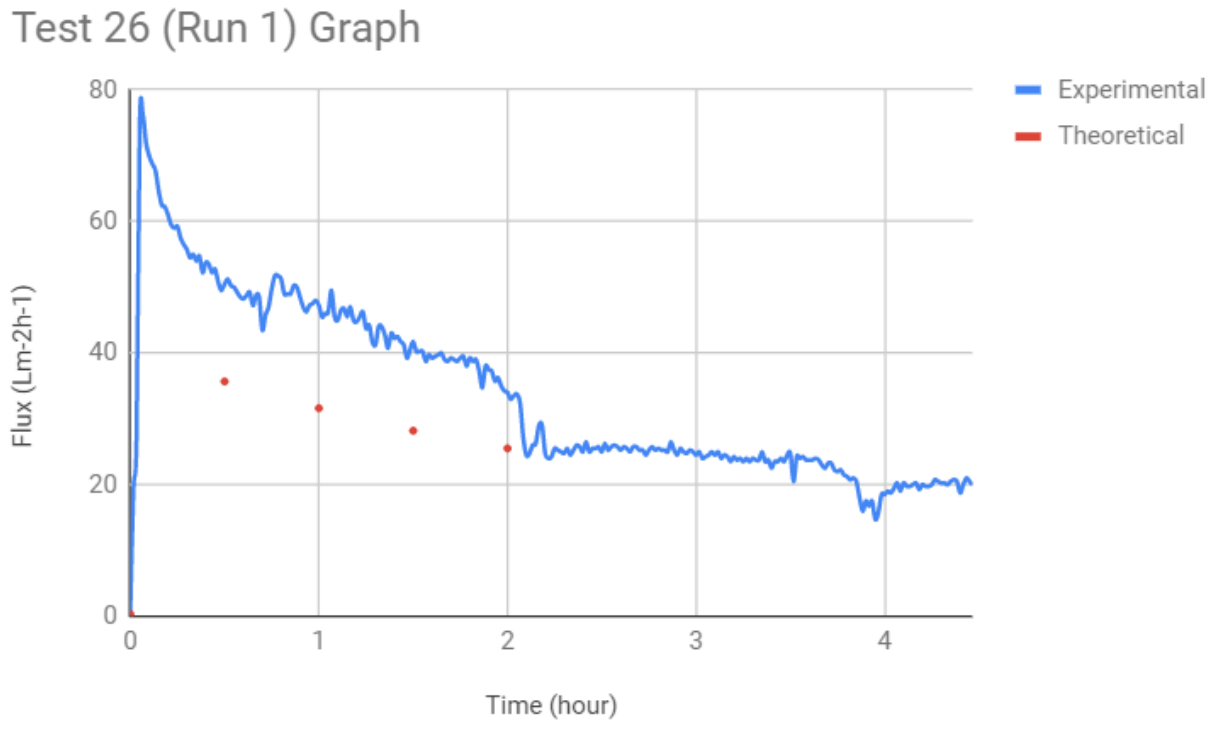

Experimental and best fit graphs of test 26 (Run 1) against time

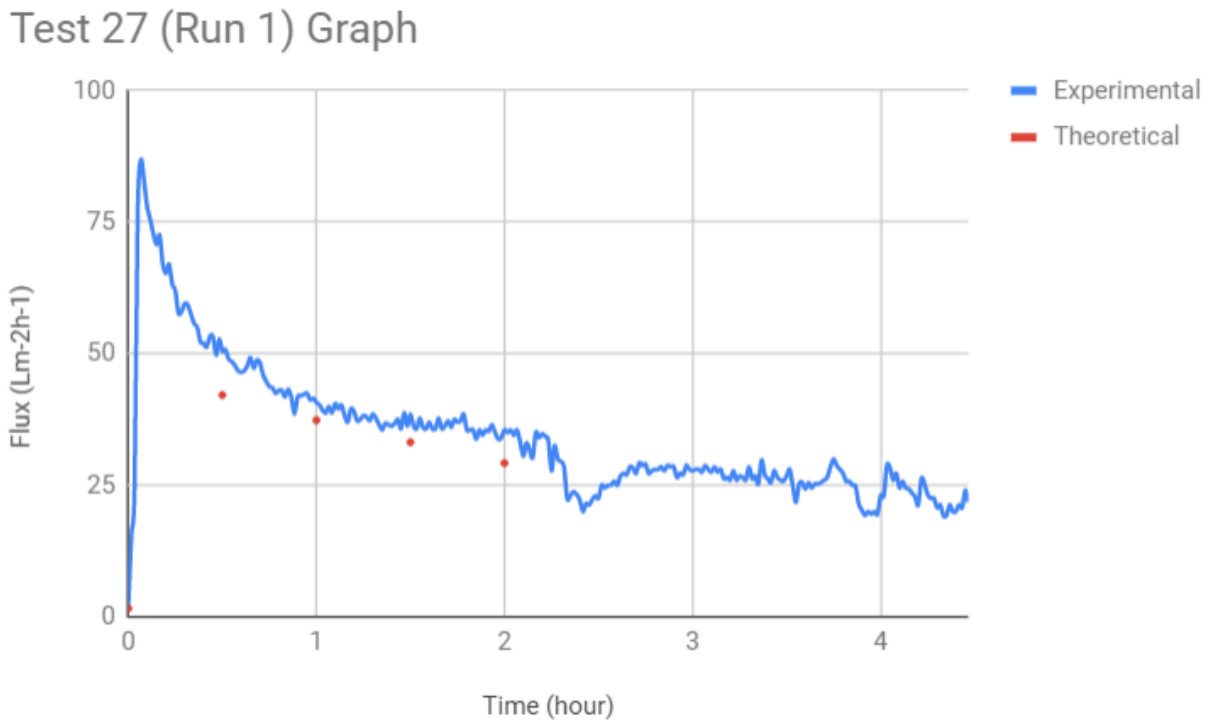

Experimental and best fit graphs of test 27 (Run 1) against time

APPENDIX B. RUN 2 GRAPHS

All the experiments performed in Run 2 are presented in this section.

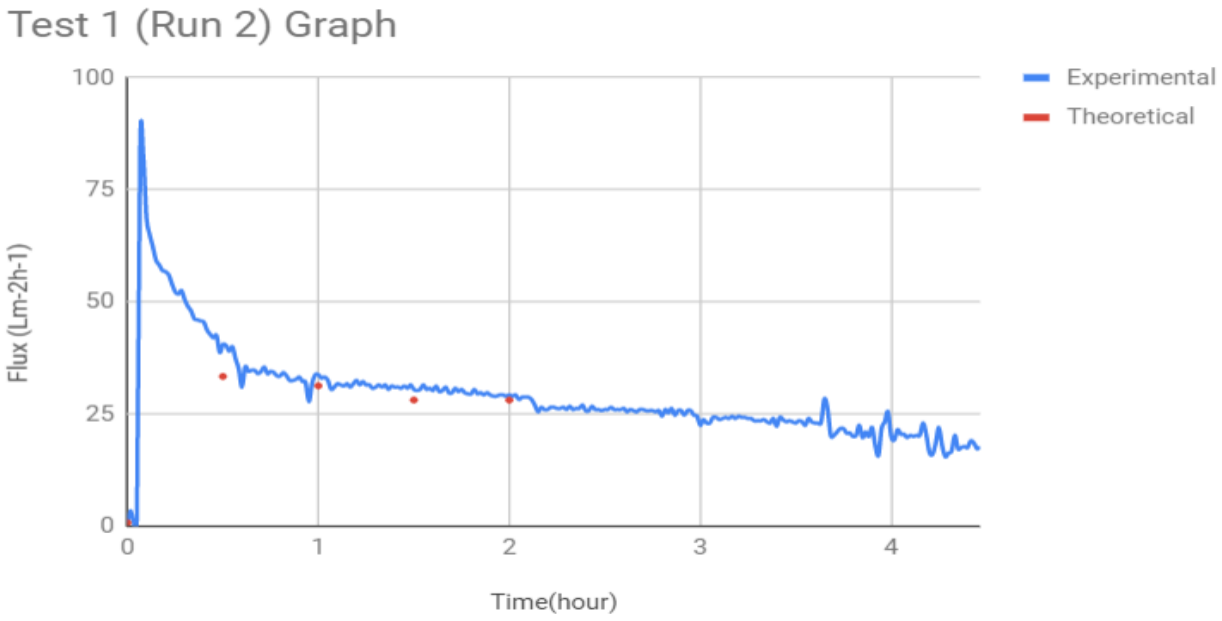

Experimental and best fit graphs of test 1 (Run 2) against time

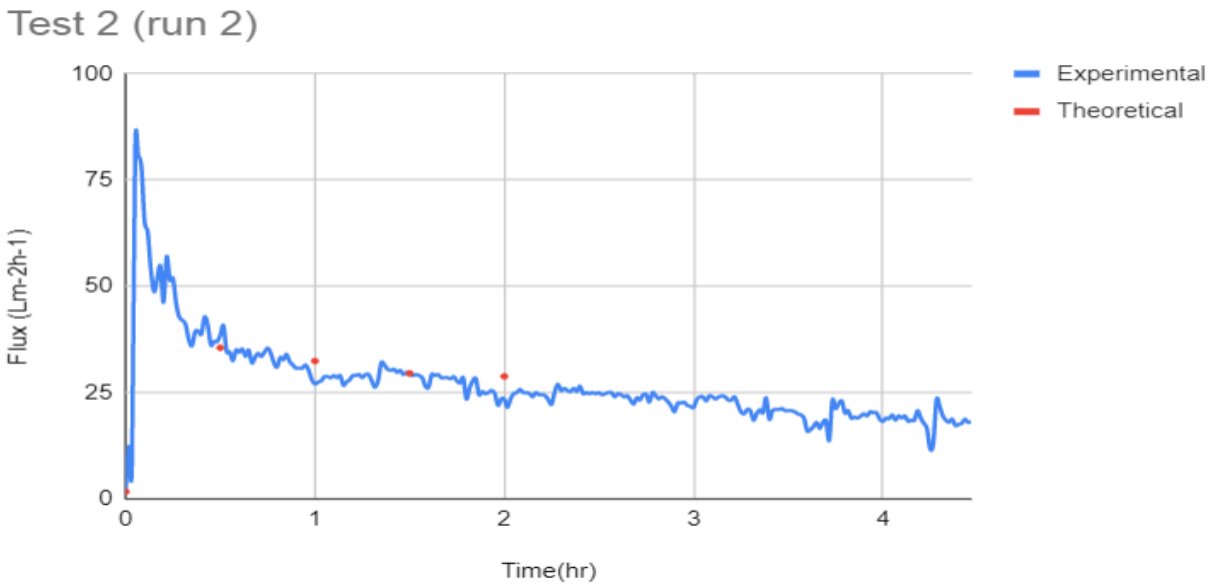

Experimental and best fit graphs of test 2 (Run 2) against time

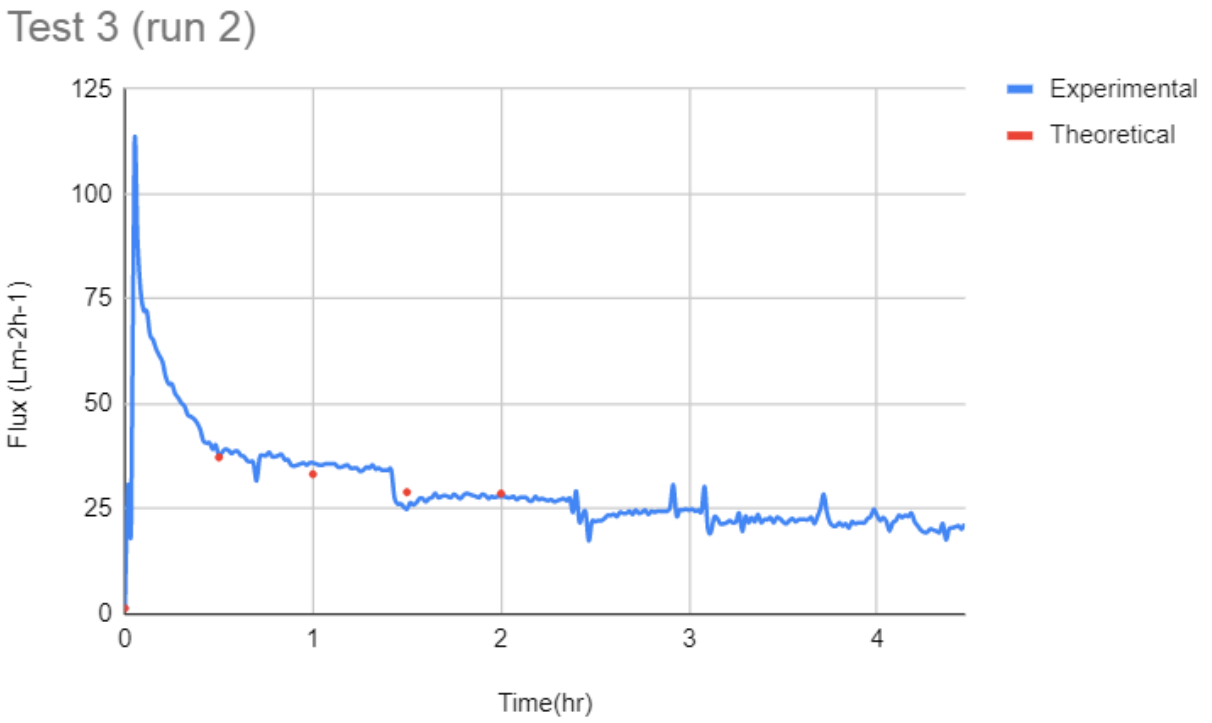

Experimental and best fit graphs of test 3 (Run 2) against time

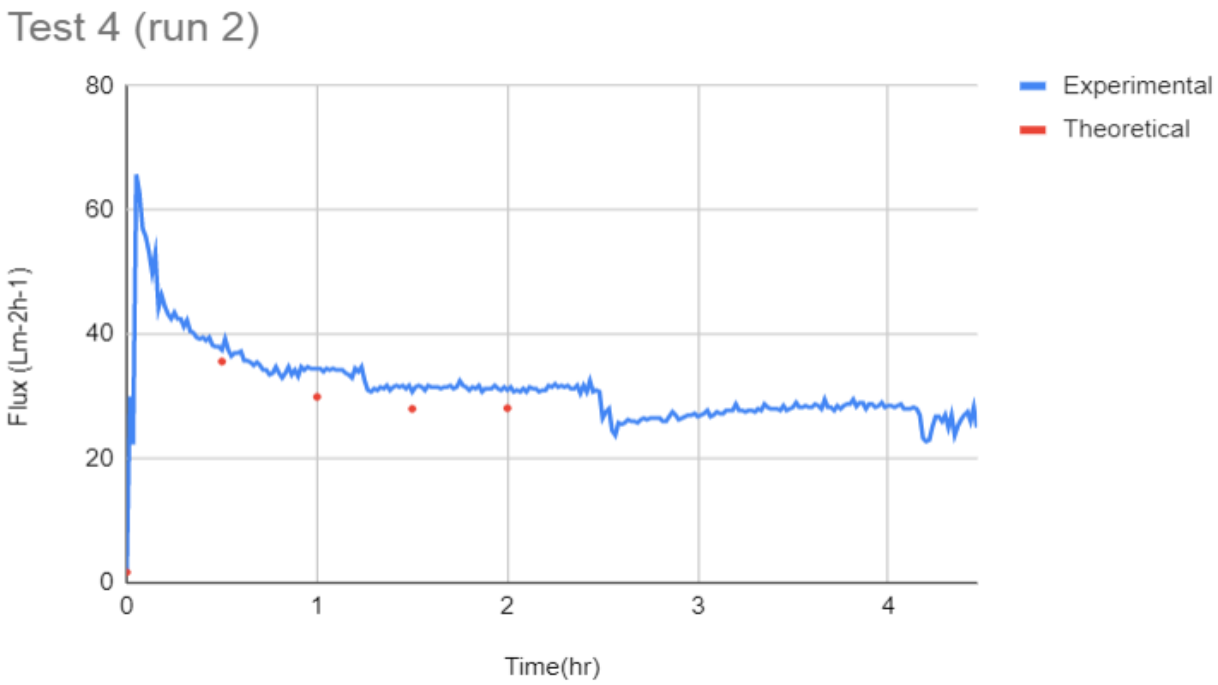

Experimental and best fit graphs of test 4 (Run 2) against time

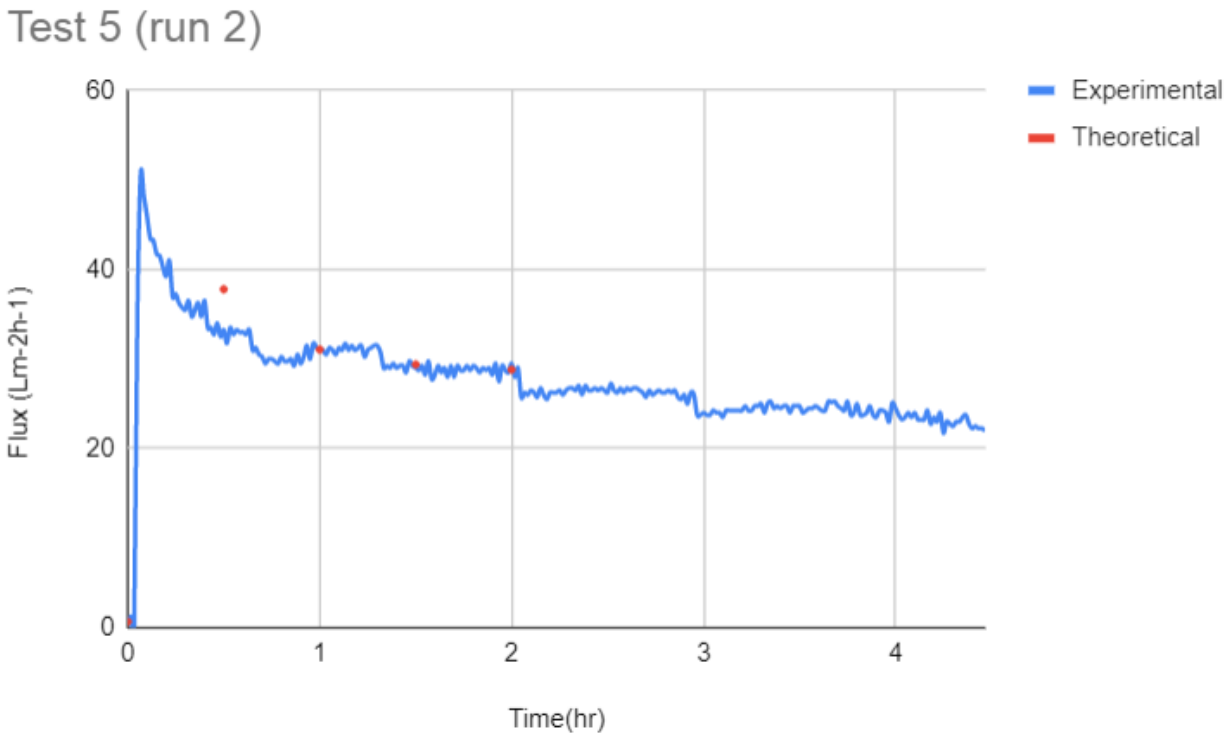

Experimental and best fit graphs of test 5 (Run 2) against time

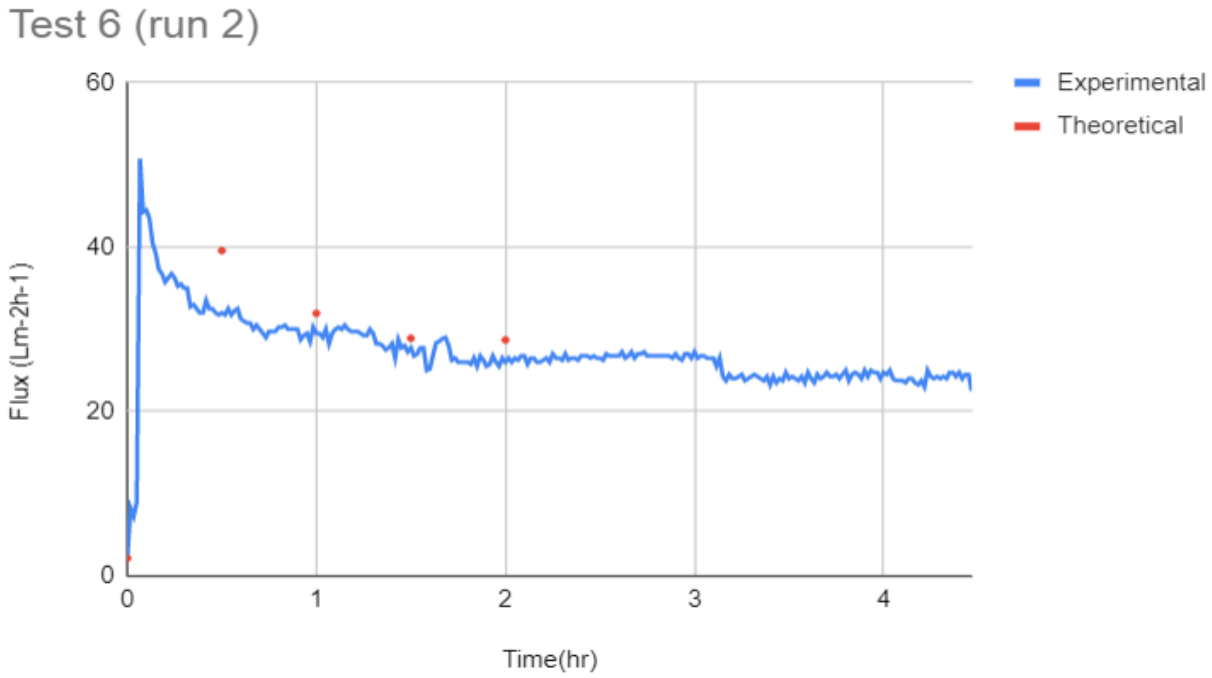

Experimental and best fit graphs of test 6 (Run 2) against time

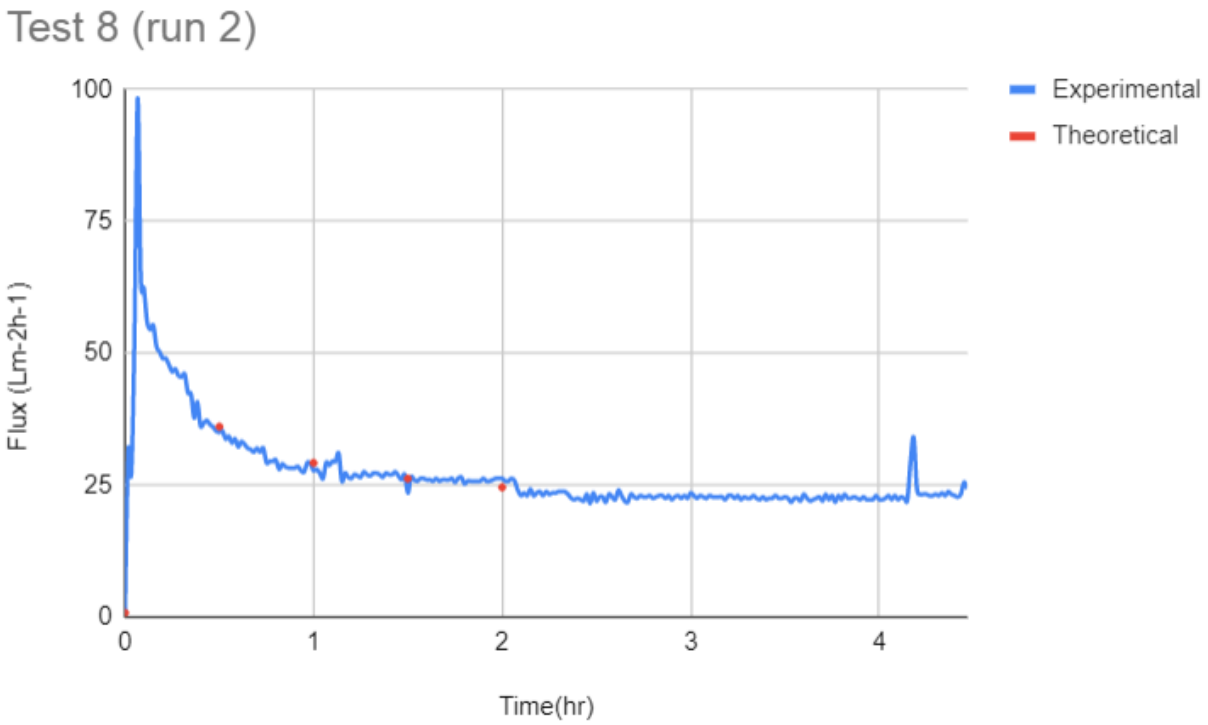

Experimental and best fit graphs of test 8 (Run 2) against time

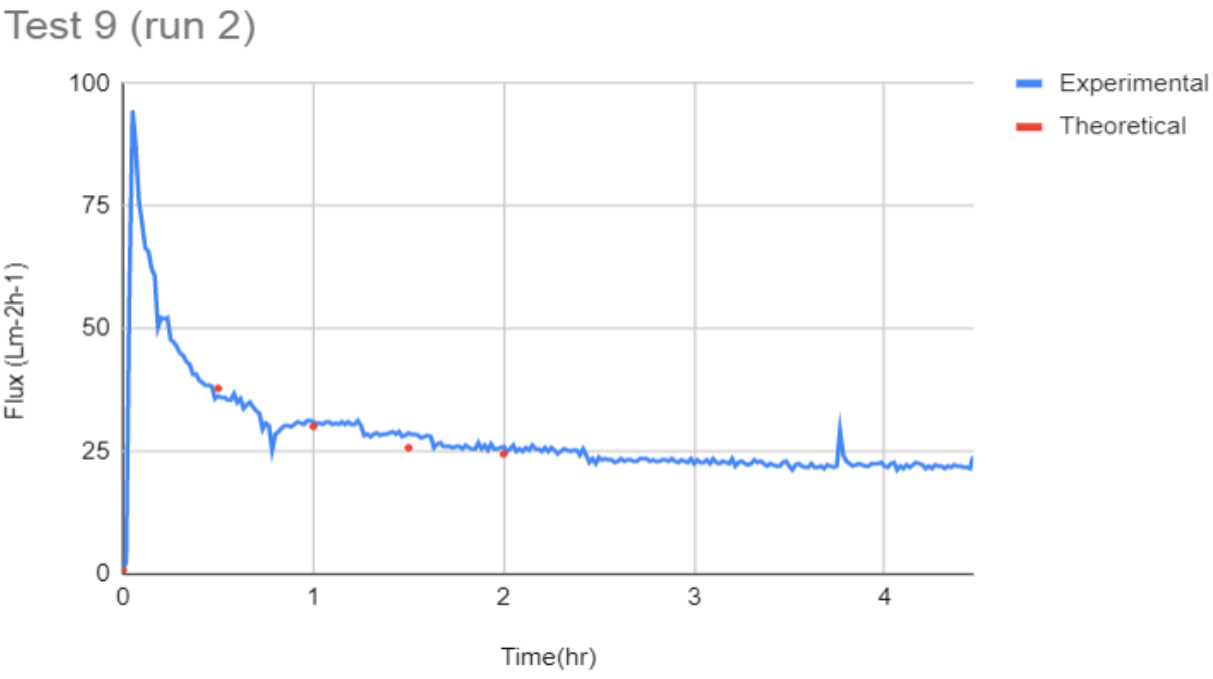

Experimental and best fit graphs of test 9 (Run 2) against time

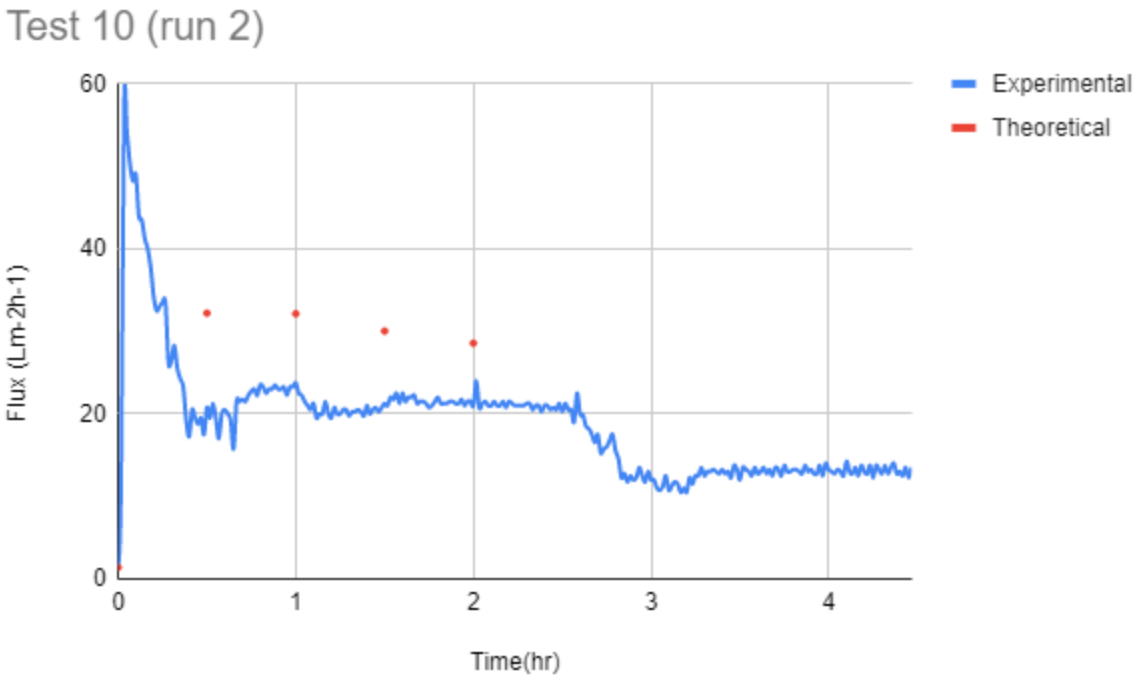

Experimental and best fit graphs of test 10 (Run 2) against time

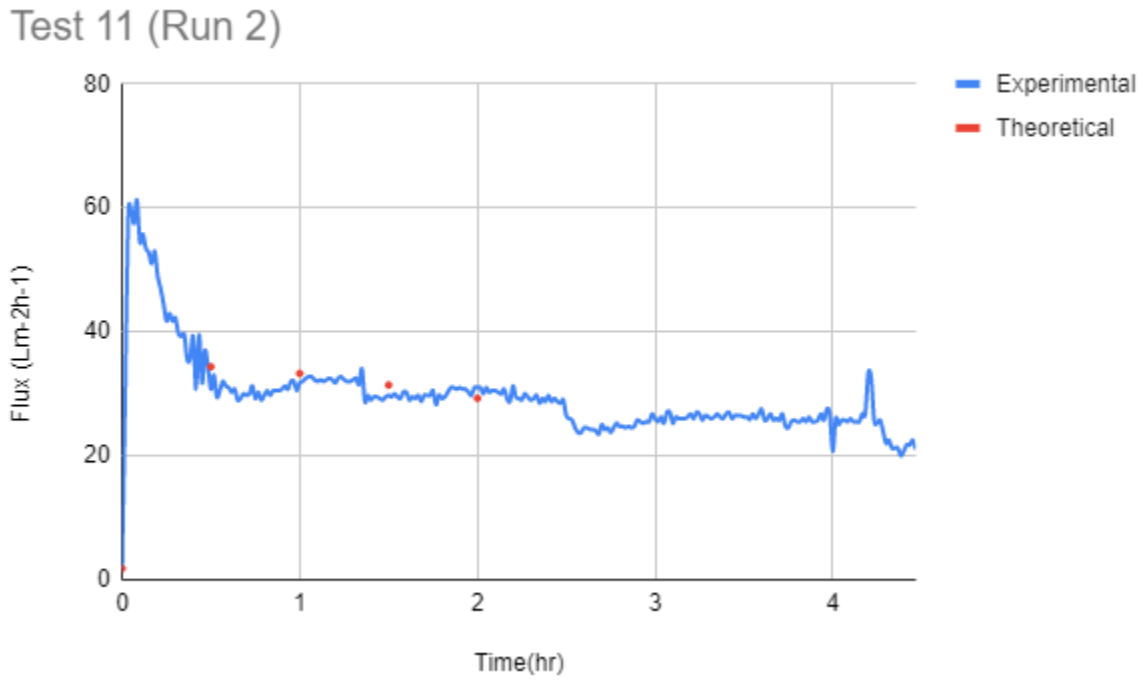

Experimental and best fit graphs of test 11 (Run 2) against time

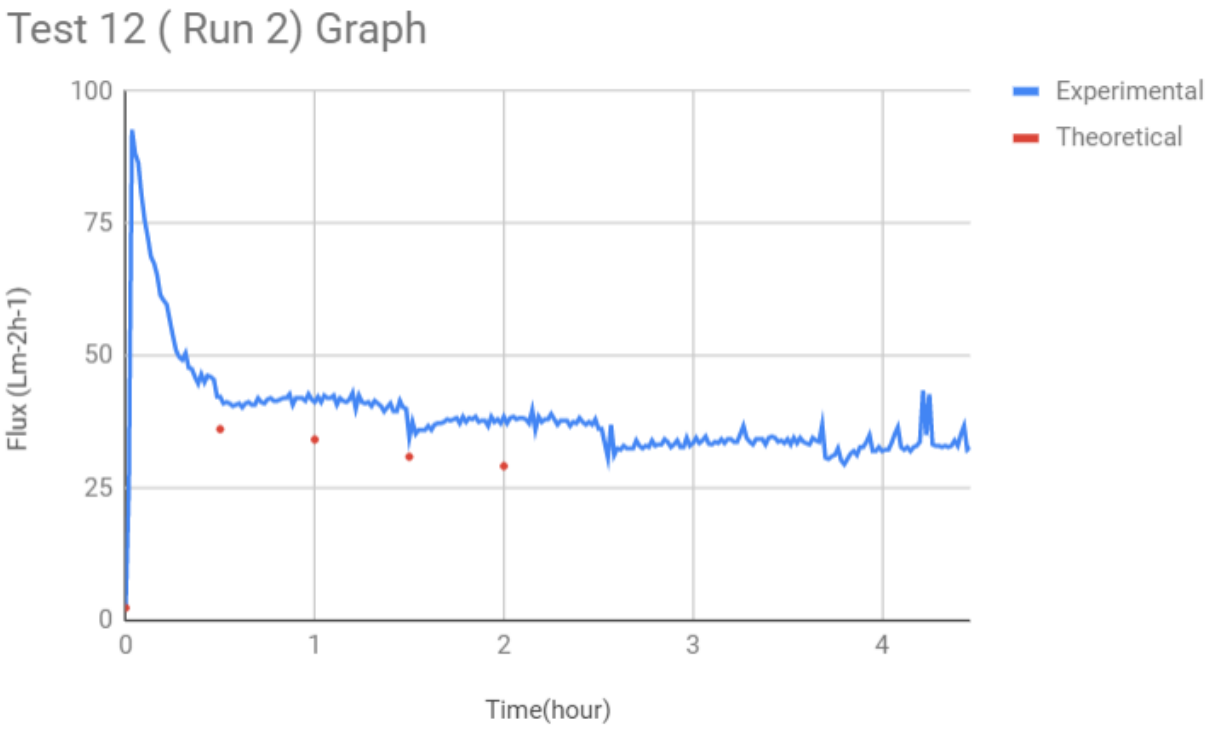

Experimental and best fit graphs of test 12 (Run 2) against time

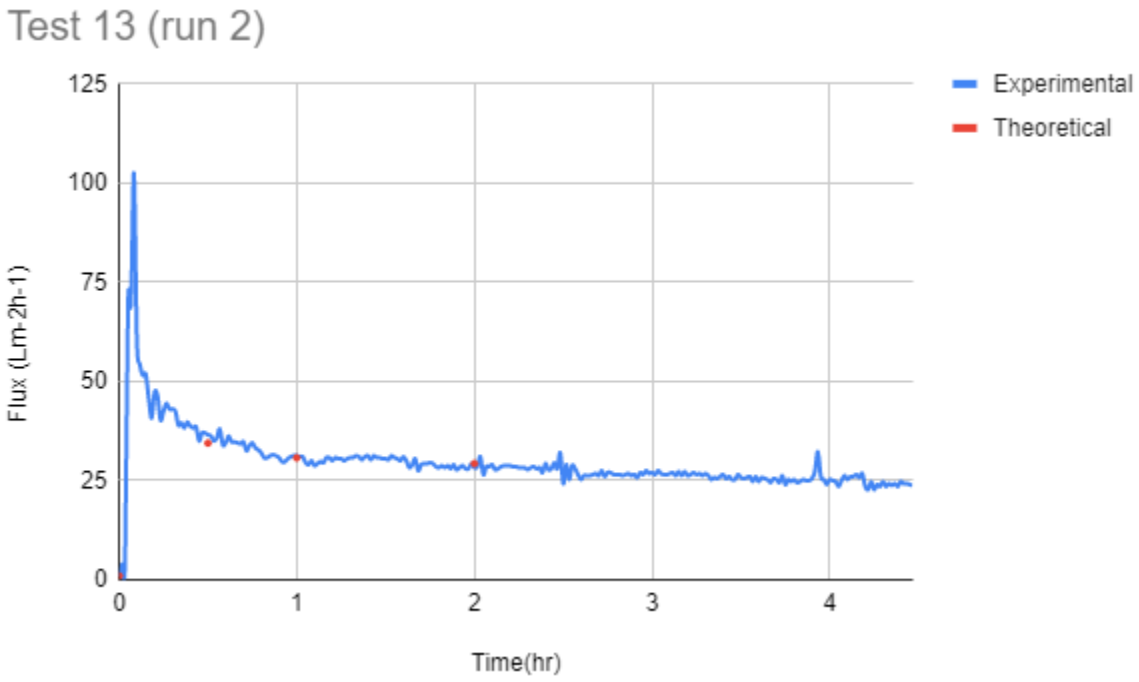

Experimental and best fit graphs of test 13 (Run 2) against time

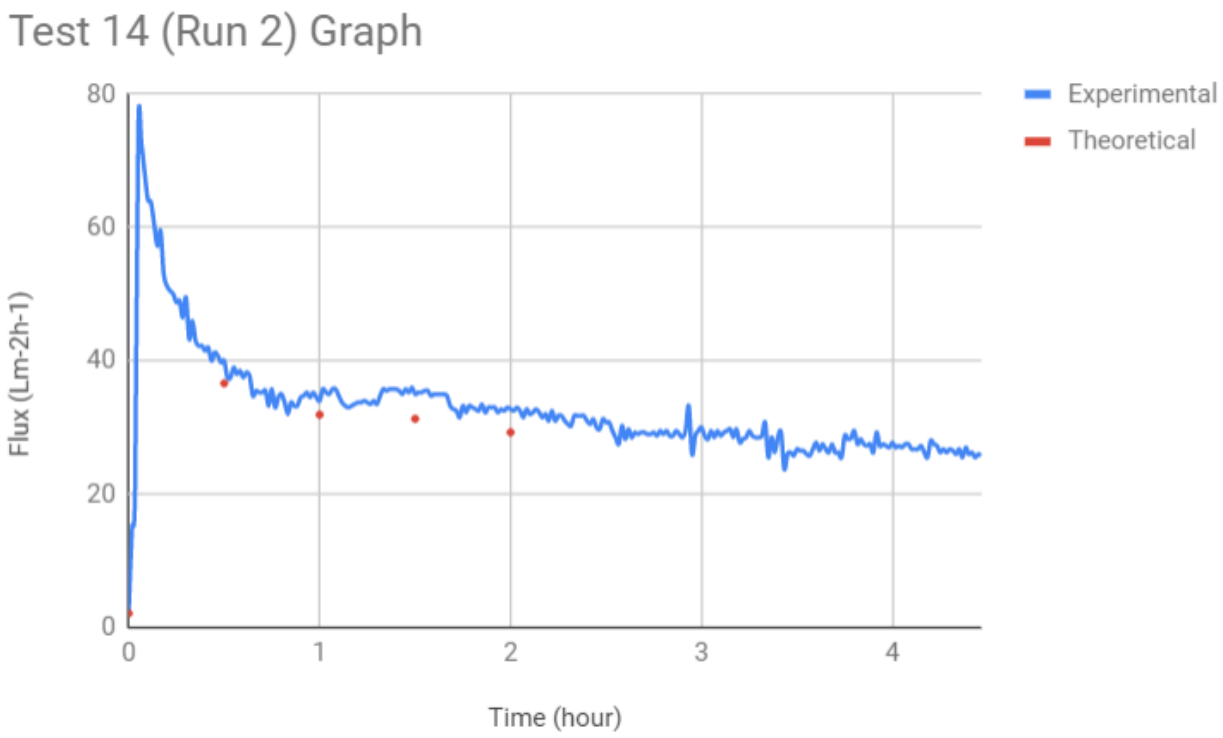

Experimental and best fit graphs of test 14 (Run 2) against time

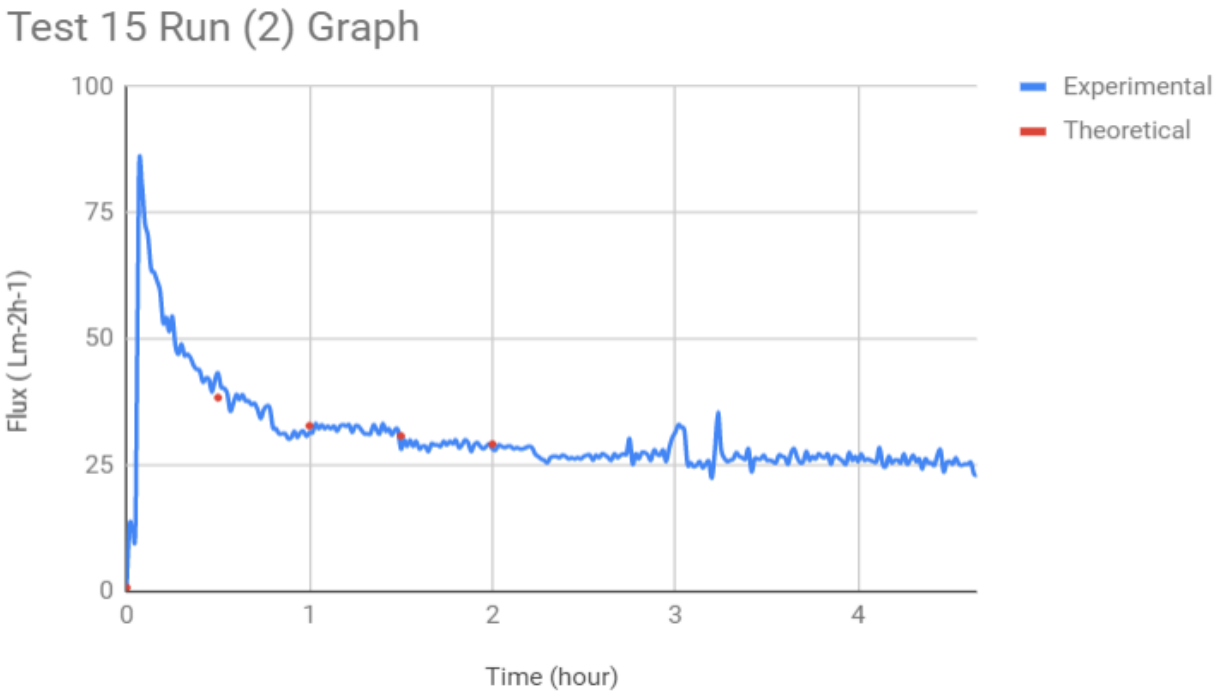

Experimental and best fit graphs of test 15 (Run 2) against time

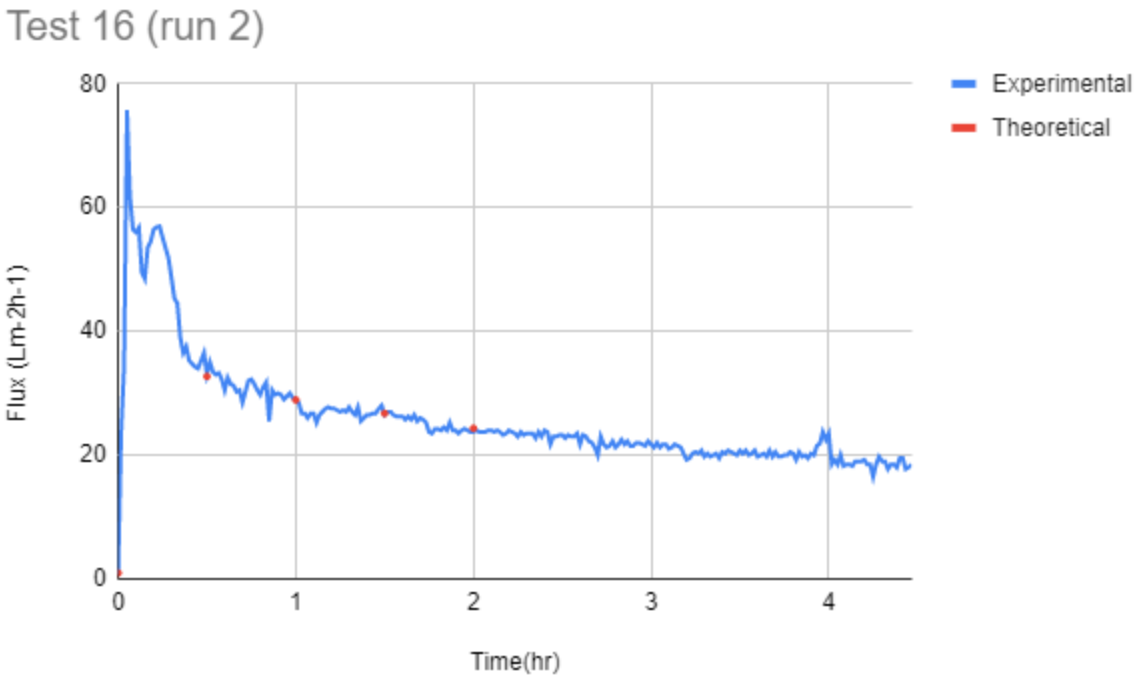

Experimental and best fit graphs of test 16 (Run 2) against time

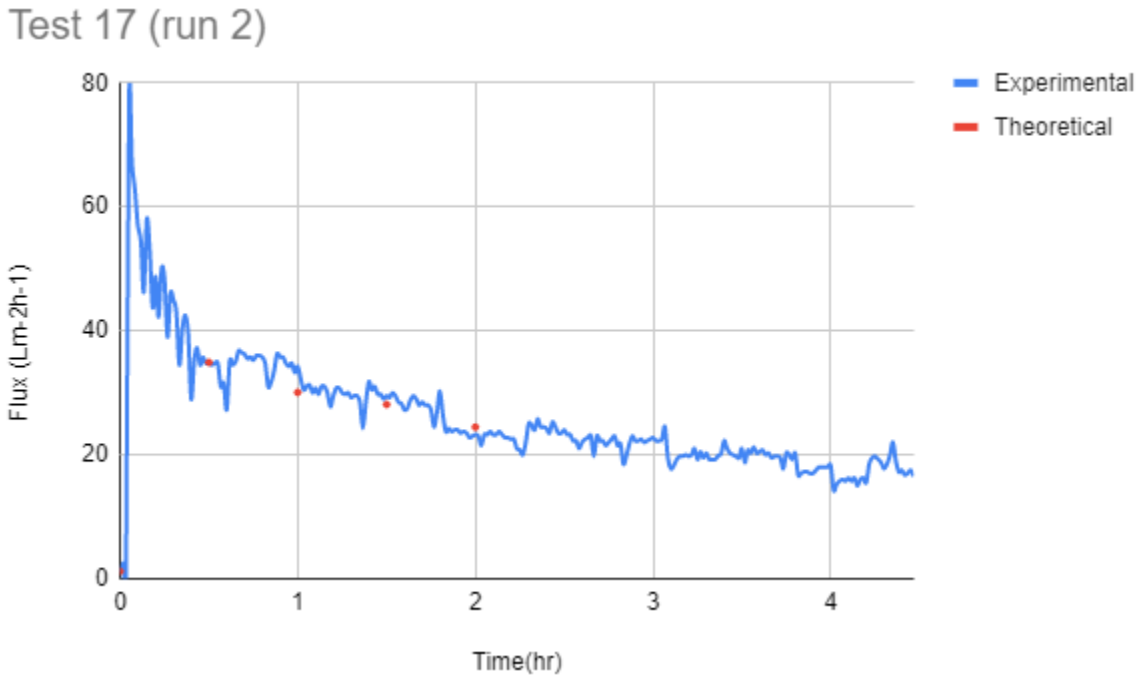

Experimental and best fit graphs of test 17 (Run 2) against time

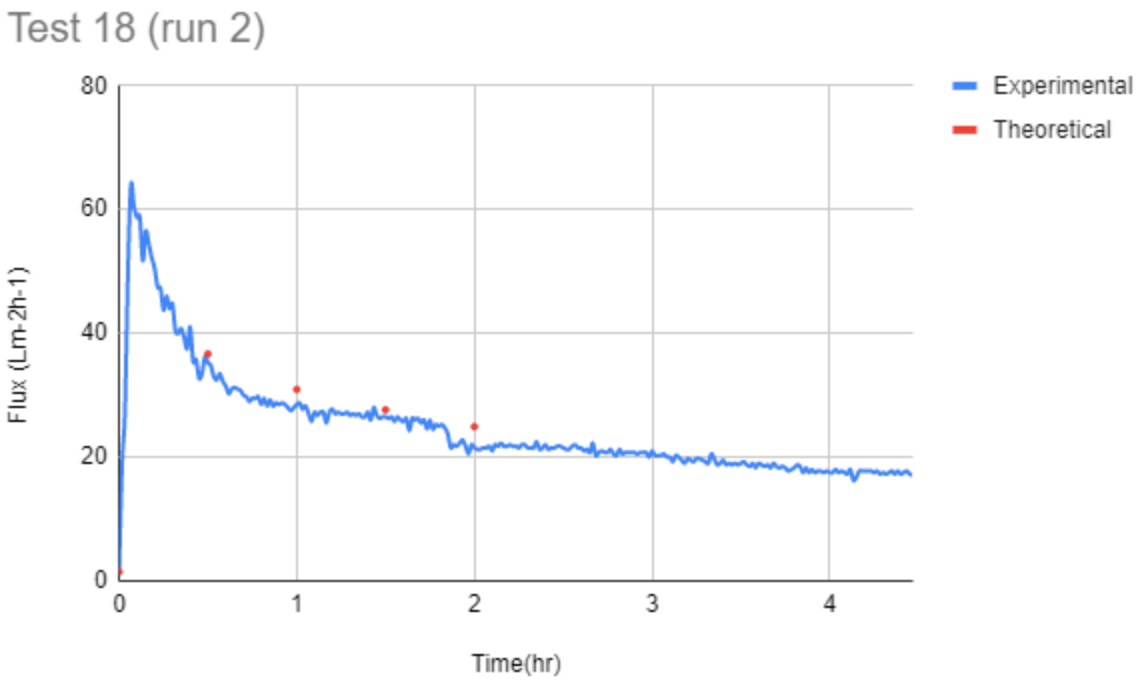

Experimental and best fit graphs of test 18 (Run 2) against time

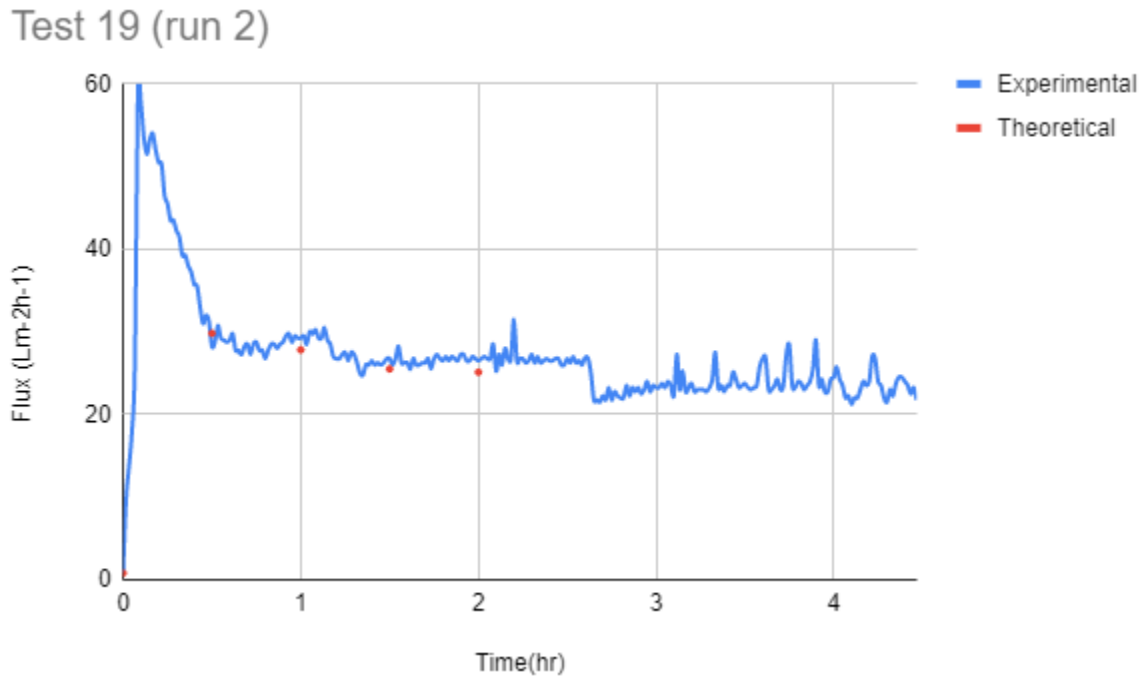

Experimental and best fit graphs of test 19 (Run 2) against time

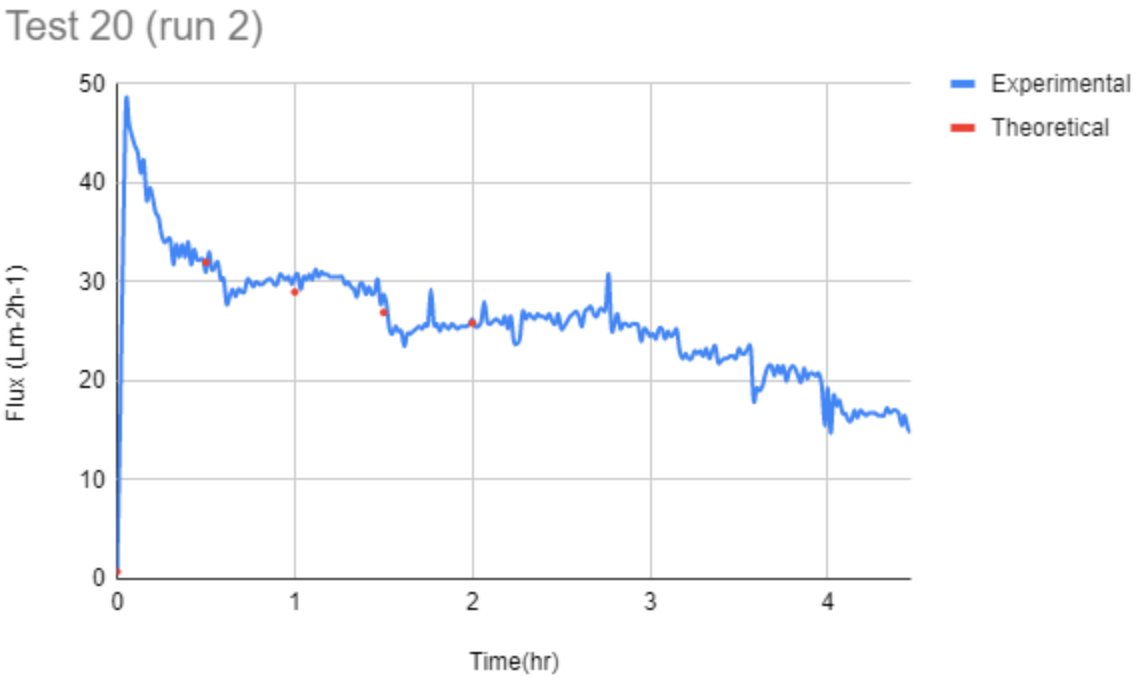

Experimental and best fit graphs of test 20 (Run 2) against time

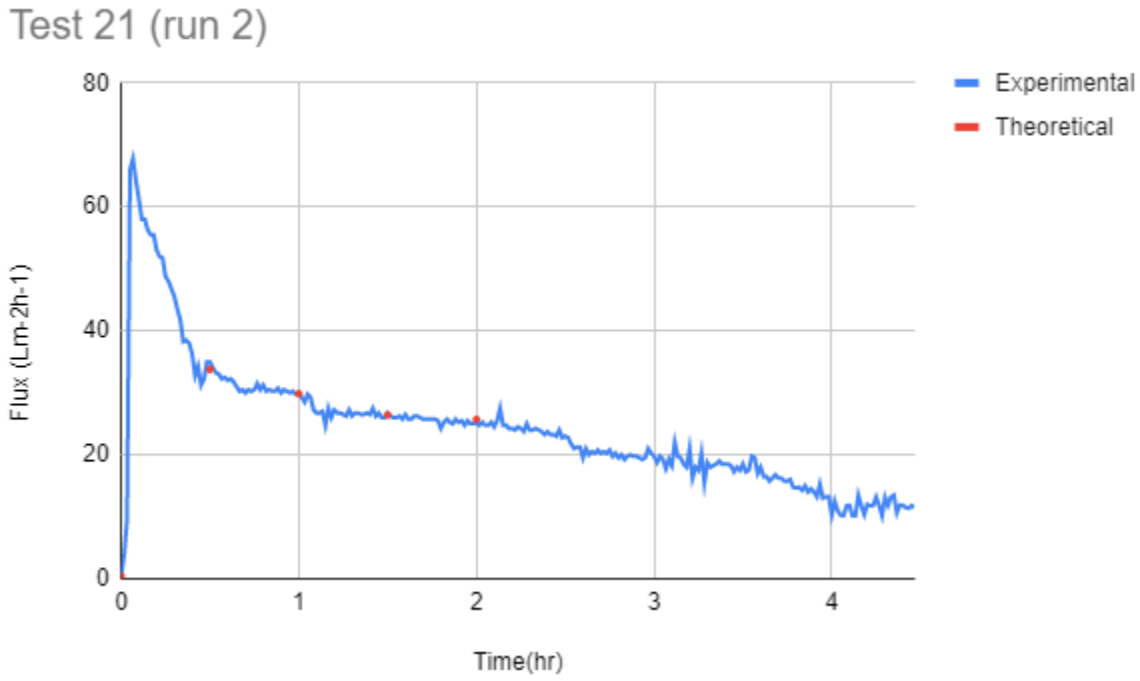

Experimental and best fit graphs of test 21 (Run 2) against time

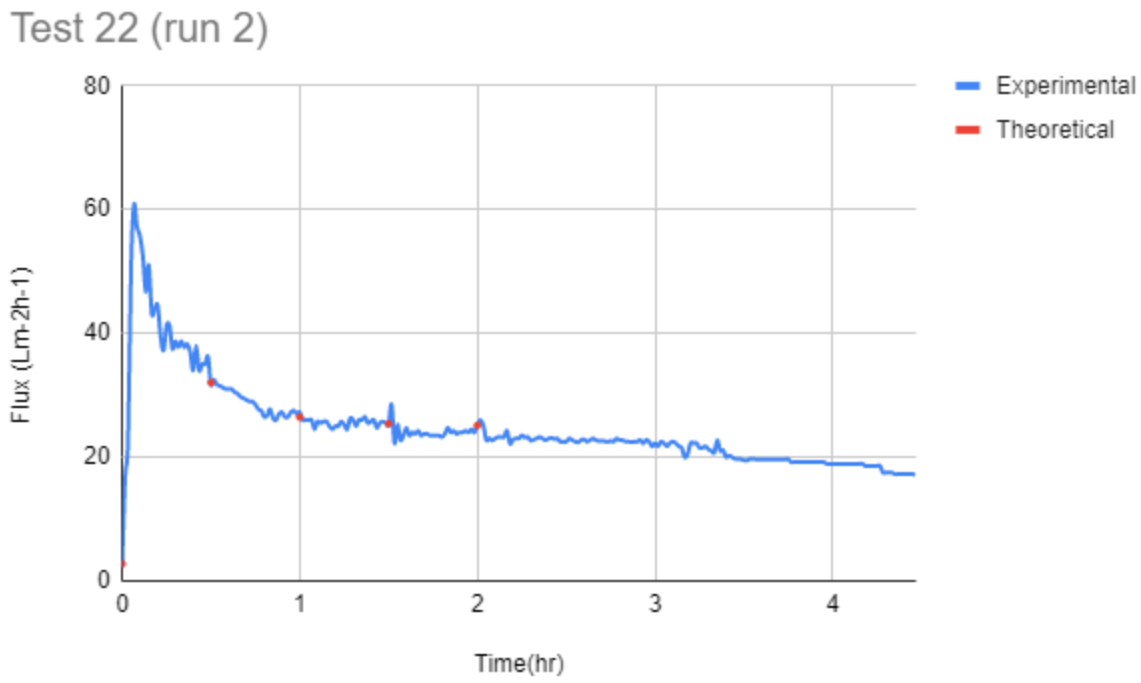

Experimental and best fit graphs of test 22 (Run 2) against time

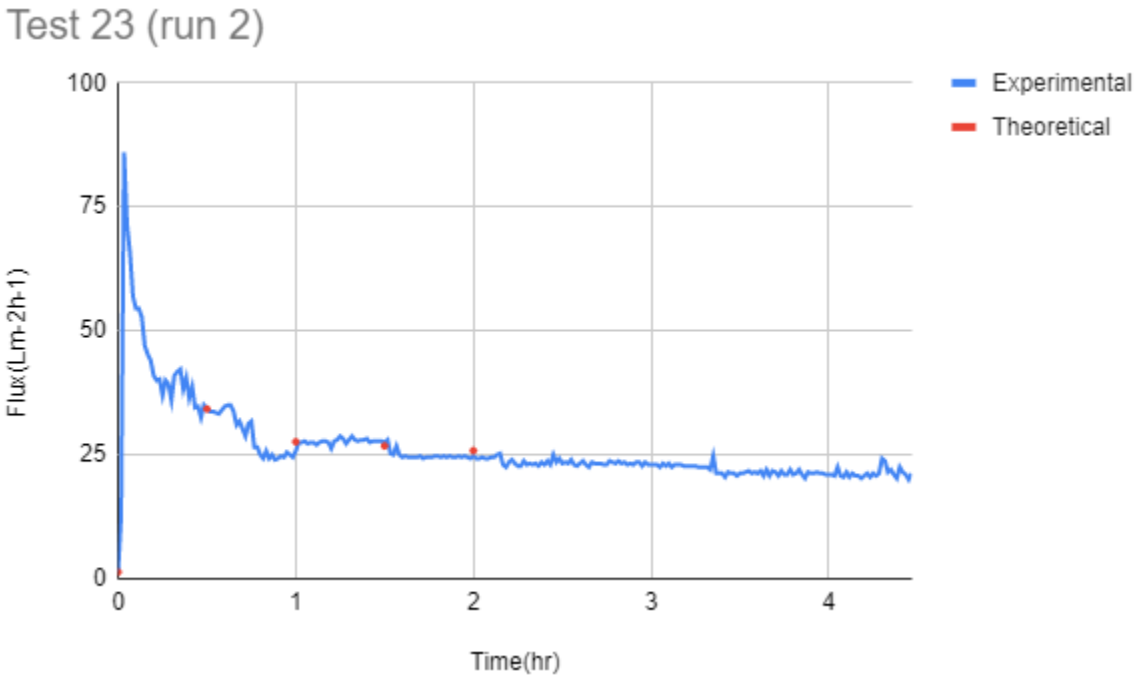

Experimental and best fit graphs of test 23 (Run 2) against time

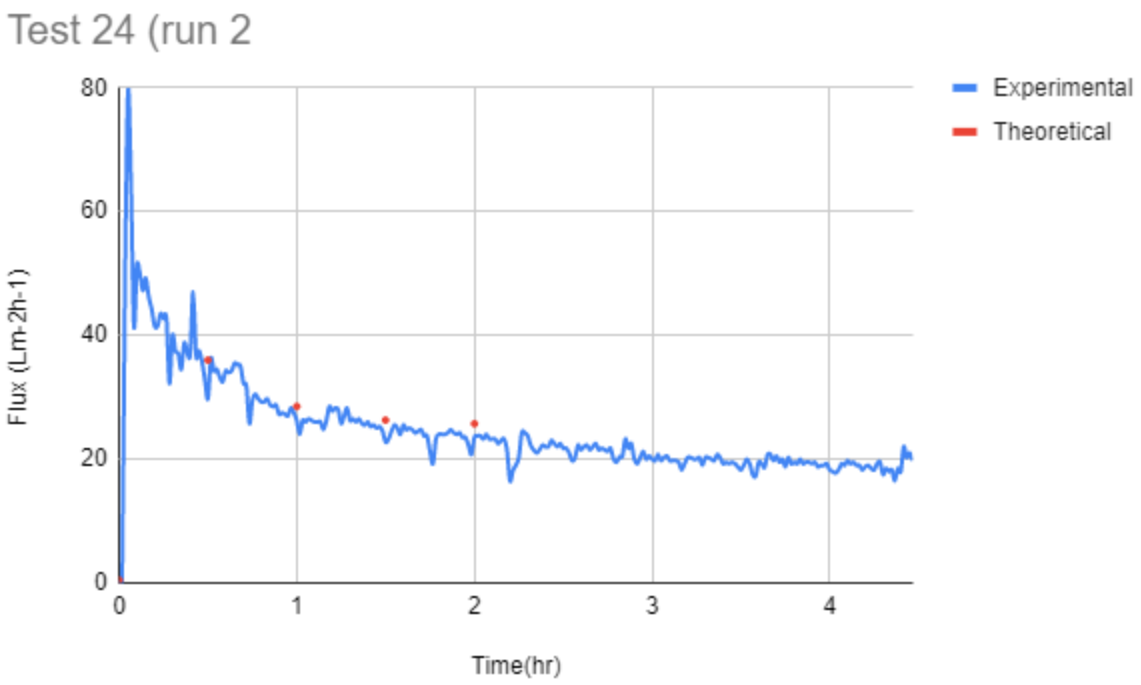

Experimental and best fit graphs of test 24 (Run 2) against time

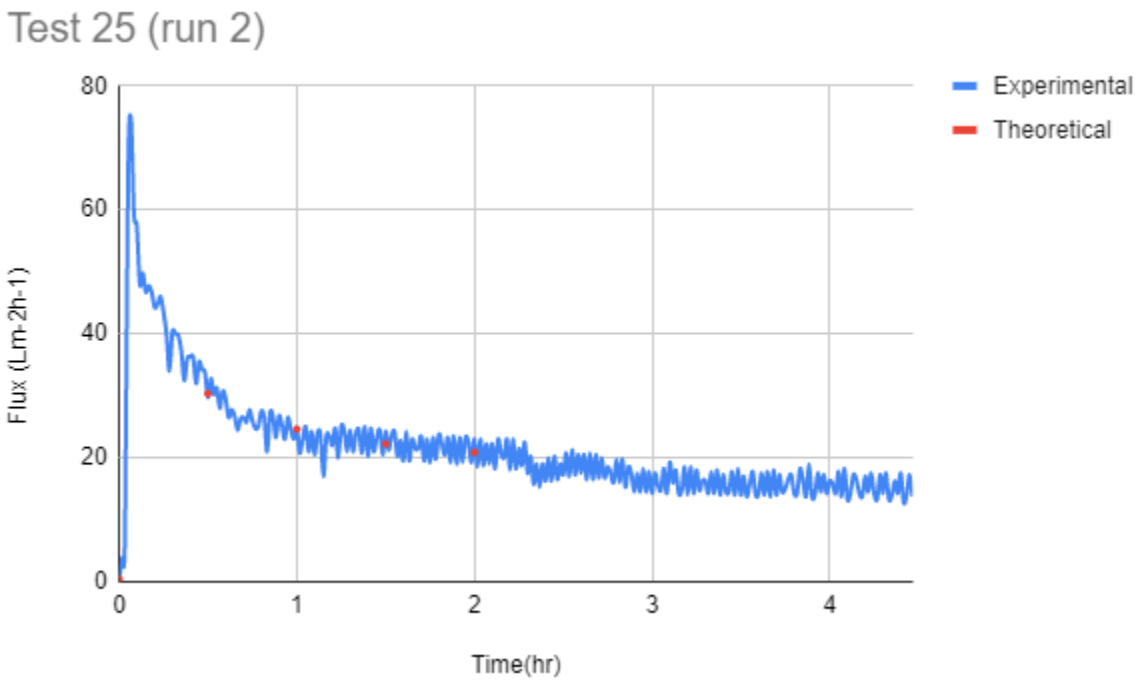

Experimental and best fit graphs of test 25 (Run 2) against time

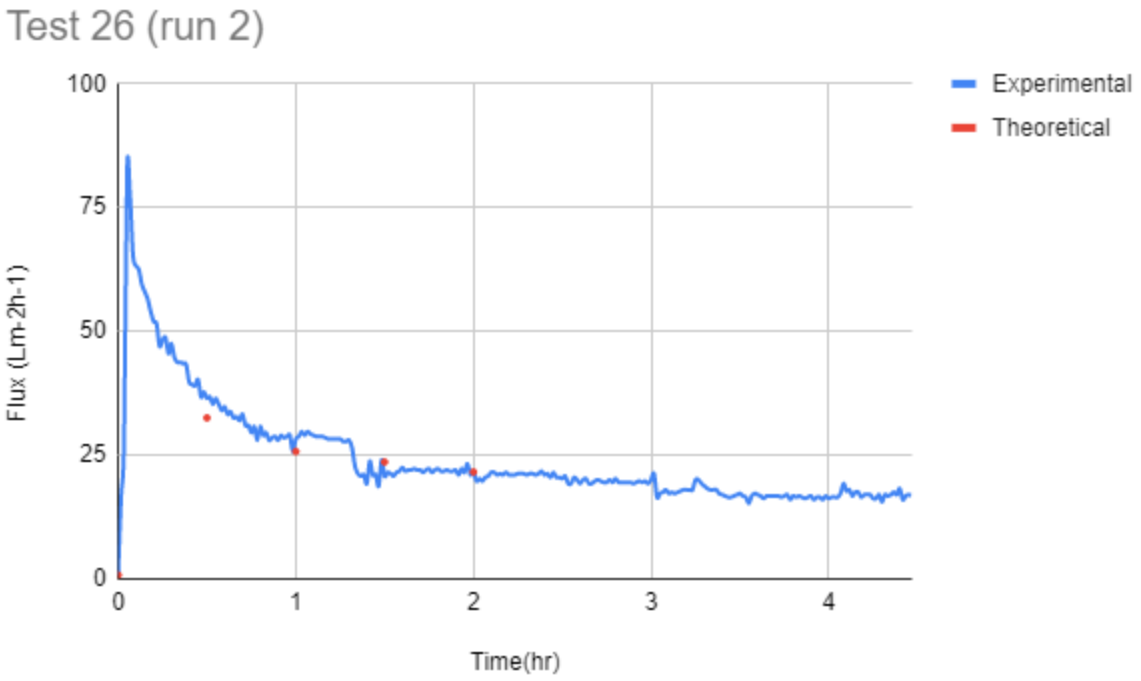

Experimental and best fit graphs of test 26 (Run 2) against time

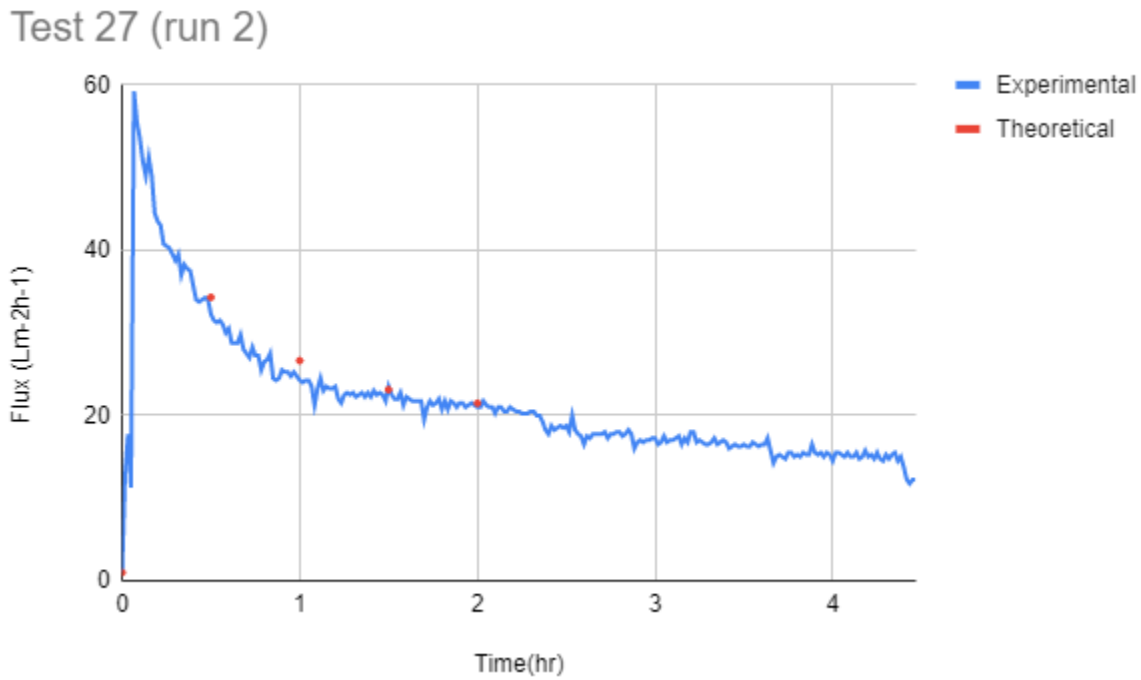

Experimental and best fit graphs of test 27 (Run 2) against time

APPENDIX C. SEM ANALYSIS OF RUN 1 HIGH FLUX MEMBRANES

The SEM images analysis results of the high flux tests of run 1 are presented in this section.

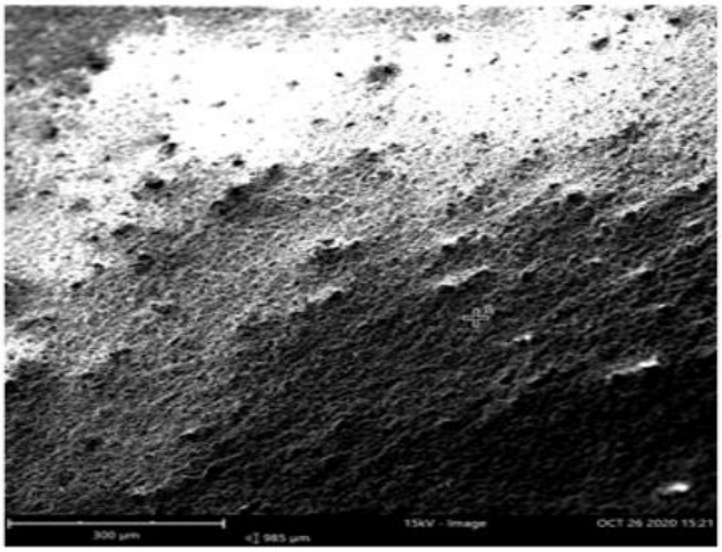

SEM analysis of Test 1 (Run 1)

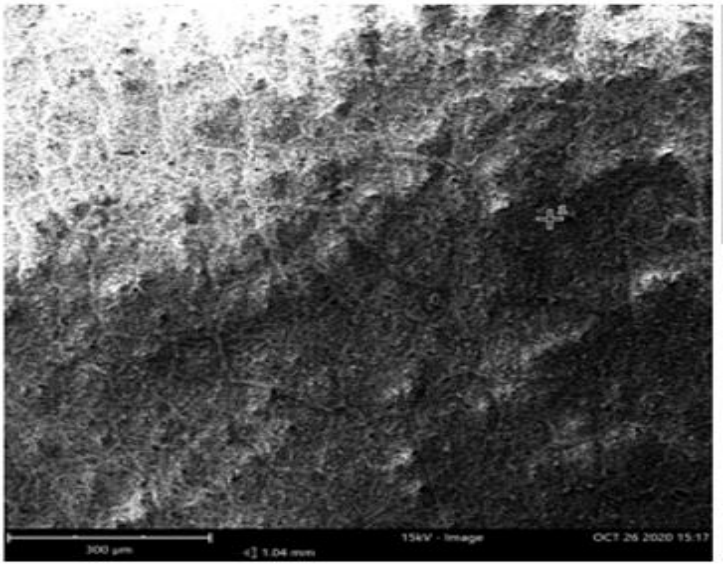

SEM analysis of Test 2 (Run 1)

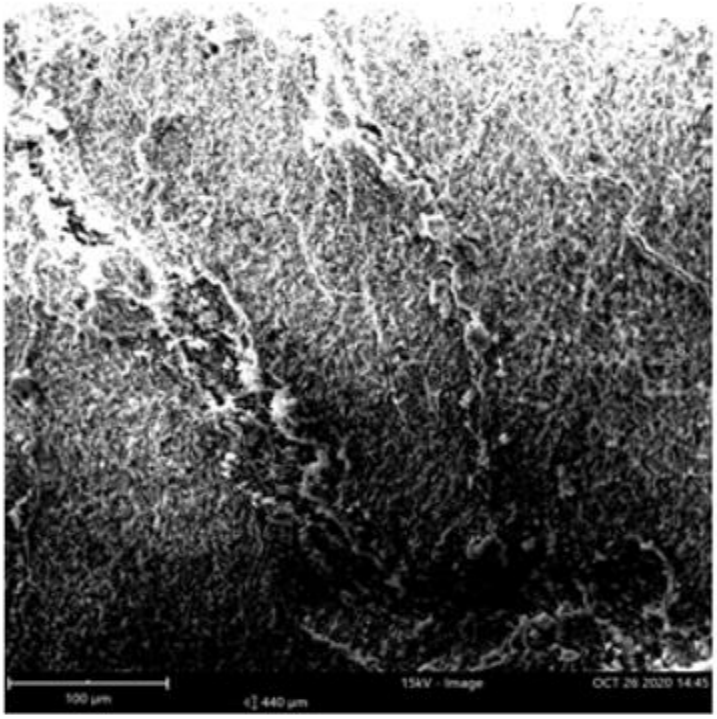

SEM analysis of Test 3 (Run 1)

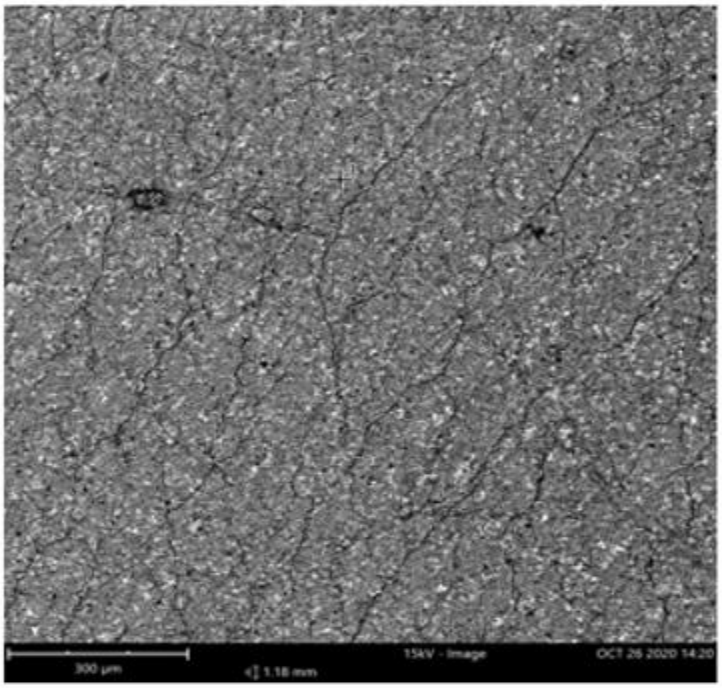

SEM analysis of Test 9 (Run 1)

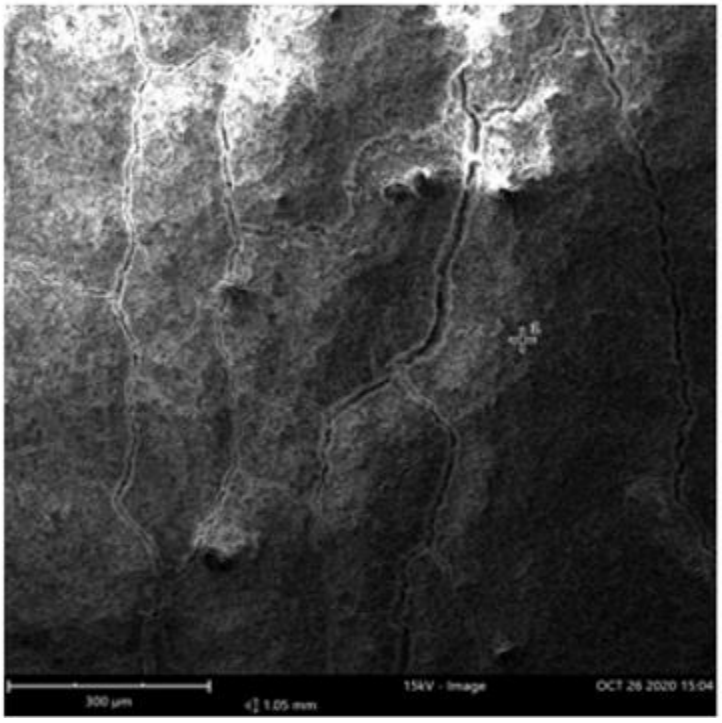

SEM analysis of Test 12 (Run 1)

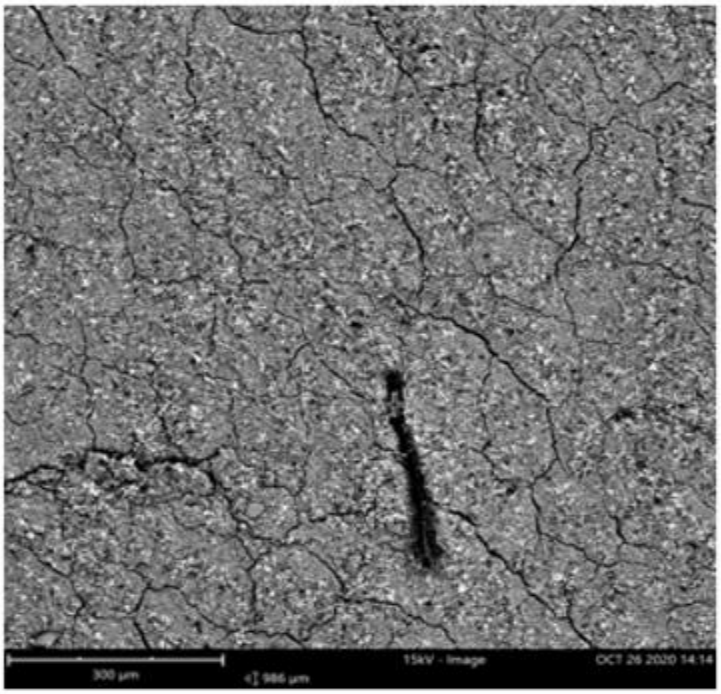

SEM analysis of Test 13 (Run 1)

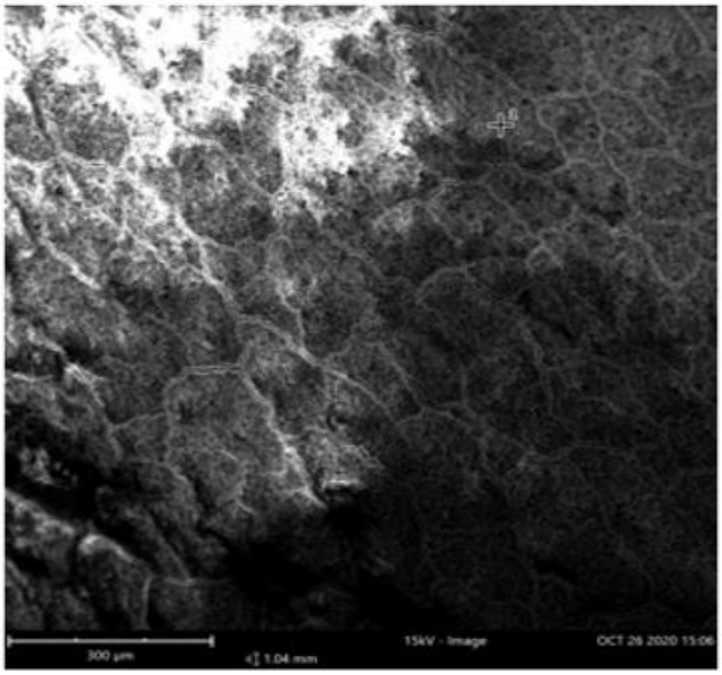

SEM analysis of Test 14 (Run 1)

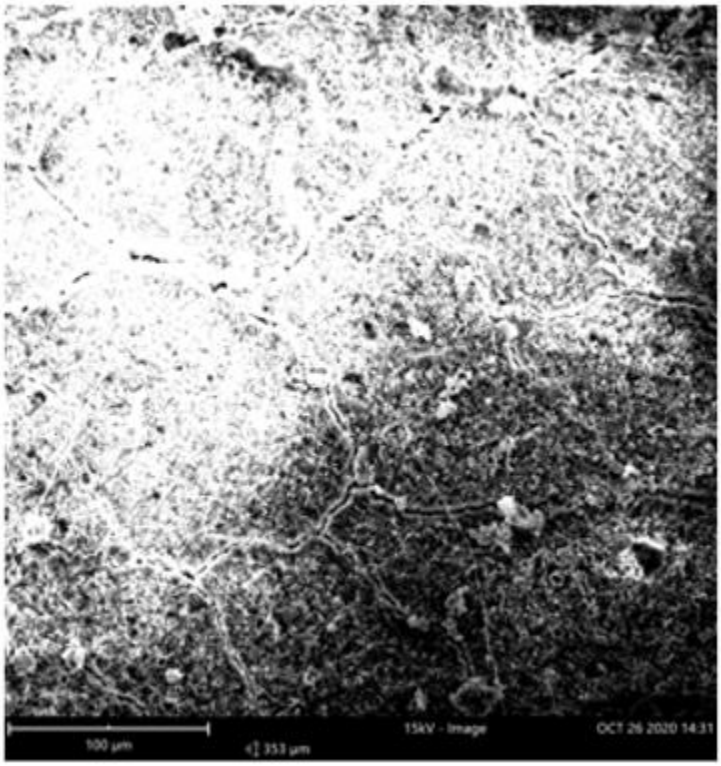

SEM analysis of Test 15 (Run 1)

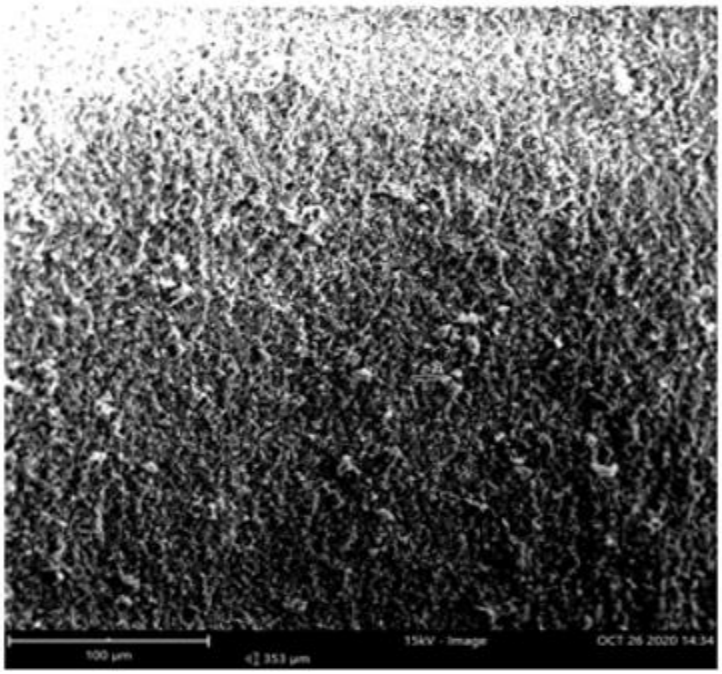

SEM analysis of Test 16 (Run 1)

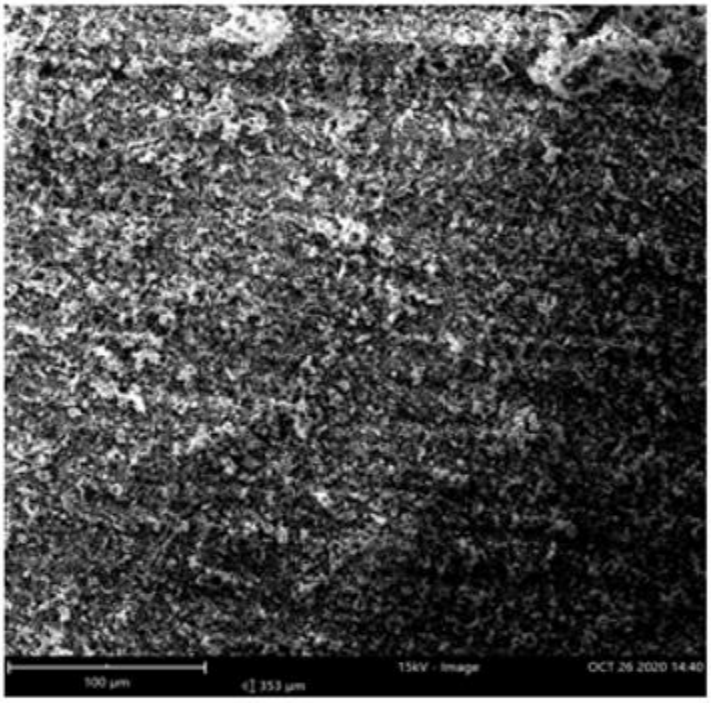

SEM analysis of Test 18 (Run 1)

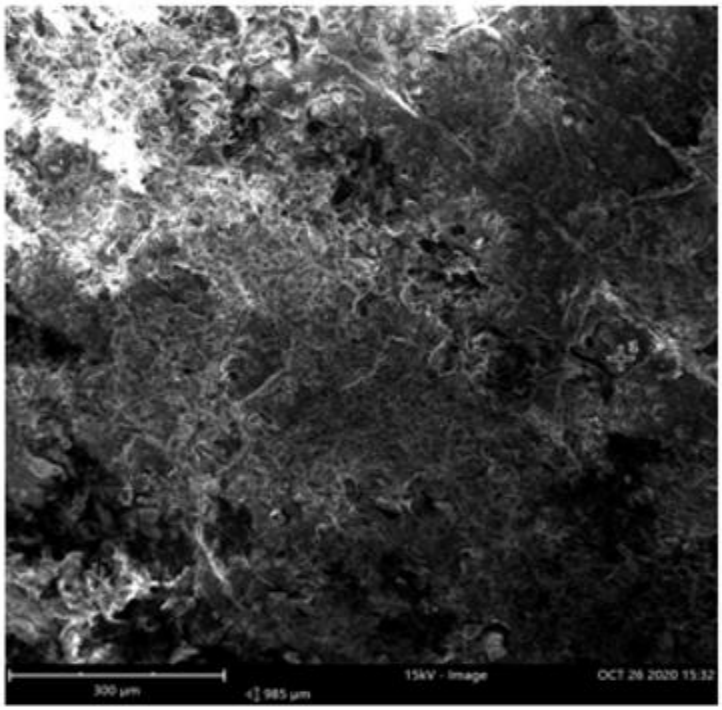

SEM analysis of Test 24 (Run 1)

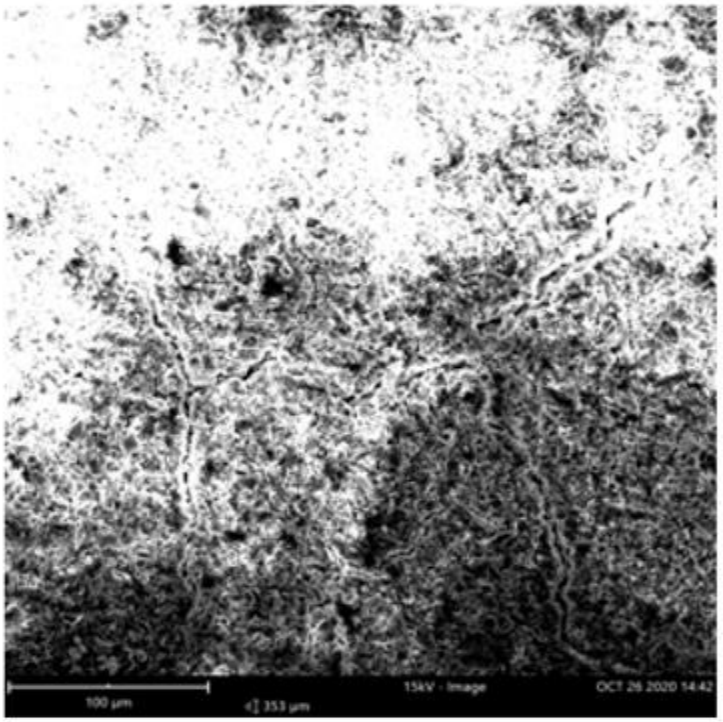

SEM analysis of Test 26 (Run 1)

APPENDIX D. SEM ANALYSIS OF RUN 2 HIGH FLUX MEMBRANES

The SEM images of the high flux tests of run 2 are presented in this section.

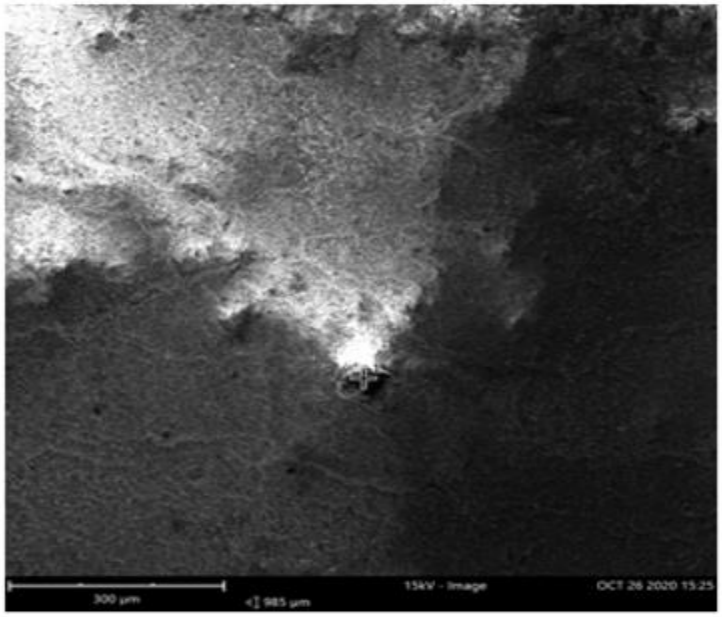

SEM analysis of Test 2 (run 2)

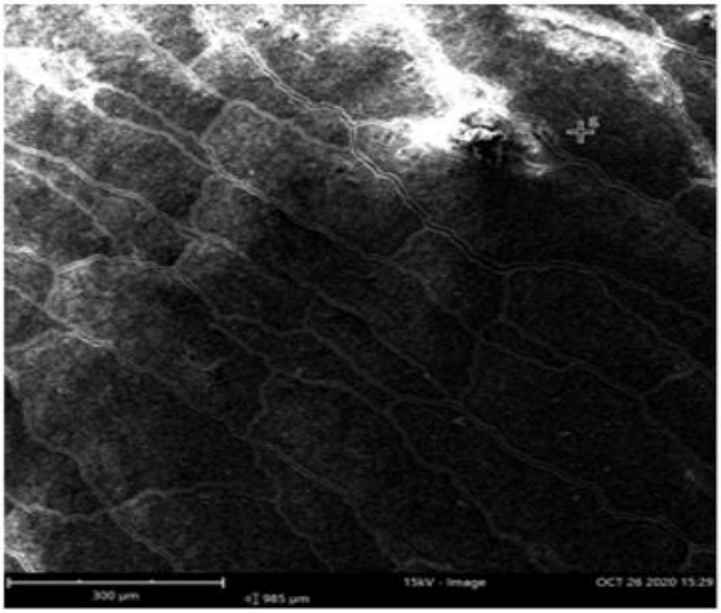

SEM analysis of Test 10 (Run 2)

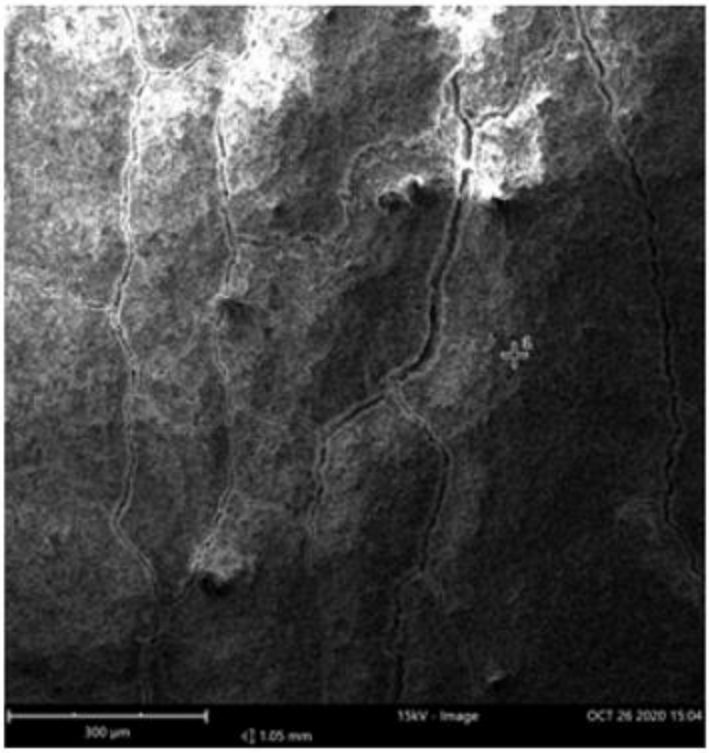

SEM analysis of Test 12 (Run 2)

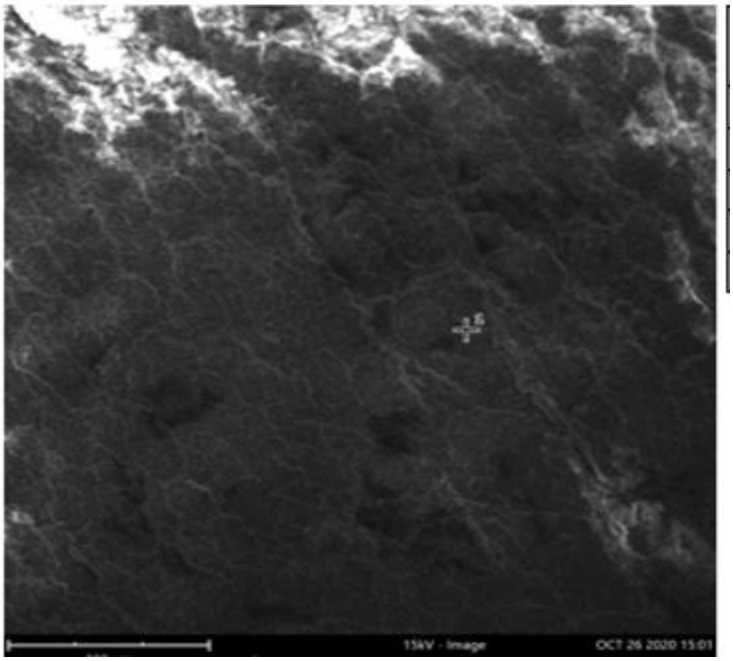

SEM analysis of Test15 (Run 2)

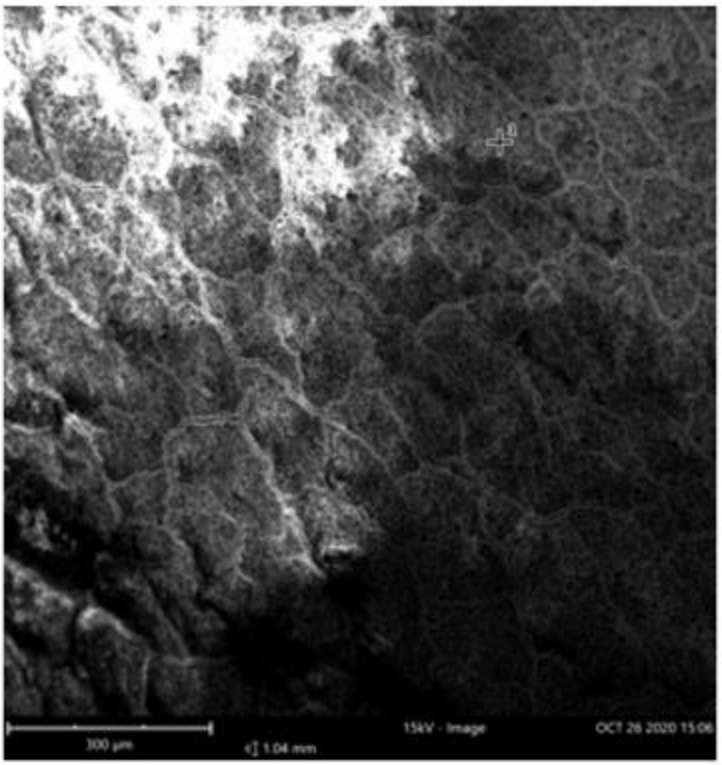

SEM analysis of Test 14 (Run 2)

PUBLICATION

Obinna Aronu & Harvey Abramowitz & Agbai George (2019). Membrane Fouling Mitigation in Water Filtration Using Piezoelectrics. 10.1115 IMECE 2019-11313, V008T09A006